University of Stavanger

Faculty of Science and Technology

MASTER'S THESIS

Study program/ Specialization: Offshore Technology / Marine and Subsea Technology	Spring semester, 2017 Open / ~~Restricted~~ access

Writer:
          Hui Zhu
	………………………………………
	          (Writer's signature)

Faculty supervisor:
Prof. Muk Chen Ong   Dr. Lin Li

Title of thesis: Study of Lifting Operation of a Tripod Foundation for Offshore Wind Turbine

Credits (ECTS): 30

Key words: Frequency domain analysis, response spectrum, limiting weather prediction, Time domain simulation, nonstationary process, lowering, lift-off	Pages: 65 + enclosure: 7 Stavanger, June 15 / 2017 Date/year

Abstract

Marine lifting operations play a key role in the installation of turbines and bottom-fixed foundations. Offshroe installations of the bottom-fixed foundations, tripod foundation in this study, are costly and risky due to the challenging environmental conditons and the bulkiness of the object. It becomes more and more challenging due to the tendency to intall larger turbines in the sites further away from shoreline. To minimize the risks and better prepare the operations, careful study and analysis are essential.

This thesis addresses numerical studies of the installation of tripod foundations using a heavy lift vessel (HLV). Both frequency and time-domain methods are applied in the study. Investigation is first carried out in the frequency domain using the response aptitude operators (RAOs) of the HLV. The wave induced rigid body motions of the vessel are calculated, represented by response spectrum and spectral moment. Thus, the vertical motion of the crane tip can be predicted, which is used as a criterion to find the limiting weather.

As the frequency domain method is based on the simplification of linear response, detailed numerical modelling and simulation of the installation system have been carried out in time domain to analyse the coupled dynamic system. The predicted limiting weather using frequency domain method is firstly verified in time domain by running stationary simulations. It is found that the predicted limiting sea states are inaccurate. The calculated limiting H_s (significant wave height) is underestimated with T_p (spectral peak period of the wave) approaching the natural periods of the installation vessel.

During the lifting operations, some potential critical events may be encountered, such as slack wire or re-hit, collision with the lifting vessel due to excessive motions of the tripod. To identify the potential risks, nonstationary simulations are conducted with emphasis on two lifting scenarios, the lift-off and the lowering phases. Moreover, comparative studies in response using two types of installation vessel, the HLV and the Jack-up, are investigated for the lowering process. Furthermore, sensitivity study on various hoisting speeds is also performed for the case onboard lift-off.

It is found that the wire tension and response of the tripod using the jack-up are relatively smaller, during the lowering process in the selected sea states, than the case utilizing floating vessel. Especially for the lowering in air, huge difference exists between the two types of installation vessels and barely any tripod motion is induced for the jack-up case thanks to the great bottom-fixed stability. Compared to the onboard lift-off, it turns out that there would be much more challenges for the lift-off from barge. Under the considered wave condition, the onboard lift-off operation can be smoothly implemented while the operation from the barge experiences snap load and re-hit.

Acknowledgement

This thesis work is finalized based on the project for the subject Marine Operation in the semester Fall 2016. The detailed works are conducted under the supervision of professor Muk Chen Ong and doctor Lin Li.

The topic was initially recommended by the supervisors for the semester project after I had expressed my interest in marine lifting operations. Initially, it seemed too challenging to follow their stringent comments. On the same token, their constructive comments, combined with their expertized know-how, are highly helpful for me to dive into the topic. Several group meetings on theoretical background and SIMA modelling were organized by doctor Li, not to mention the random drop-by to her office. It would not go smooth without her assistance and devotion. Professor Ong has also presented some precious advices. I would like to take this opportunity to express my sincere appreciation to them.

Hui Zhu

June 2017

Stavanger, Norway

Contents

List of Figure

List of Table

1   Introduction

1.1   Background and motivation

Wind is a clean, free and readily available renewable energy source. Everyday around the world, wind turbines are capturing the wind's power and converting it to electricity. Besides the on-land wind farms, offshore wind industry grows fast. The installation of offshore wind farms continues to increase, which are driven by many factors. The potential energy produced from wind is directly proportional to the cube of the wind speed. As a result, only a small increment of the wind speed can produce a significantly larger amount of electricity. Compared to the wind plants on land, higher wind speeds and low turbulence intensity offshore can result in up to 50% higher energy production (WindEurope, 2017). Since more wind energy can be captured offshore, together with other positive factors, like technology transfer from oil and gas industry, offshore wind industry has boomed around the world, especially in Europe around the North Sea and the Baltic Sea. It is predicted that offshore wind will provide a growing share and reach one third all the wind generated energy by 2050 (IEA, 2013). As illustrated in the Figure 1.1, cumulative capacity of the offshore wind will keep growing in the coming decade.
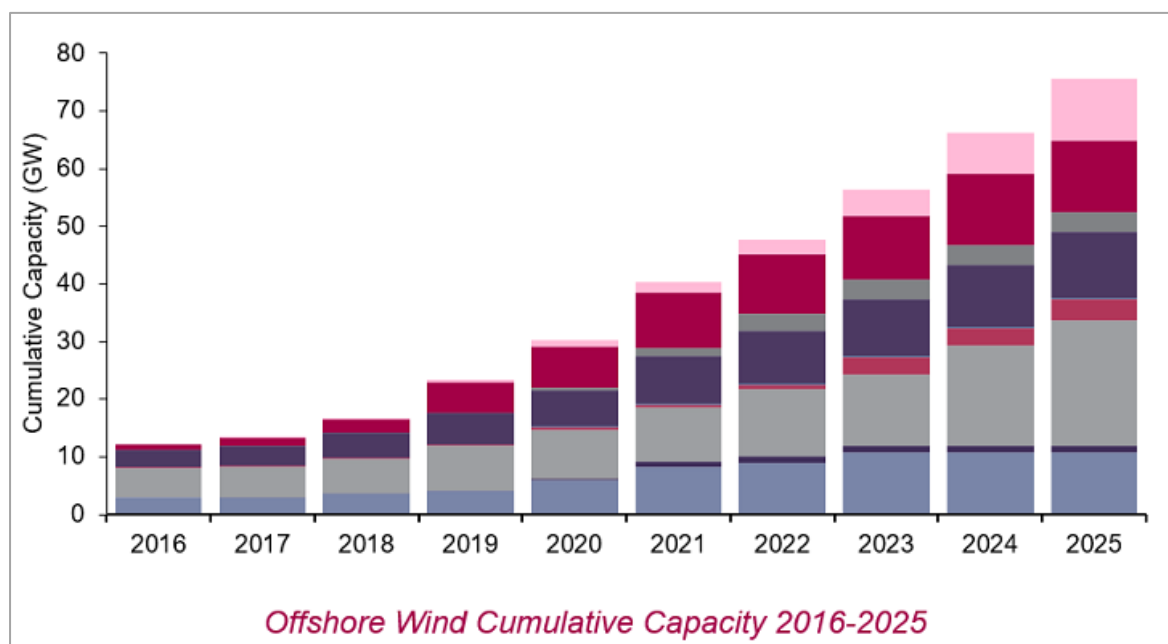
Figure 1.1 World offshore wind market forecast from Douglas-Westwood

The Figure 1.2 shows that offshore wind farms tend to move into deeper waters. Projects, irrespective of under construction, consented or planned, follow the same trend. Aside from the aim to search for greater wind condition, it is the result of the lack of available and proper sites close to shore. Moreover, the rated capacity of offshore wind turbines becomes larger and has grown 62% over the past decade. The averaged rated capacity of turbines installed in 2016 was 4.8 MW, 15.4% larger than 2015 (WindEurope, 2017). To withstand bigger loads from the larger turbine and the harsher environment, more robust substructures are needed which brings more challenge to the offshore installation.

In addition, price of offshore wind was expecting to gradually decrease so that the wind energy could be competitive in the energy market. Surprisingly, the anticipation is coming true. According to online report, a spectacular drop in price, by any measure, which has certainly defined a range for 'the new normal' in mature northern European offshore wind markets at well below €100/MWh (GWEC, 2016). This is another driving factor for efficient and reliable offshore installation.
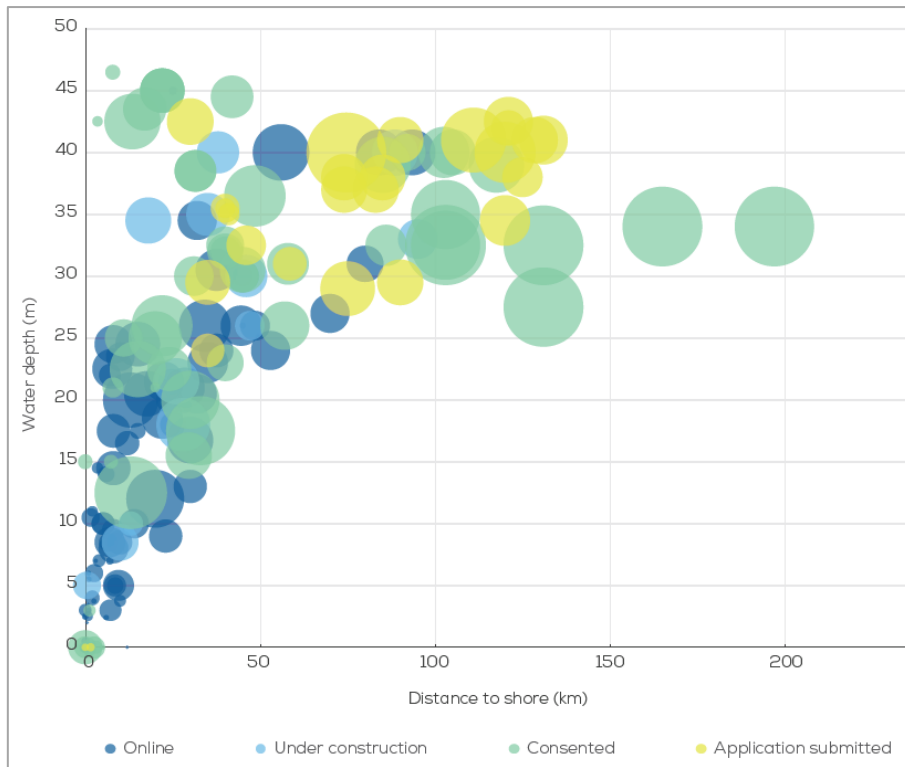
Figure 1.2 Average water depth, distance to shore of bottom-fixed, offshore wind farms by development status. (WindEurope, 2017)

Tripod foundation is normally composed of one large central column which connects to three pile sleeves through diagonal braces. The central column penetrates water surface even after its installation so that tower and turbine structure can be easily connected on. The foundation is anchored into the seabed using steel piles on each corner. Thanks to the pile anchoring which provides a stable foundation, the tripod has proven useful at deep sites and varying soil conditions. The design of the tripod gives it sufficient strength to be placed in deep waters, while maintaining the advantage of minimal sea bed preparation. Figure 1.3 shows a typical profile of tripod structure.
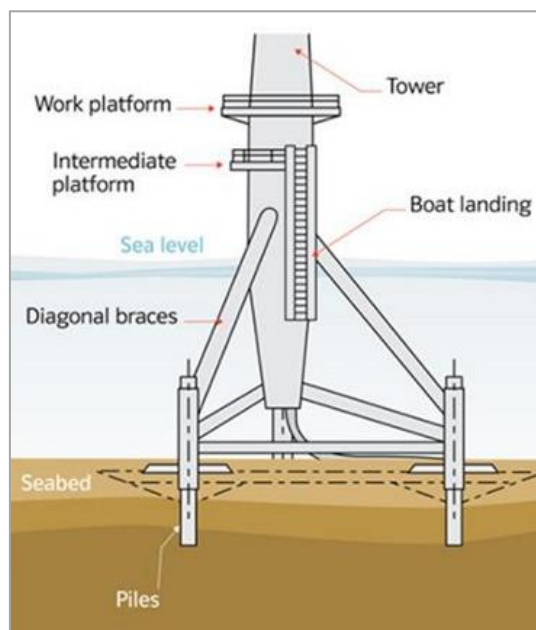
Figure 1.3 Typical tripod structure (4Coffshore, 2013)

Marine lifting operations play a key role in the installation of turbines and bottom-fixed foundations. They are typically carried out by a floating or jack-up crane vessel. A jack-up provides a stable working platform while the installation and retrieval of the jack-up legs are time consuming. Floating vessels with onboard heavy crane are more effective especially for the mass installation of wind farms, because of their fast transit among specific turbine sites. Figure 1.4 and Figure 1.5 shows installation operation carried out by a floating vessel and a jack-up respectively.

Figure 1.4 Tripod installation by HLV (HeavyLiftSpecialist, 2013)

Figure 1.5 Tripod installation by jack-up vessel (Overdick GmbH & Co KG, 2012)

Tripods are transported onboard of the installation vessel or a transport barge to the offshore site, after the manufacturing at shipyard. Lifting and installation can then be carried out after necessary weather window analysis. For proper installation, the foundations are to be lifted off, positioned and lowered to the sea bed by use of a floating or a jack-up vessel with onboard cranes. For subsea lifting, the operation process can be divided into 5 phases.

Number	Phase
1	Lift off
2	Object hanging in air
3	Splash zone crossing
4	Deeply submerged
5	Landing
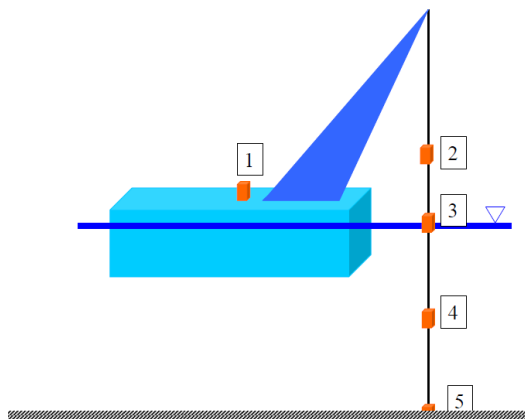
Figure 1.6 Five phases of a marine lifting

1.2   Literature reviews

In contrast to the installation in the oil and gas industry which are normally tailor made for the specific project, repetitive operations are implemented for the units in an offshore wind farm. For efficient mass installation operations, it is crucial to build accurate numerical models to predict the system behaviour.

Regarding operational limits, it is believed that an increasing need to determine the operational limits based on quantified responses will occur, even though practical experience still plays an important role in the design of marine operations (Birkeland, 2016). Limiting conditions of crane vessel operations by model tests and calculations were investigated in (Clauss, et al., 1990). Operational limits in terms of H_s were established based on the selected limiting parameter – the vertical load motion.

In (Li, et al., 2016a) new methodology was established to obtain the operational limits based on limiting parameters obtained from different numerical approaches. Further study was conducted in (Li, et al., 2016b) by investigating which factors are crucial in the numerical modelling to achieve an accurate basis for establishing the operation limits.

During the lowering or the lift-off operation, the dynamic properties of the lifting system changes continuously following the varying position of the tripod. It is vital to select proper time-variant system properties like the hydrodynamic coefficients, for precise response analysis of the lifting system. To determine accurate hydrodynamic coefficients, model tests or computational fluid dynamics are normally required.

For slender structures, strip theory based on Morison's formula with varying draft was used to approximate the wave forces in (Li, et al., 2013). It turned out in (Li, et al., 2015a) that the conventional Morison's formula might overestimate the responses of the lifting system since the diffraction and radiation had been neglected. To address the issue, new approaches were proposed to account for the radiation damping on the basis of the Morison's formula and strip theory.

1.3   Scope and purpose

The marine lift and installation involves multi-bodies that includes the heavy lift vessel, the object to be lifted (the tripod) and the transport barge if engaged. During the lifting operations, the lifting system may experience changes in dynamic properties. The involvement of running winch, no matter for the lift-off or the lowering of tripod, makes the process non-stationary. For a dynamic coupled model of the installation system, their motions can be solved in frequency or time domain. Frequency domain method can be applied for analysis of responses resulting from a stationary process like the floating vessel alone under wave condition. In contrast, if the dynamic system is non-linear and the resulting processes are non-stationary, time domain simulations need to be carried out.

Subject to rigid body motions, the floating heavy lift vessel (HLV) itself can be investigated in frequency domain. Its behaviour can be checked by looking at the response amplitude operators (RAOs) which is further clarified in the theory part.

For the coupled non-linear installation system, numerical modelling and analysis are expected to get an understanding how they interact with each other, especially during the non-stationary process. For this purpose, the software SIMO, issued by the company MARINTEK, is going to be used. SIMO is a non-linear time domain simulation program used for the analysis of rigid body motions and multibody systems.
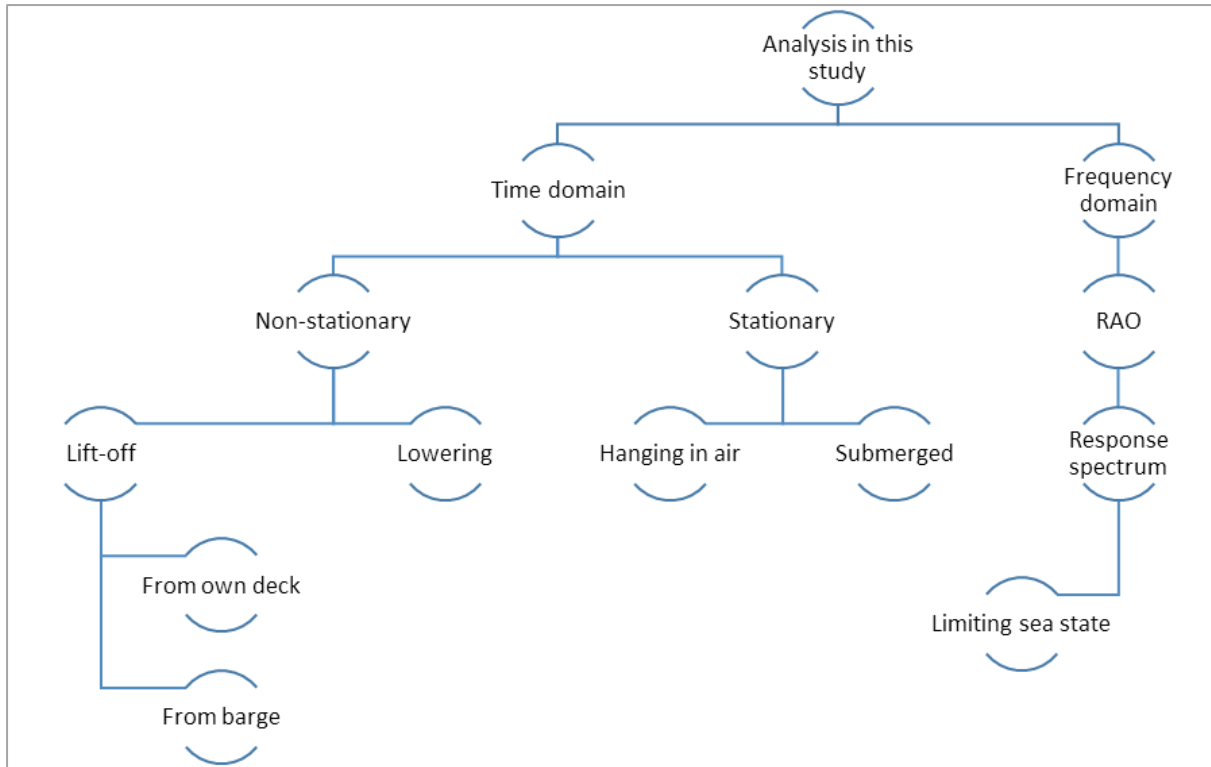
Figure 1.7 General scope of this thesis work

Lifting operations of the tripod foundations at the offshore installation site are to be studied in this thesis. Investigation is first carried out in frequency domain in Chapter 4, starting from RAOs of the HLV. Based on the linear wave theory and linear response process (Haver, 2007), (Birkeland, 2016)wave induced rigid body motions of the vessel can be calculated in the frequency domain, represented by response spectrum and spectral moment. Concerning certain critical response parameter, like the vertical motion of the crane tip in this study, limiting weather can be predicted based on probabilistic acceptance criteria.

The calculated limiting sea states in frequency domain can only be treated as preliminary assessments since it is carried out on the basis of the decoupled rigid body motion (HLV only). Besides, the wave induced motions are supposed to follow the linear response process.

For the dynamic lifting system, numerical models are to be built as introduced in Chapter 5, followed by eigenvalue analysis which presents eigenfrequency of the rigid body or the coupled system under certain loading condition. Time domain simulations of the coupled lifting system are carried out in Chapter 6. The predicted limiting sea states using frequency domain method are cross checked in time domain by running stationary simulations. Consequently, the attention is shifted to the time-varying non-stationary processes, the lowering and the lift-off. Potential critical events may occur during the processes, such as slack wire, collision with the lifting vessel due to excessive tip motion of the tripod or even re-hit between the tripod and transport barge during the lift-off. All the cases are simulated and analysed in detail in the Chapter 6.

2 Installation system and site condition

In this study, site 15 North Sea Centre is chosen as the installation site which was shortlisted for a potential offshore wind farm project. Wave data on the installation site, presented in scatter diagrams are available. The installation operations of the tripod foundations, are going to be carried out by a heavy lift vessel (HLV). Detailed characteristics of the installation system, together with the site conditions, are illustrated in this chapter.

2.1 Tripod foundation

The advantage of the tripod is that it is suitable for greater water depths while at the same time only a minimum of preparations is required at the site before installation, compared to other types of foundation like gravity-based foundation. The design of the tripod foundation gives it sufficient strength to be placed in deeper waters, while maintaining the advantage of minimal sea bed preparation. This extra strength should also give turbines using this foundation more resilience to hurricanes and tropical storms.

Depend on the capacity of the wind turbine, the weight of the tripod foundation can reach around 1000 tons, which presents new challenge for offshore installation. Table 2-1 shows the main parameters of the tripod foundation in this study (Xu, 2016).

Table 2-1 Main parameters of tripod foundation

Item	Value
Total height [m]	65
Centre column outer diameter [m]	5.7
Brace outer diameter [m]	1.2-3.15
Tripod mass [tons]	885

2.2 Installation vessel

Taking into account the weight and dimension of the tripod foundation, only the vessels with capable enough lifting cranes can be employed for this installation work.

The one chosen for the duty in this study is a mono-hull heavy lift vessel (HLV). The crane is capable of performing lifts of up to 5000 tons at an outreach of 32m in fully revolving mode. The main hook featured a clear height to the main deck of the vessel of maximum 100m. The vessel has been designed with a combination of dynamic positioning system and eight catenary mooring line system. The positioning system allowed the operation in close proximity to other structures, which makes it possible to lift the tripods from adjacent transporting barge.

Table 2-2 Characteristics of installation vessel

Item	Value
Length overall [m]	183
Length between perpendiculars [m]	171.6
Breadth [m]	47
Depth from deck [m]	18.2
Operational draught (crane lifting mode) [m]	10.2
Transit draught [m]	7.5

In addition to the main hook, auxiliary hook with 800 tons lifting capacity and whip hoist with 200 tons' capacity are also fitted. Now that the weight of the tripod is over 800 tons, only the main hook will be utilized. Working radius chart, figure 2.1, shall be referred to sort out reasonable lifting position.
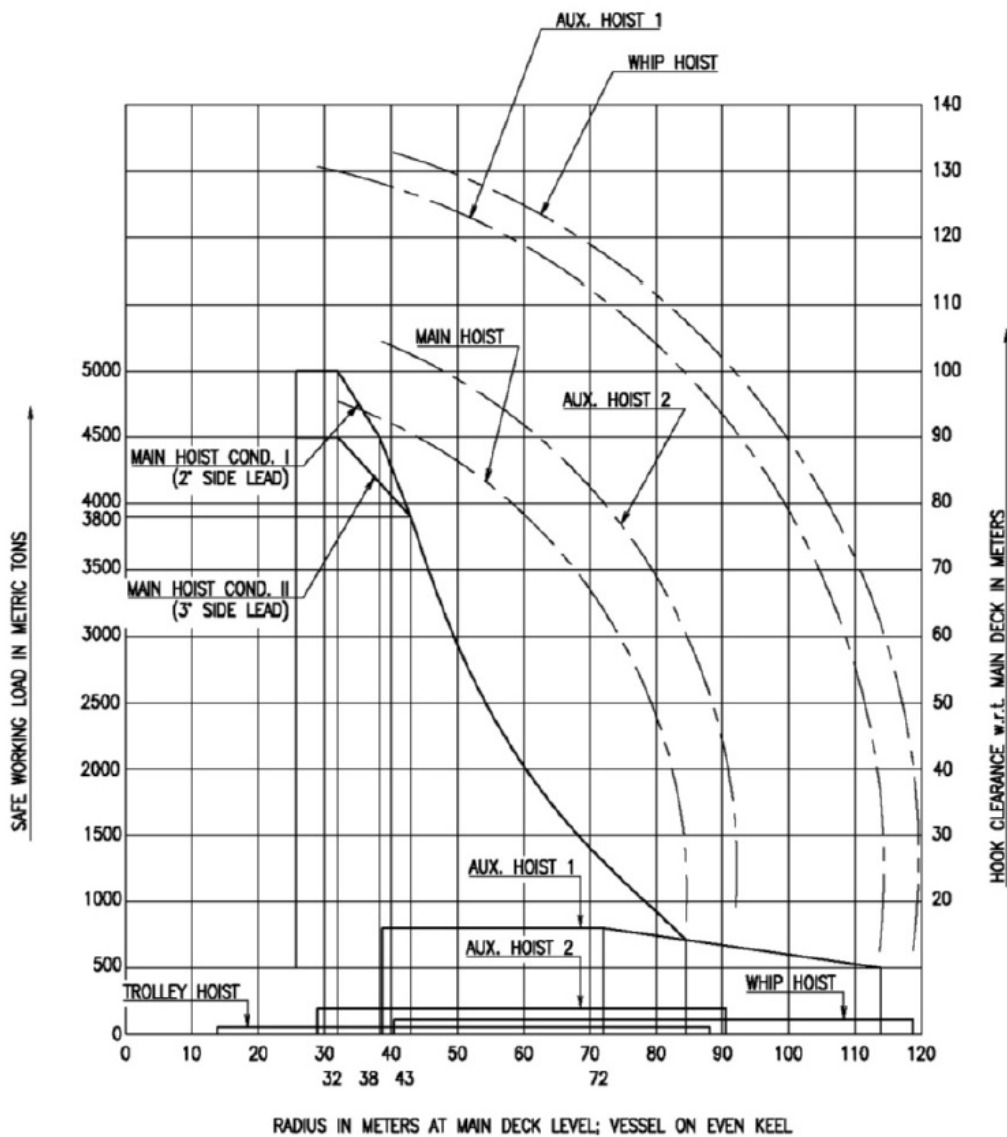
Figure 2.1 Load-radius chart of the heavy lift crane

Given the total height of the tripod 65m, approximately 80m lifting clearance from vessel deck will be required, taking into consideration the height of lifting blocks and some clearance allowance. Reading from the load chart in Figure 2.1, the maximum allowable working radius for the main hoist, with 80m lifting height, is around 57m for crane centre. Should the crane be orientated in the transverse direction, the lifting distance away from ship side is about 33.5m (subtracting half width of the vessel). Due to the huge volume of the tripod, around 25m protrusion distance from geometric centre in footprint, there is not much clearance left between the lifted tripod and ship side hull, even the crane boom aligned in the transverse direction during the lifting (lowering) operation. Although it will help mitigate the tripod's motion to orientate the crane boom towards mid-ship (approaching ship-side in the meantime), enough clearance to ensure safe operation is of the utmost importance. Hence, lifting operation is decided to be carried out in transverse direction in this study.

2.2.1 Coordinates of the crane tip during the installation

On the premise of ensuring reasonable lifting operation, such as safe clearance from ship side as clarified earlier, the exact location (coordinates) of the crane tip during the installation can be decided by further referring to General Arrangement of the ship (Appendix A).

The coordinates of the crane tip, relative to the origin of the vessel which is the basis for the crane tip motion calculation in frequency domain analysis and further for the modelling and simulation in the time domain, is decided as (-81.7, 53.5, 88).

Table 2-3 Coordinates of the crane tip during the installation

	X	Y	Z
Crane Tip	-81.7	53.5	88

2.2.2 Operational requirements of the vessel

Generally, there would be some operational requirements for the safety of heavy lift operations, from the general specification of the vessel or manual of the heavy lift crane.

Normally, for marine lift, there would be some limitation on maximum angle of vessel roll and pitch which can be easily checked based on the given transfer functions of the vessel. It is not included in this study and more attention is paid to sorting out the limiting sea state through probabilistic calculation in frequency domain (Haver, 2016). In this case, another limiting criterion is of concern, the acceptable vertical motion of crane tip. Referring to the master thesis (Andersen, 2012), the concerned limiting criteria for the chosen heavy lifting vessel (HLV) are listed in the table 2.4.

Table 2-4 Limiting values for the operation of the HLV

Significant wave height (H_s)	$\leq$	2.5 [m]
Vertical motion of crane tip	$\leq$	0.3 [m]

2.3 Environmental conditions on the installation site

Installation site is chosen as site 15 North Sea Centre which was considered as potential site for renewable energy project (Li, et al., 2015b).

Figure 2.2 Installation site - 15 North Sea Centre (Li, et al., 2015b)

Marine operations are highly dependent on environmental conditions. Hence, prediction of the operational weather window is critical. Especially the impact from waves, wind and current are of interest, but also other environmental parameters as ice, the impact of tides and marine growth may be considered. Waves are of special interest as they directly affect the motions of an installation vessel.

Hourly wave data at the subject site from April to September in the years 2001 - 2010 are available, and 10-year scatter diagram has been compiled accordingly (Li, et al., 2016c).

Table 2-5 Ten-year scatter diagram of Hs and Tp at the installation site

Tp (s) / Hs (m)	1-2	2-3	3-4	4-5	5-6	6-7	7-8	8-9	9-10	10-11	11-12	12-13	13-14	14-15	15-17	Sum
0-0.2	0	0	8		0	3	13	0	1	6	0	0	12	0	0	43
0.2-0.4	3	44	461	334	74	47	80	67	46	37	27	10	6	13	12	1261
0.4-0.6	0	86	633	1803	788	245	152	221	165	81	28	20	31	12	13	4278
0.6-0.8	0	31	707	2233	1632	686	215	242	177	180	60	26	33	14	13	6249
0.8-1.0	0	3	228	2428	2008	1201	327	270	320	263	46	24	15	11	4	7148
1.0-1.2	0	0	44	1486	1816	1151	595	265	181	235	89	36	34	7	7	5946
1.2-1.4	0	0	3	590	1677	1017	524	278	165	194	80	36	7	13	1	4585
1.4-1.6	0	0	0	175	1403	878	428	233	73	91	81	45	19	4	2	3432
1.6-1.8	0	0	0	41	930	837	381	233	36	38	45	45	10	6	2	2604
1.8-2.0	0	0	0	2	472	765	324	176	66	27	15	19	38	22	4	1930
2.0-2.2	0	0	0	1	191	818	265	165	38	20	14	14	24	2	1	1553
2.2-2.4	0	0	0	0	56	569	328	140	50	9	4	10	20	1	0	1187
2.4-2.6	0	0	0	0	14	361	269	110	38	16	2	11	17	1	0	839
2.6-2.8	0	0	0	0	1	239	267	112	34	9	2	1	12	0	0	677
2.8-3.0	0	0	0	0	0	101	218	134	45	16	3	2	22	2	0	543
3.0-3.2	0	0	0	0	0	35	170	77	65	16	3	0	7	4	0	377
3.2-3.4	0	0	0	0	0	4	133	44	42	8	6	0	2	0	0	239
3.4-3.6	0	0	0	0	0	1	117	53	51	12	3	0	0	0	0	237
3.6-3.8	0	0	0	0	0	1	59	48	41	12	4	0	0	0	0	165
3.8-4.0	0	0	0	0	0	0	44	26	43	13	5	1	0	0	0	132
4.0-5.0	0	0	0	0	0	0	35	82	112	85	16	0	0	0	0	330
5.0-6.0	0	0	0	0	0	0	0	8	31	75	25	1	0	0	0	140
6.0-7.0	0	0	0	0	0	0	0	0	0	18	7	0	0	0	0	25
Sum	3	164	2084	9093	11062	8959	4944	2984	1820	1461	565	301	309	112	59	43920

Based on the scatter diagram, statistical distribution of the wave condition, probability distribution function (PDF) and cumulative distribution function (CDF), can be plotted.
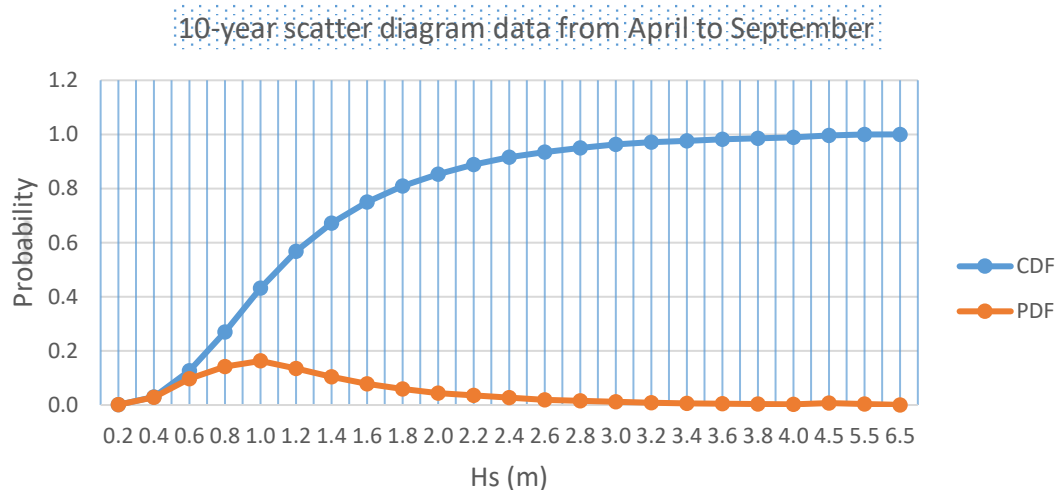
Figure 2.3 Probability distributions of the 10-year data

Reading from the plotted figure, the probability of the waves lower than 2.5m (operational requirement of the HLV) can reach 90%. In this case, it seems really positive to carry out the operation. But for the risky and costly offshore installation operation, further study shall be carried out to predict the limiting weather based on certain critical response criteria or even to conduct numerical simulations for deep understanding of the performance of the dynamic coupled installation system.

3　Theoretical Background

The intention of this chapter is to provide the theoretical background on waves and wave induced motions, based on which the performance of the rigid body (the HLV) and the affiliated point on it (the crane tip) would be evaluated. Consequently, the theory behind the limiting weather prediction would be introduced.

As introduced in above chapter, to ensure safe operation of the offshore installation work, weather condition shall be verified and certain limiting sea state shall be guaranteed. Following the lectures on marine operation (Haver, 2016), the limiting sea state in terms of certain critical parameter can be determined by spectral analysis in frequency domain. In this study, the critical parameter would be the vertical motion of the crane tip.

3.1　Wave theory

In general, wave can be generated in many different ways:

- Waves generated by blowing wind, over a fetch length for a duration of time.

- Waves generated by astronomical forces: tides.

- Waves generated by earthquakes or submarine landslides: Tsunamis.

- Waves generated by moving objects.

Wind generated waves are of main concern. In reality, waves are very irregular, especially wind waves. Even so, they can be seen as a superposition of many simple and regular harmonic wave components, each with its own amplitude, length, period or frequency and direction of propagation. Such a concept can be very handy in many applications which allow one to predict very complex irregular behaviour in terms of much simpler theory of regular waves (Journée & Massie, 2001).

3.1.1　Regular waves

Regular waves are characterised with same periodic form in each cycle. Through linearized boundary conditions, linear wave theory results in regular waves with sinusoidal shape.

The surface profile of the sinusoidal-shape wave can be expressed in cosine or sine function of both the position x and the time t:

$$\zeta = \zeta_a \cos(kx - \omega t) \qquad (3\text{-}1)$$

In which:

ζ_a, wave amplitude

ω, circular wave frequency

k, wave number
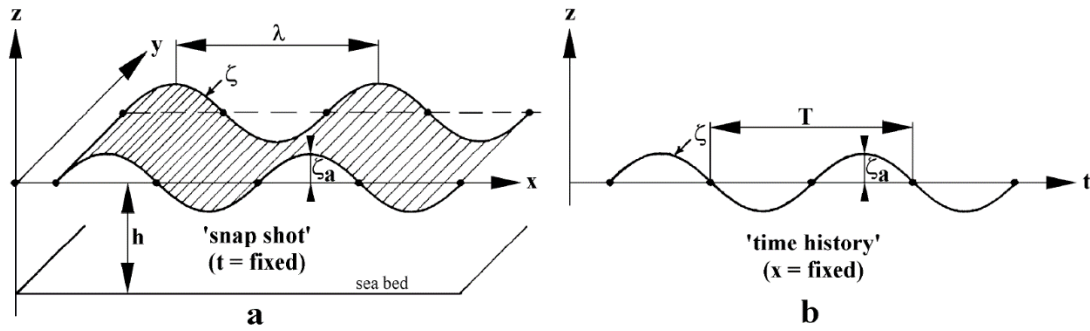
Figure 3.1 Regular wave definitions (Journée & Massie, 2001)

3.1.2   Irregular Waves

The equation (3-1) describes a regular sinusoidal wave with amplitude ζ_a which propagates in the positive x-direction. Since irregular waves can be seen as superposition of a series of sinusoidal waves, the wave elevation of long crested irregular sea can be written as a large number of regular wave components:

$$\zeta(t) = \sum_{n=1}^{N} \zeta_{a_n} \cos(k_n x - \omega_n t + \epsilon_n) \tag{3-2}$$

In which, for each component n:

ζ_{a_n}, wave amplitude component

ω_n, circular frequency component

k_n, wave number component

ϵ_n, random phase angle component

In order to investigate how the energy in the sea is distributed on the various frequencies, wave spectrum $S_\zeta(\omega_n)$ is introduced and related to wave elevation as below:

$$S_\zeta(\omega_n) \cdot \Delta\omega = \sum_{\omega_n}^{\omega_n + \Delta\omega} \frac{1}{2}\zeta_{a_n}^2(\omega) \tag{3-3}$$

Where, $\Delta\omega$ is a constant difference between two successive frequencies. By letting $\omega \rightarrow 0$, the definition of the wave energy spectrum becomes:

$$S_\zeta(\omega_n) \cdot d\omega = \frac{1}{2}\zeta_{a_n}^2 \tag{3-4}$$

Figure 3.2 gives a graphical interpretation of the relation between the wave energy spectrum and the time history wave elevation record.
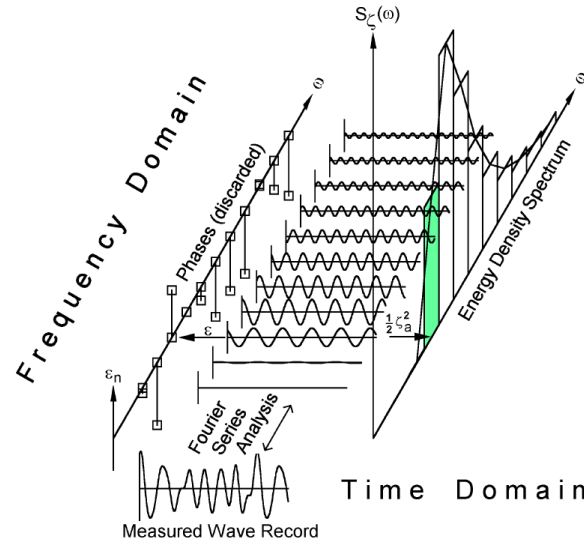
Figure 3.2 Wave energy spectrum (Journée & Massie, 2001)

Then, the variance σ_ζ^2 of the water surface elevation can be expressed as:

$$\sigma_\zeta^2 = \int_0^\infty S_\zeta(\omega) \cdot d\omega \tag{3-5}$$

3.2 Wave spectrum and directional spreading

The sea state can be described as random process presented as a spectrum S(ω) as explained, based on the following assumptions:

- The wave surface elevation process is stationary in a short term, i.e. the mean value and variance will be constant in a short time interval.

- The wave elevation is Gaussian distributed with a mean value of zero and a variance of σ^2.

- The process is ergodic, i.e. a single time series is representative of the whole process.

From long periods of observations, various wave spectra have been constructed to reflect these wave data. These spectra can then, by adding the correct parameters, reproduce a sea state for the user to deploy in his calculations. Many models have been developed, dependent on location varied measurements and different input parameters. Pierson-Moskowitz (PM) spectrum and JONSWAP spectrum are frequently applied for wind seas.

3.2.1 Pierson-Moskowitz spectrum and JONSWAP spectrum

The Pierson-Moskowitz spectrum was developed for fully developed seas generated by local winds in the Northern Atlantic Ocean.

The Pierson-Moskowitz (PM) spectrum $S_{PM}(\omega)$ is given by,

$$S_{PM}(\omega) = \frac{5}{16} H_S^2 \omega_p^4 \, \omega^{-5} \exp\left(-\frac{5}{4}\left(\frac{\omega}{\omega_p}\right)^{-4}\right) \tag{3-6}$$

Where, $\omega_p = 2\pi/T_P$ is the angular spectral peak frequency.

The JONSWAP (Joint North Sea Wave Project) spectrum was the result of a multinational measuring project from the south-eastern parts of the North Sea. The JONSWAP spectrum is formulated as a modification of the Pierson-Moskowitz wave spectrum for a developing sea state in a fetch limited situation (DNV, 2011a).

Then, the JONSWAP $S_J(\omega)$ spectrum can be expressed as below,

$$S_J(\omega) = A_\gamma S_{PM}(\omega) \gamma^{\exp\left(-0.5\left(\frac{\omega-\omega_p}{\sigma\omega_p}\right)^2\right)}$$

(3-7)

Where

$S_{PM}(\omega)$, Pierson-Moskowitz spectrum

γ, non-dimensional peak shape parameter

σ, spectral width parameter

$\sigma = \sigma_a$, for $\omega \leq \omega_p$

$\sigma = \sigma_b$, for $\omega \geq \omega_p$

$A_\gamma = 1 - 0.287 \ln(\gamma)$, a normalizing factor
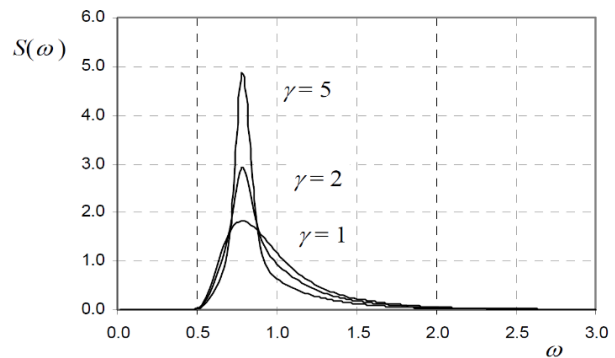
Figure 3.3 JONSWAP spectrum for γ=1, γ=2 and γ=5 [6]

Average values for the JONSWAP experiment data are $\gamma = 3.3$, $\sigma_a = 0.07$ and $\sigma_b = 0.09$. The peak shape parameter typically varies between 1 and 7, and for $\gamma = 1$ the JONSWAP spectrum reduces to the Pierson-Moskowitz spectrum.
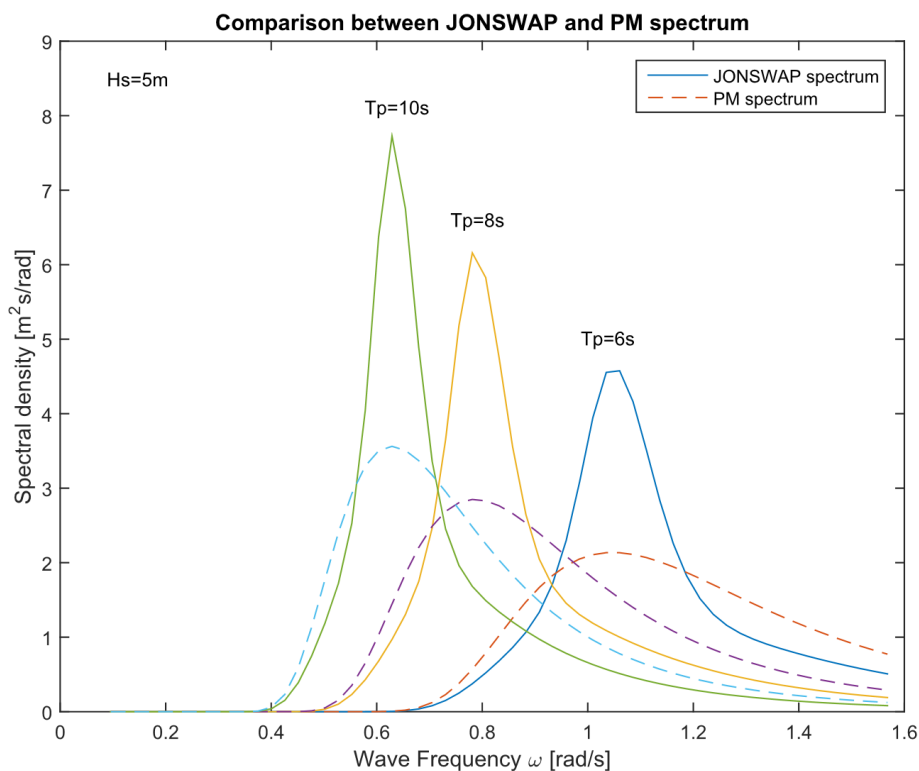
Figure 3.4 JONSWAP (γ=3.3) versus PM spectrum for different peak periods

13

The JOSWAP spectrum is expected to be a reasonable model in the following interval and should be used with care outside this range.

$$3.6 < T_p/\sqrt{H_s} < 5 \tag{3-8}$$

3.2.2   Torsethaugen spectrum

In the sea state of combined wind sea and swell which is not uncommon in Norwegian sea, a two-peak spectrum like Torsethaugen spectrum will be the right one to apply. The Torsethaugen spectrum is basically summing up of two JONSWAP spectrums one of which represents a wind-dominated sea state and the other represents the swell-dominated sea state.

$$S(\omega) = S_{wind\ sea}(\omega) + S_{swell}(\omega) \tag{3-9}$$

Wind sea and swell are assumed to be uncorrelated and in general they will travel in different directions. The complete build-up of this spectrum is quite complex and this study will be carried out based on the two wind sea spectrums, PM spectrum and JONSWAP spectrum.

3.2.3   Directional spreading

So far, unidirectional wave energy spectra have been considered. These spectra describe an ideal condition where one assumes waves to travel in the same direction with parallel wave crests, which are referred to as long crested waves. In reality, the wave energy spectrum derived from a record of surface elevations for a particular point will invariably consist of contributions from several different wave directions. It can result from varied wind directions, influence of coastlines and uneven bottom topography.

Directional short crested wave spectra $S(\omega, \theta)$ may be expressed in terms of the unidirectional wave spectra (DNV, 2011a),

$$S(\omega, \theta) = S(\omega) \cdot D(\theta) \tag{3-10}$$

Here, $D(\theta)$ is a directional spreading function. θ is the angle between the direction of elementary wave trains and the main wave direction of the short-crested wave system. The total energy in the spectrum will however remain unchanged and the directional spreading function fulfils the requirement:

$$\int_0^{2\pi} D(\theta)\, d\theta = 1 \tag{3-11}$$

Then, for a two-peak spectrum expressed as a sum of a swell component and a wind-sea component, the total directional frequency spectrum $S(\omega, \theta)$ can be expressed as:

$$S(\omega, \theta) = S_{wind\ sea}(\omega) \cdot D_{wind\ sea}(\theta) + S_{swell}(\omega) \cdot D_{swell}(\theta) \tag{3-12}$$

This directional spreading factor is neither taken into consideration in this study. While, concerning vessel response which would be discussed in following sections, the spreading coefficient is not negligible. Owing to the spreading, vessel would experience some amount of "beam sea" even if it is orientated in head sea.

3.3 Response amplitude operator (RAO) of the vessel

A free-floating vessel can experience 6 degrees of freedom (DOF) movements which comprises 3 translational motions, surge, sway and heave, together with 3 rotational motions, pitch, roll and yaw, as shown in the Figure 3.5.
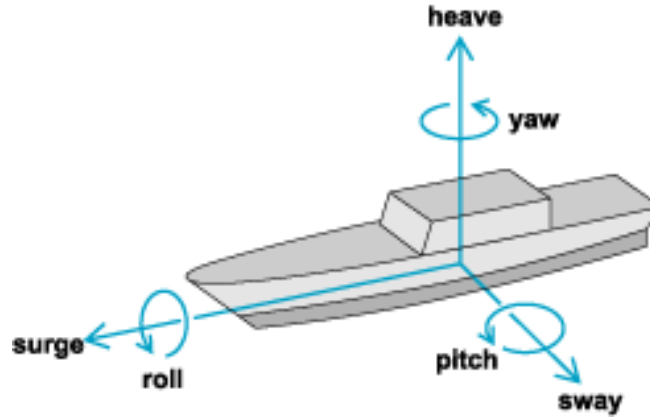
Figure 3.5 The six degrees of motions of a vessel (Gudmestad, 2015)

The response amplitude of a vessel can be normalized with respect to the amplitude of the wave, expressed in the ratio of amplitudes between vessel motion and wave elevation. For a linear system, the normalized response is invariant with the wave amplitude at a wave frequency. If a normalized response function is constructed for a range of frequencies for a given vessel, then this function is called Transfer Function, so called because it allows the transfer of the exciting waves into the response of the structure. Because of the invariance of the normalized response for a linear system, the RAO is unique (Chakrabarti, 1987).

In general, the transfer function is the ratio between the complex response amplitude and the wave amplitude. It is a function of frequency f or angular frequency ω, and it gives both the amplitude scaling and phase shift of response relative to wave component. For each degree of freedom, the function is complex and can be expressed as:

$$H_i(\omega) = A_i(\omega)\exp(i\varphi_i(\omega)) \tag{3-13}$$

Where

$H_i(\omega)$, transfer function in the i-th degree of freedom

$A_i(\omega)$, amplitude of the transfer function

ω, angular frequency of interest

$\varphi_i(\omega)$, phase angle

The absolute value of the transfer function is often referred to as the response amplitude operator (RAO), which is also a function of frequency.

$$RAO = \left|H_i(\omega)\right| = \left|A_i(\omega)\exp\left(i\varphi_i(\omega)\right)\right| \tag{3-14}$$

3.4 Combined transfer function of crane tip

As explained and shown in the Figure 3.5, the six DOF motions of a floating vessel, translations (surge, sway and heave) and rotations (roll, pitch and yaw), can be denoted as displacements (η_1, η_2 and η_3)

and rotations (η_4, η_5 and η_6). For an arbitrary point on the floating vessel with local coordinates (x_p, y_p, z_p), the motions of the point can be expressed in following equation (Faltinsen, 1990):

$$\boldsymbol{s} = (\eta_1 + z_p\eta_5 - y_p\eta_1)\boldsymbol{i} + (\eta_2 - z_p\eta_4 + x_p\eta_6)\boldsymbol{j} + (\eta_3 + y_p\eta_4 - x_p\eta_5)\boldsymbol{k} \tag{3-15}$$

Where, $\boldsymbol{i}$, $\boldsymbol{j}$ and $\boldsymbol{k}$ are the unit vectors point along the local x-, y- and z-axis respectively. To apply the equation, it is assumed that the ship hull is slender, and that the ship motions are small so that the water plane area does not change much.

It is clear that the point-motions along each of these axes are built up by the motions of three DOFs at the origin in the coordinate system. The total vertical motion of the point, such as the crane tip of our interest, is denoted by:

$$\boldsymbol{s}_v = \eta_3 + y_p\eta_4 - x_p\eta_5 \tag{3-16}$$

Besides the heave motion η_3, the vertical motion of the rigid-body point is also affected by the body roll and pitch induced at the point (x, y). More contribution from the roll and pitch part if the point is far away the body rotation centre. For the crane tip case, it can help to alleviate the vertical motion by orientating the crane boom toward mid-ship and by locating the crane tip near ship side as far as reasonable.

As clarified, the transfer function describes the relation between the harmonic excitation and its linear response and it is simply the ratio of response amplitude to wave amplitude.

$$H_i(\omega) = \frac{\eta_{i,a}}{\zeta_a} \tag{3-17}$$

Rearrange the above equation and substituting the complex expression for $H_i(\omega)$:

$$\eta_{i,a} = H_i(\omega) \cdot \zeta_a = A_i(\omega)\exp(i\varphi_i(\omega)) \cdot \zeta_a \tag{3-18}$$

Then, the total motion in vertical direction can be expressed as:

$$\begin{aligned}\boldsymbol{s}_v &= H_3(\omega) \cdot \zeta_a + y_p H_4(\omega) \cdot \zeta_a - x_p H_5(\omega) \cdot \zeta_a \\ &= \left[H_3(\omega) + y_p H_4(\omega) - x_p H_5(\omega)\right] \cdot \zeta_a \end{aligned} \tag{3-19}$$

Here, the part, $H_3(\omega) + y_p H_4(\omega) - x_p H_5(\omega)$, is the combined vertical transfer function for the specific point and it can be denoted as $H_v(\omega)$.

By summing up the complex transfer function of each DOF, $H_v(\omega)$ can be shown as:

$$\begin{aligned}H_v(\omega) &= H_3(\omega) + y_p H_4(\omega) - x_p H_5(\omega) \\ &= A_3(\omega)\exp(i\varphi_3(\omega)) + y_p \cdot A_4(\omega)\exp(i\varphi_4(\omega)) - x_p \cdot A_5(\omega)\exp(i\varphi_5(\omega)) \end{aligned} \tag{3-20}$$

3.5   Response spectrum and spectral moment

3.5.1   Response spectrum

The response spectrum is defined as the response energy density of a structure due to the input wave-energy density spectrum. Linked by the transfer function or RAO, response spectrum, like the wave spectrum, can be defined. For a linear system, the function RAO is squared and at a given frequency the square of the RAO is multiplied by the wave spectrum to evaluate the response spectrum value at that frequency. Symbolically,

$$S_R(\omega) = [RAO(\omega)]^2 S(\omega) \tag{3-21}$$

Where S_R is the response spectrum, S is the wave spectrum, and ω is the wave angular frequency.

Given the amplitude and phase angle of the transfer functions for each DOF (data from Dr. Li), together with the local coordinates of a specific point (clarified in the above section 4.2.2), the combined transfer function and further the response spectrum of the specific-position crane tip can be calculated.

$$S_{R,v}(\omega) = [H_v(\omega)]^2 S(\omega) \tag{3-22}$$

Where,

H_v, the combined vertical transfer function.

$S_{R,v}$, response spectrum resulting from the combined transfer function

3.5.2   Response spectral moment

Based on the calculated response spectrum, response spectral moment m_n of general order n can be defined as a function of the angular frequency ω:

$$m_n = \int_0^\infty \omega^n S_R(\omega)\, d\omega \tag{3-23}$$

Where, S_R is the response spectrum.

Response variance σ_R^2, equal to the zeroth response spectral moment, can be expressed as:

$$\sigma_R^2 = m_0 = \int_0^\infty S_R(\omega)\, d\omega \tag{3-24}$$

Average zero-up-crossing period for response, T_z, can be estimated by:

$$T_z = T_{R,m_{02}} = 2\pi \sqrt{\frac{m_0}{m_2}} \tag{3-25}$$

Number of response cycles in 1-hour can be shown as:

$$n_{1h} = N = \frac{3600}{T_z} \tag{3-26}$$

3.6   Limiting sea state in terms of critical crane tip motion

Since lifting operations takes place in relatively calm weather, the motions of the crane vessel can be computed from linear wave theory and the motions can be assumed to be Gaussian distributed (DNV, 2011b). For the Gaussian process, distribution of its global maxima follows Rayleigh distribution (Haver,

2016). The distribution of 1-hour global response maxima can be expressed as, by assuming the global maxima in 1-hour as a statistically independent and identically distributed.

$$F(X) = \left\{1 - exp\left\{-\frac{1}{2}\left(\frac{X}{\sigma}\right)^2\right\}\right\}^{n_{1h}}$$

(3-27)

Where, standard deviation of the response, σ, is the only parameter.

Concerning one critical response parameter, e.g. vertical motion of crane tip Z_{lim}, the probability of exceeding the limiting value during 1-hour sea sate can be shown as,

$$P[Z_{1h} > Z_{lim}] = 1 - \left\{1 - exp\left\{-\frac{1}{2}\left(\frac{Z_{lim}}{\sigma}\right)^2\right\}\right\}^N$$

(3-28)

The probability of exceedance is a measurement of the risk taken for the marine operation. Low probability of exceedance is preferred for relatively safe operation. In reality, the allowable probability of exceedance (acceptance criteria) depends on the cost and consequences due to the failure.

Given an acceptance criterion, q_{1h}, the marine operation can only be carried out on the premise of satisfying the blow equation,

$$1 - \left\{1 - exp\left\{-\frac{1}{2}\left(\frac{X}{\sigma}\right)^2\right\}\right\}^N \leq q_{1h}$$

(3-29)

After transformations of the above equation,

$$\sigma \leq \frac{Z_{lim}}{\sqrt{-2\ln[1 - (1 - q_{1h})^{1/N}]}}$$

(3-30)

Hence, the limiting sea state in parameters of H_s and T_p, can be written as,

$$\sigma_{z,lim}(H_s, T_p) = \frac{Z_{lim}}{\sqrt{-2\ln[1 - (1 - q_{1h})^{1/N}]}}$$

(3-31)

4 Frequency domain analysis

Based on the linear wave theory and linear response process (Haver, 2007), wave induced rigid body motions of the vessel can be calculated in the frequency domain, represented by response spectrum and spectral moment. The vertical motion of the crane tip is thus obtained, which is used as the limiting parameter to predict the limiting sea states based on probabilistic acceptance criteria.

RAO	Response spectrum	Limiting sea state
• the HLV • the crane tip	• Crane tip position 1 • Crane tip position 2	• Direction of wave propagation • wave spectrum • Crane tip postion
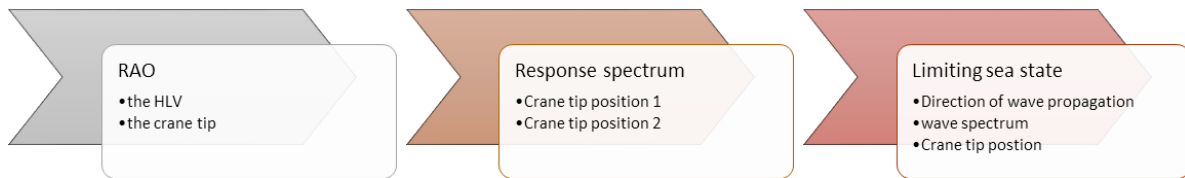
Figure 4.1 Workflow of the analysis in the frequency domain

4.1 Response amplitude operator (RAO) of the vessel

Based on the forgoing theory, investigation can continue and go into calculations, with transfer functions of the HLV from Dr. Li. In the given file, titled in System Description File, the motion amplitudes and phases of the first order motion transfer functions, corresponding to various directions in certain frequency range, are included. All motions in the system description file are referred to the coordinate system in which the origin is set to be in still water level and at mid-ship.

Vessel RAO can be simply plotted in MATLAB by importing data from the system description file and getting the absolute value of the complex transfer functions. Further calculation following the theory part can be carried out by coding in MATLAB and consequently the plotting. Relevant MATLAB codes are attached in the Appendix.

The frequency ranges in the file cover [0.0959, 1.568] in rad/s, which correspond to the periods [4, 60] in second. Wave directions in the given file cover 180 degrees from following sea to heading sea. Based on the fact that vessel bow would often be orientated against the apparent wave direction to reduce vessel motions in operation, only the wave heading between 180 and 90 degrees are to be taken into consideration in following study.

Table 4-1 Direction of incoming waves and its designation

Figure 4.2 Definition of wave heading direction (Xu, 2016)

Direction of the incoming wave	Designation
0^0	Idir1
15^0	Idir2
30^0	Idir3
45^0	Idir4
60^0	Idir5
75^0	Idir6
90^0	Idir7
105^0	Idir8
120^0	Idir9
135^0	Idir10
150^0	Idir11
165^0	Idir12
180^0	Idir13

4.1.1   Results and discussion

For heave motion of the vessel, it can be seen from Figure 4.3 that the largest response amplitude operator (RAO) occurs in idir7 (90-degree, beam sea). Value of the RAOs decreases with rising wave direction up to idir13 (180-degree, head sea). The RAO of vessel roll (Figure 4.4) generally follows the same trend as the vessel heave that the value reduces with increasing wave direction. Moreover, it is obvious that the RAO is peaked at the frequency around 0.5 rad/s. Furthermore, significant difference can be found among the peaks resulting from varied wave directions and the values approach zero with heading sea. Regarding the RAO of vessel pitch (Figure 4.5), it is obvious that the values are much smaller in the beam sea (idir7) and the peak occur in idir9 (120-degree).

In short, the minimum values occur in head sea (180-degree incoming wave direction) for both heave and roll. While, concerning pitch, the minimum value of RAO occurs in idir7 (beam sea). Hence, it is kind of interesting to investigate which wave direction would prevail in the RAO of the crane tip which results from the motion combination among the heave, the roll and the pitch.
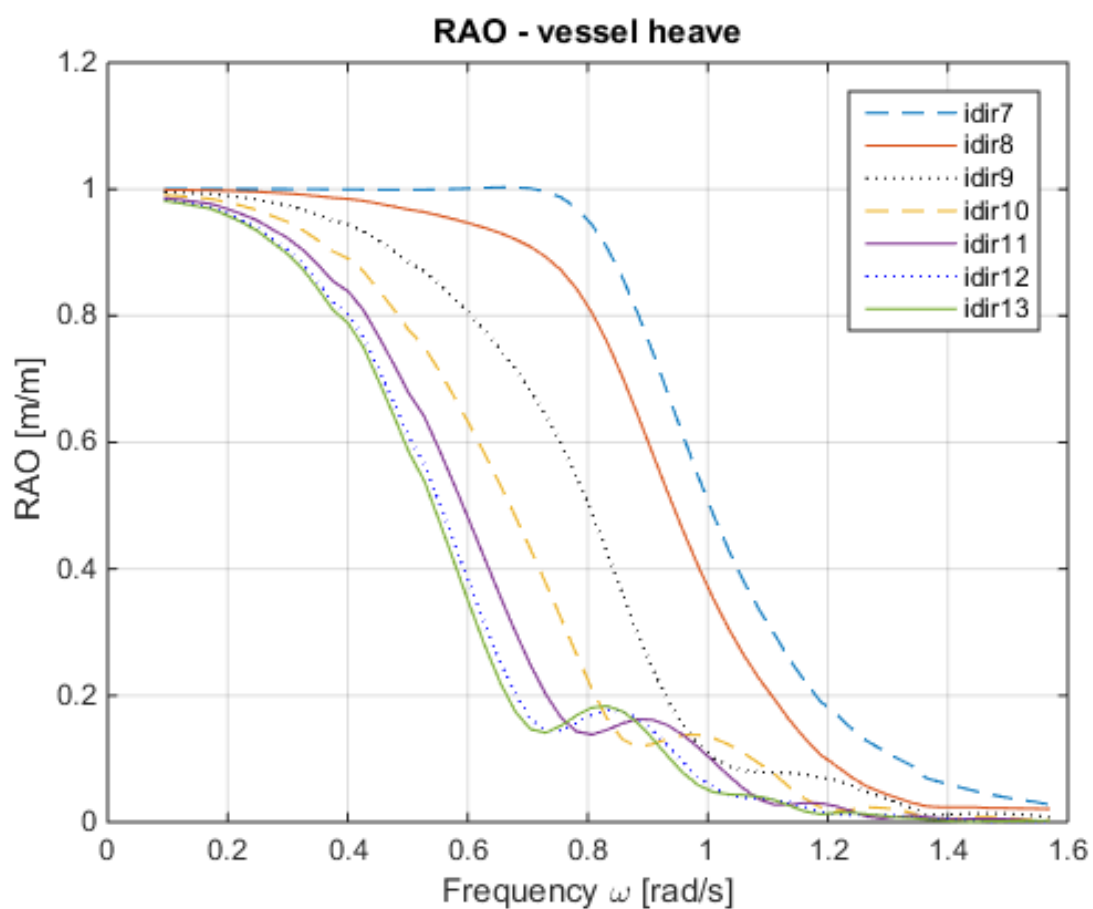
Figure 4.3 Response amplitude operator of vessel heave
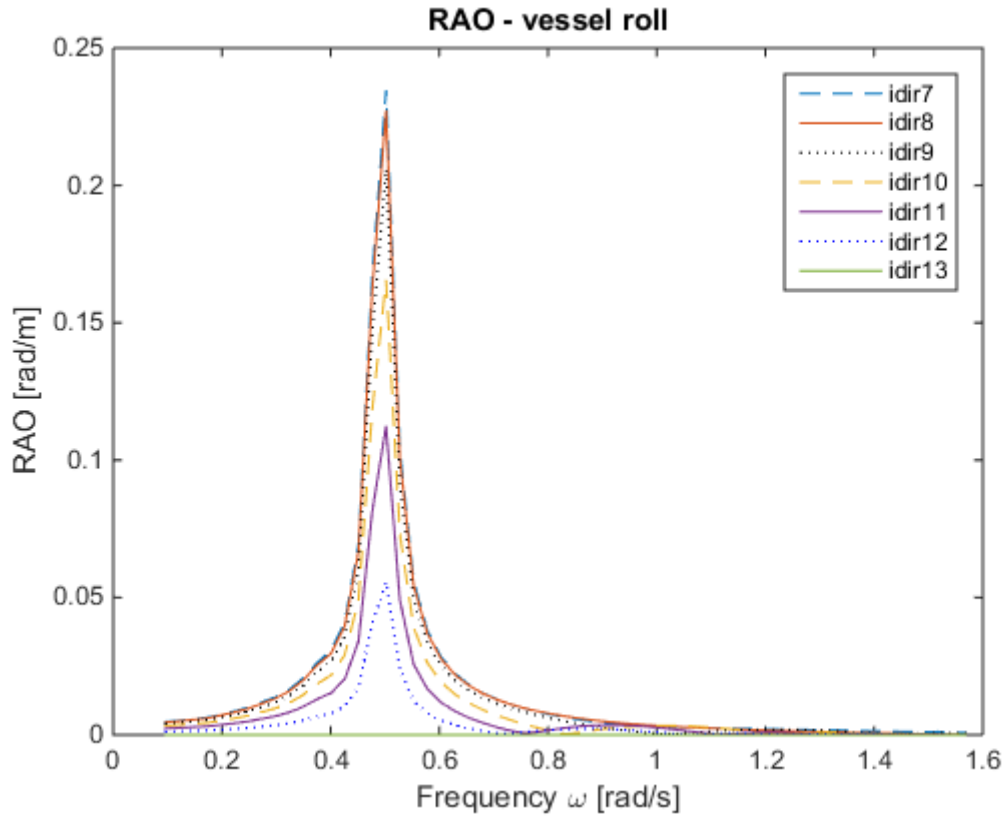
Figure 4.4 Response amplitude operator of vessel roll
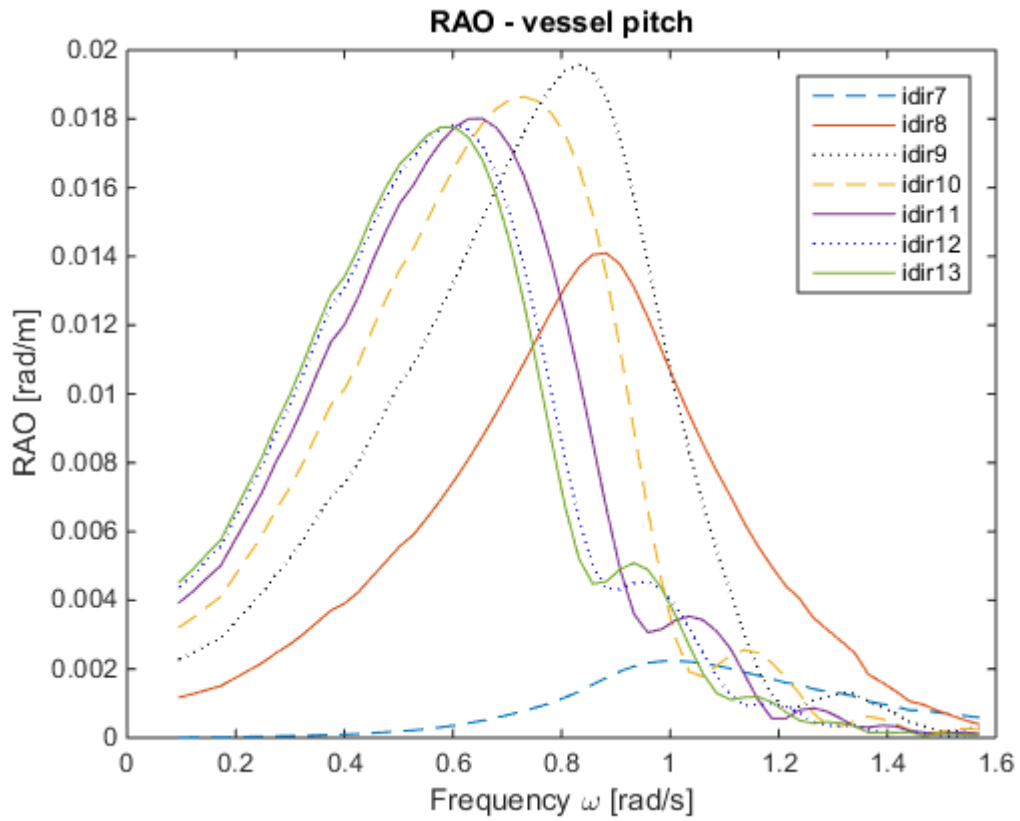
Figure 4.5 Response amplitude operator of vessel pitch

4.2   RAO of crane tip

Vertical motion of crane tip as the critical response parameter is of interest. The vessel motions which can contribute to the vertical displacement of the crane tip, including heave, roll and pitch as explained, are of our concern. Consequently, the RAO for the vertical motion of crane tip can be calculated and plotted by use of MATLAB.

Due to the reason that the combined vertical motion of certain point is related to its coordinates, another crane-tip-location is assumed (-10.5, 53.5, 88) as a comparison to the determined point-position (-81.7, 53.5, 88). The assumed position is closer to mid-ship and pitch motion would be theoretically alleviated to some degree.

Table 4-2 Coordinates of the crane tip during installation

	X	Y	Z
Crane Tip (decided position)	-81.7	53.5	88
Crane Tip (assumed position)	-10.5	53.5	88

4.2.1   Results and discussion

It is clear from the following figures that, for both the crane tip positions, the RAO values are peaked at around the same frequency as the vessel roll. For both crane tip positions, the lowest RAO occur in the wave direction idir13 (head sea). Meanwhile, the difference resulting from the varying crane tip positions, is not obvious except that the largest value for the assumed crane tip position (Figure 4.6) is a bit smaller than the counterpart in Figure 4.7 (determined position, further away from mid-ship).
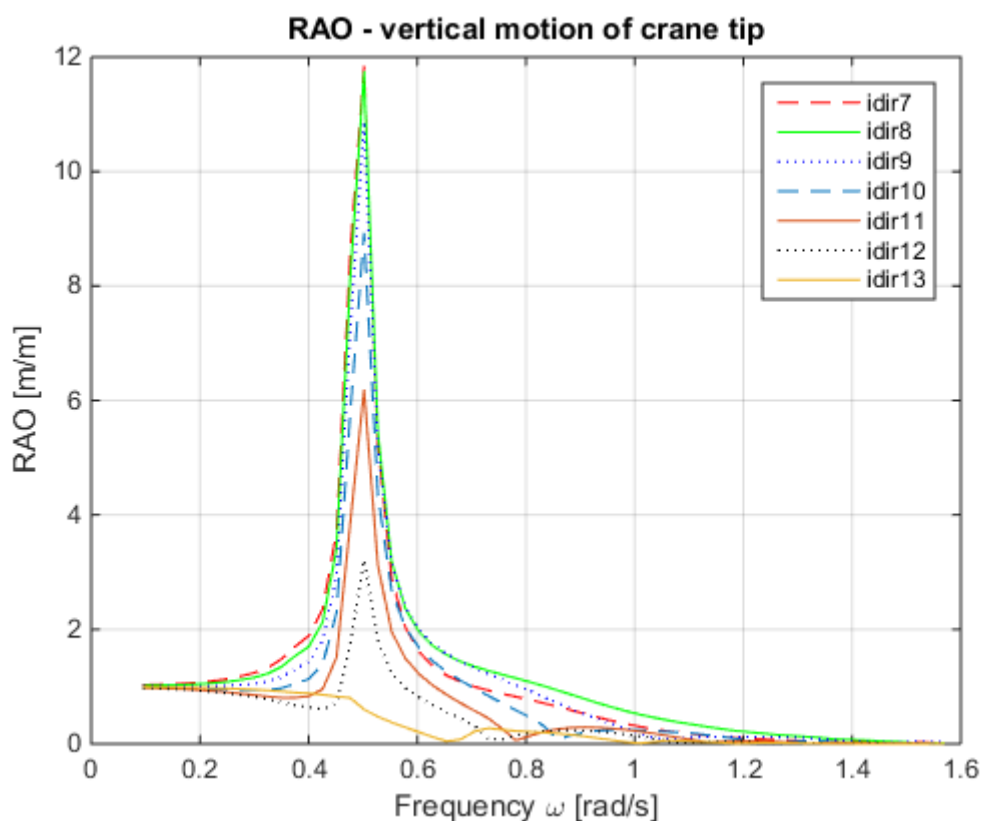
Figure 4.6 RAO for vertical motion of crane tip (assumed position)
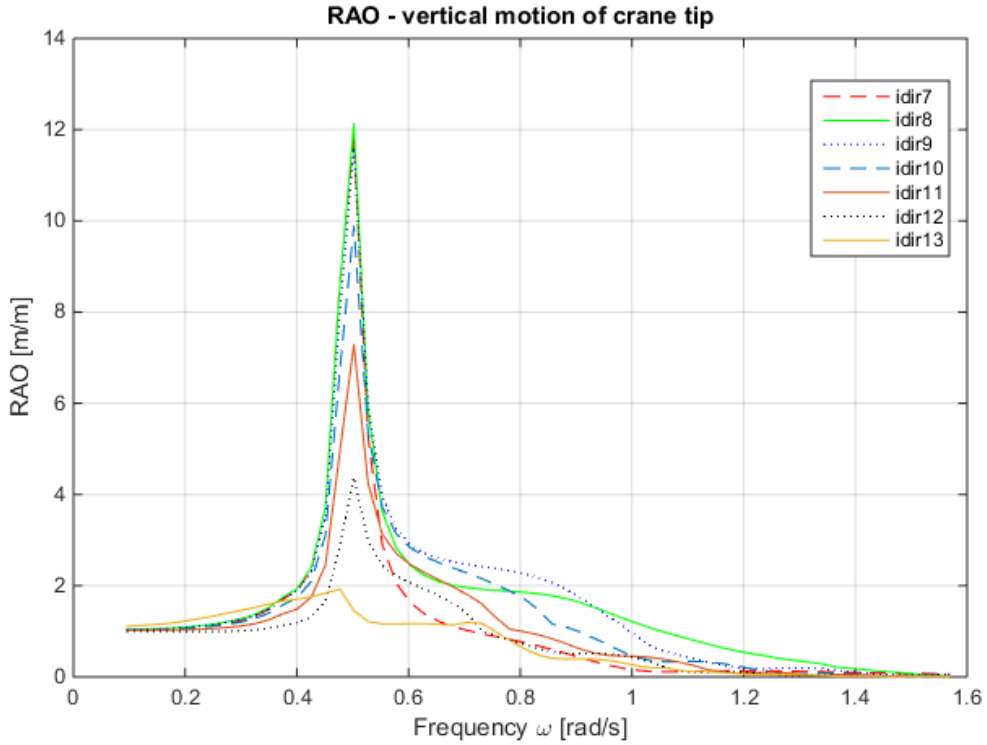
Figure 4.7 RAO for vertical motion of crane tip (decided position)

4.3 Response spectrum

It is necessary to define the key parameters of the wave spectrum before the calculation can proceed further. Now that the installation site is in North Sea area, it is reasonable to apply JONSWAP spectrum. Referring to the scatter diagram Table 2-5, the following wave conditions, with relatively high probability, are chosen for the study.

Table 4-3 Typical wave conditions

	Case 1	Case2	Case3
H_s [m]	1.25	1.25	2.5
T_p [s]	6	12	6

As clarified, for wave spectrum, the parameter T_p corresponds to the spectral peak frequency f_P with inverse relation to each other. With different T_p, the shape of wave spectrum is supposed to shift following the peak frequency, as shown in the Figure 3.4. By comparison between Case 1 and Case 2, it is anticipated to find out the influence from the varying Tp. In same logic, the influence from different Hs is investigated by studying the case 1 and case 3.

4.3.1 Results and discussion

Huge difference can be found due to the varied crane-tip position in the Figure 4.8, peak value of response spectrum for the determined position is significantly larger than the peak at the assumed position which is much closer to mid-ship. It does demonstrate that it helps a lot to mitigate the

23

response by locating the crane tip toward mid-ship during installation as far as reasonable. The largest peaks of the response spectra occur at the frequency around 0.9 rad/s which is not exactly in line with the 6s-T_p (corresponding to the angular frequency of 1.05 rad/s) and even further away from the peak frequency for the RAO of the vertical motion of crane tip (0.5 rad/s as in Figure 4.6 and Figure 4.7 in Case 1 ($H_s = 2.5\ m$).
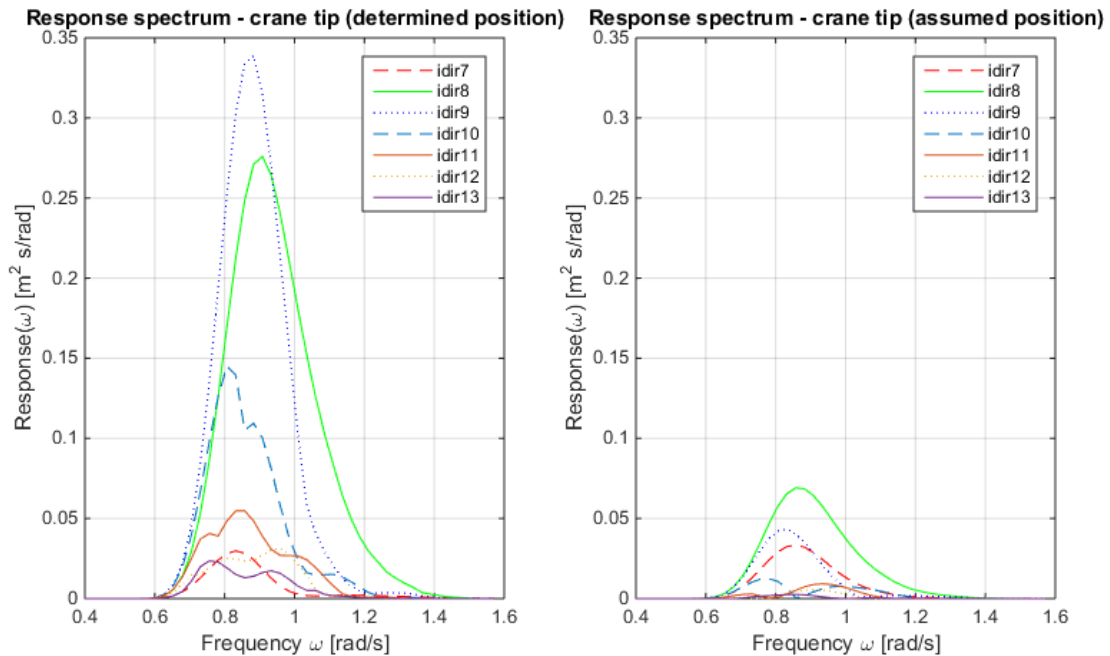
Figure 4.8 Response spectrum of crane tip (Hs=1.25m and Tp=6s)
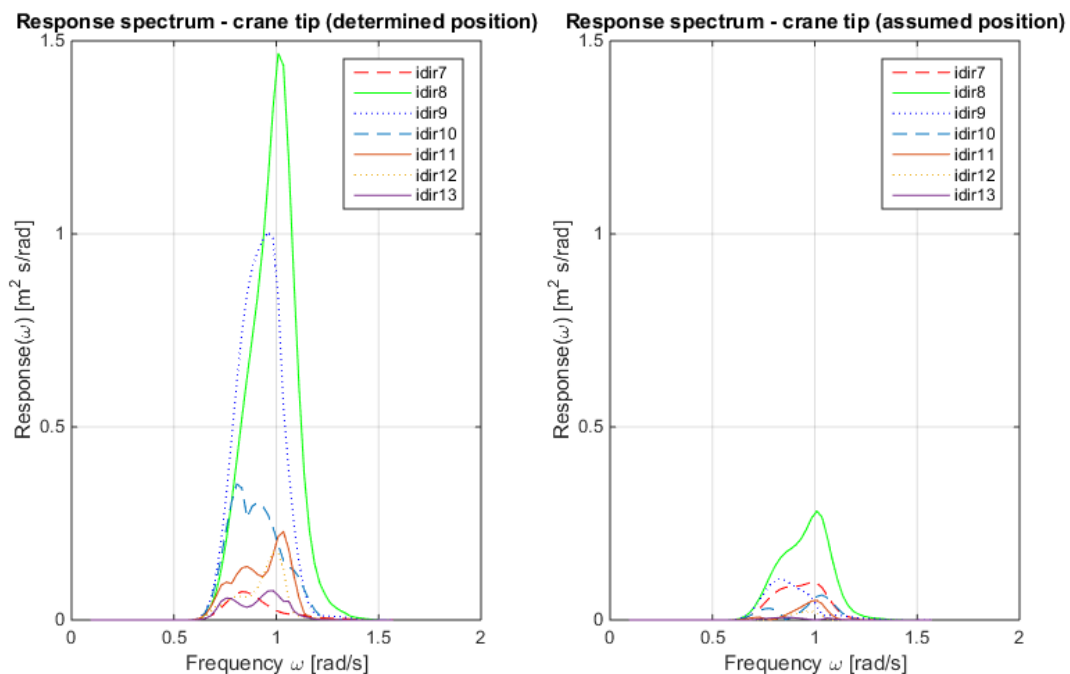
Figure 4.9 Response spectrum of crane tip (Hs=2.5m and Tp=6s)

For the Case 3 with $H_s = 2.5\ m$, as shown in the Figure 4.9, huge difference between the two crane tip positions is as obvious as the case 1. Moreover, the peak values are scaled up many times compared

to the values in Case 1. In addition, the peak frequency (1rad/s) of the highest response (idir8) almost coincide with the input peak period (corresponding to the circular frequency of 1.05 rad/s) now.

While, for the Case 2 with 12s spectral peak period, the corresponding peak frequency in JONSWAP spectrum would be 0.5 rad/s, same as the peak frequency of the RAO of the crane tip motion. In this case, reading from the Figure 4.10, the difference because of the varied position is relatively minor and both the peak values are extremely high due to the resonance effect. The fact that the wave frequency (period) is close to the peak frequency of the RAO of the crane-tip vertical motion (dependent on natural frequency of vessel roll), is deemed as resonant condition which can induce extremely high motions regardless of the crane-tip position.
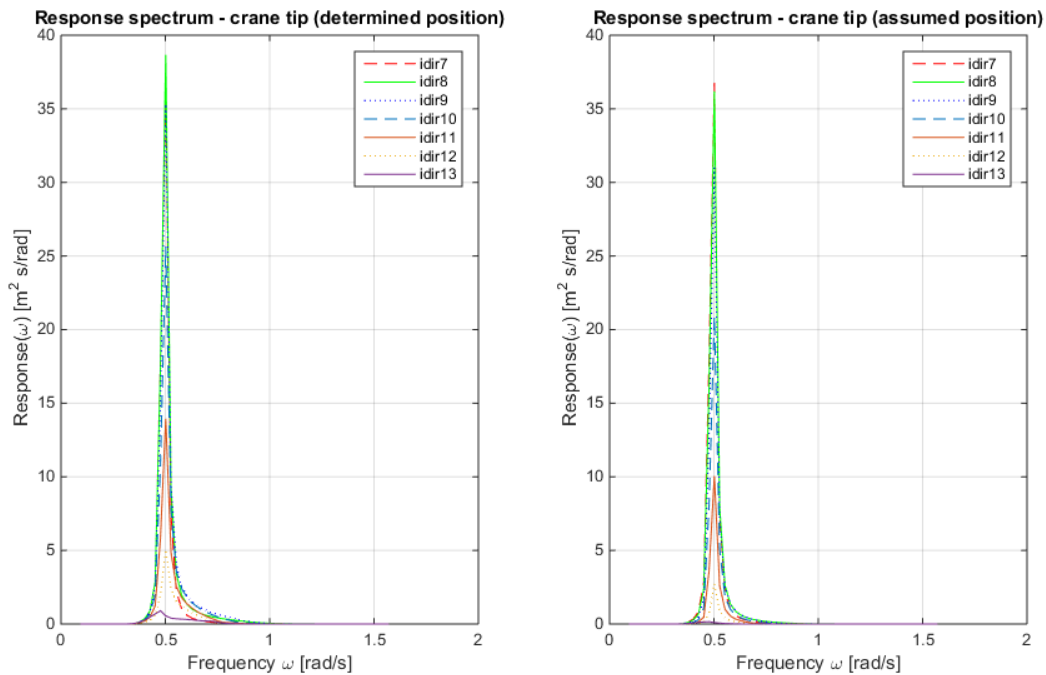
Figure 4.10 Response spectrum of crane tip (Hs=1.25m and Tp=12s)

4.4 Limiting sea state based on the critical crane tip motion

Based on the theories, limiting sea state can be determined and plotted in MATLAB through iteration, by increasing the significant height H_s (for a given T_p) until the limiting standard deviation $\sigma_{z,lim}$ exceeded.

The critical response parameter and acceptance criteria (q_{1h}, probability of exceedance) shall first be clarified. In this study, critical response parameter is the vertical motion of crane tip Z_{lim} which shall be no more than 0.3m as clarified in Section 2.2.2. Acceptance criteria is assumed to be 0.05.

Table 4-4 Critical parameters

Limiting value of crane tip motion Z_lim [m]	0.3
Allowable probability of exceedance q_1h	0.05

In addition, as verified and explained, the HLV shall be orientated toward the apparent wave direction during installation. Now, limiting sea state for the determined crane tip position, in heading sea, can be calculated and plotted.

4.4.1   Results and discussion

Reading from the Figure 4.11, extremely larger significant wave heights can be tolerated with reducing peak period, e.g. almost 16m H_s allowable for waves with 4s spectral peak period, which seems too positive to believe.
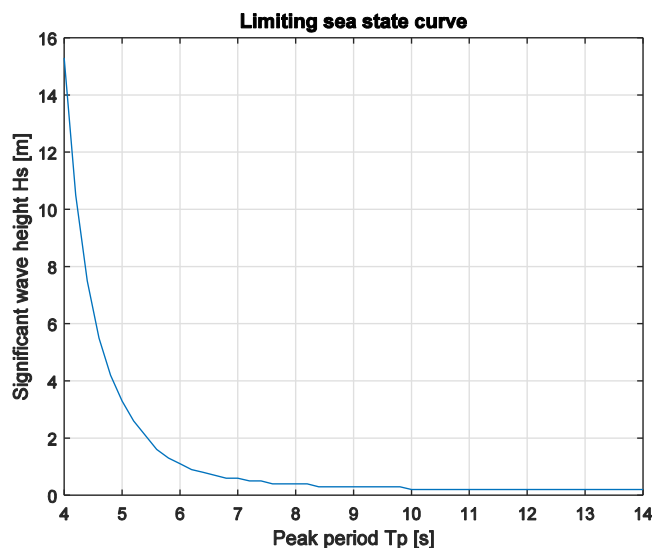
Figure 4.11 Limiting sea state curve in idir13

As clarified in the beginning of this chapter, the frequency ranges in the study cover [0.0959, 1.568] in rad/s, which correspond to the periods [4, 60] in second. In this case, the JONSWAP spectra is not fully covered and has more deficiency in the wave conditions with lower T_p (larger angular frequency), as shown in the Figure 4.12. For the case with 4s peak period (corresponding to 1.6 rad/s peak frequency), around half of the wave spectrum is lost. The partial absence of the wave spectrum will induce smaller value for the zeroth response spectral moment, which leads to underestimate of the response standard deviation. While, the insufficiency is much less and relatively tolerable with larger T_p, e.g. 6s as shown in the Figure 4.12, owing to the high concentration around the peak period in JONSWAP spectrum.
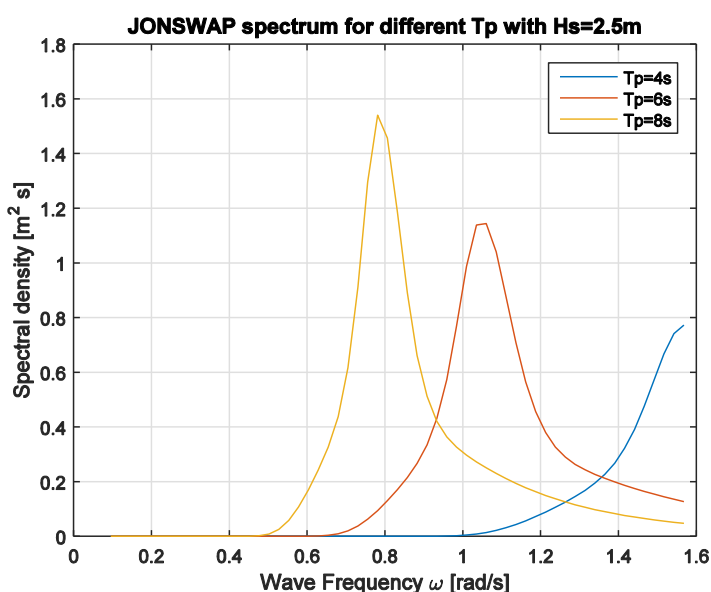
Figure 4.12 JONSWAP spectrum in the chosen frequency range

According to the hindcast data referring to the scatter diagram in Table 2-5, there is no so critical waves at all, with so high H_s but low T_p.

In addition, operational requirement of the vessel as clarified in Section 2.2.2, shall be taken into consideration. Even though the calculated limiting sea state for larger peak periods are reasonable enough, it shall never be more than 2.5m according to the operational requirements of the vessel. Thus, the curve would be capped, as shown in the Figure 4.13.
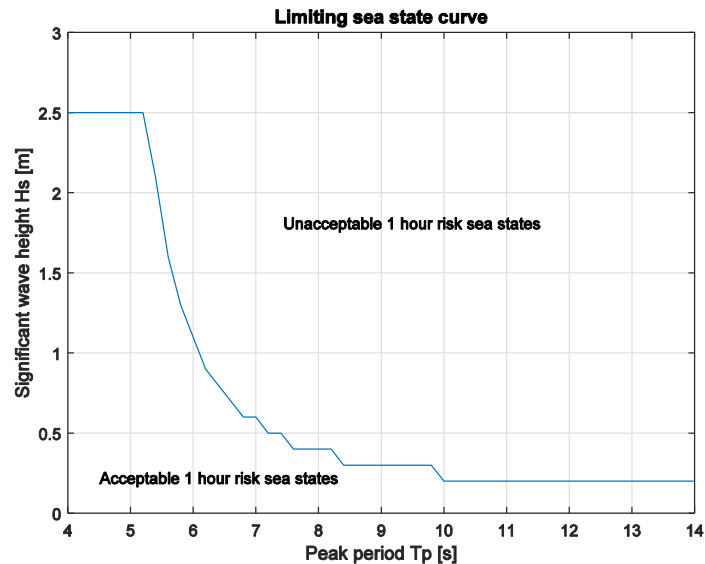
Figure 4.13 Limiting sea state curve in idir13 capped by operational requirements
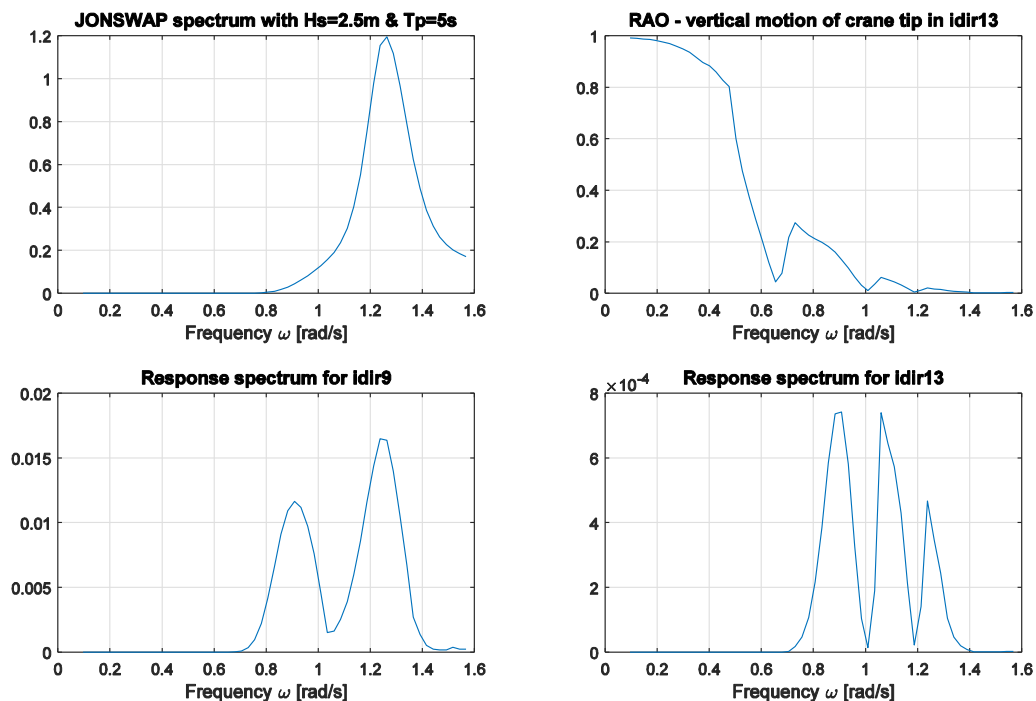
Figure 4.14 Wave and response spectrum with Tp=5s and Hs=2.5m

As we can see from the Figure 4.13, for the sea state with 5s peak period, it is still acceptable to operate with up to 2.5m H_s in heading sea (idir13). But how about in other directions of wave

27

propagation, e.g. idir9. It seems really negative by preliminary judgement from the Figure 4.14 since the peak of the response spectrum in idir9 is about dozen times larger than the case in idir13.

4.4.2   Sensitivity studies

To have a thorough understanding of the influence from different parameters like direction of coming waves, wave spectrum and crane tip position, case studies are planned on each parameter.

Table 4-5 Case study concerning varied parameters

Case1		Case2		Case3	
Direction of wave propagation		Wave spectrum		Crane tip position	
idir13 (180 degree)	idir9 (120 degree)	**JONSWAP**	PM	**(-81.7, 53.5,88)**	(-10.5, 53.5,88)

Note: the parameters in bold are the default input for all the cases.

For the Case 1, it is clear from the Figure 4.15 that the limiting sea state curve in idir9 (in red) is lower than the curve for idir13, which signifies that milder sea states are required in idir9 due to much more volatile vessel response in this direction of wave propagation. The influences are so obvious that the allowable H_s lowers down from around 1m to about 0.3m for the waves with T_p equal to 6s. This is another solid proof of the importance to orientate vessel toward the primary wave direction.
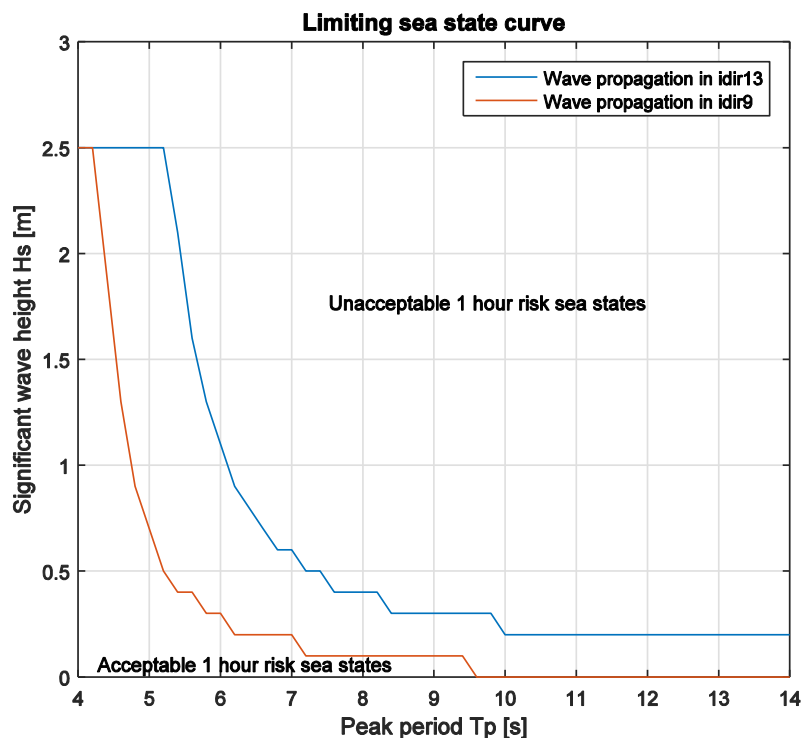
Figure 4.15 Limiting sea states in different wave directions – Case1

In the second case, the deviation between the two curves is minor and the two curves seem tangling together. Theoretically, around the peak period of 12s corresponding to the resonance frequency (0.5rad/s, discussed earlier), the area of the response spectrum (response variance) in the chosen limited frequency range would be larger for JONSWAP owing to its peak shape. While, in the lower peak periods, the spectrum projected area or the response variance for the JONSWAP spectrum should be smaller than the counterpart of PM spectrum because its peak shape will leave thinner tail in the peak frequency range of the crane-tip-motion RAO. In short, compared to the PM spectrum, the

response standard deviation in JONSWAP spectrum is supposed to be smaller in lower peak periods and larger following the increasing peak periods. Hence, the trend for JONSWAP in the Figure 4.16, higher curve in the lower periods and lower curve on the right side, agrees with the above theoretical deduction as milder sea state is required for bigger standard deviation of the response and vice versa.
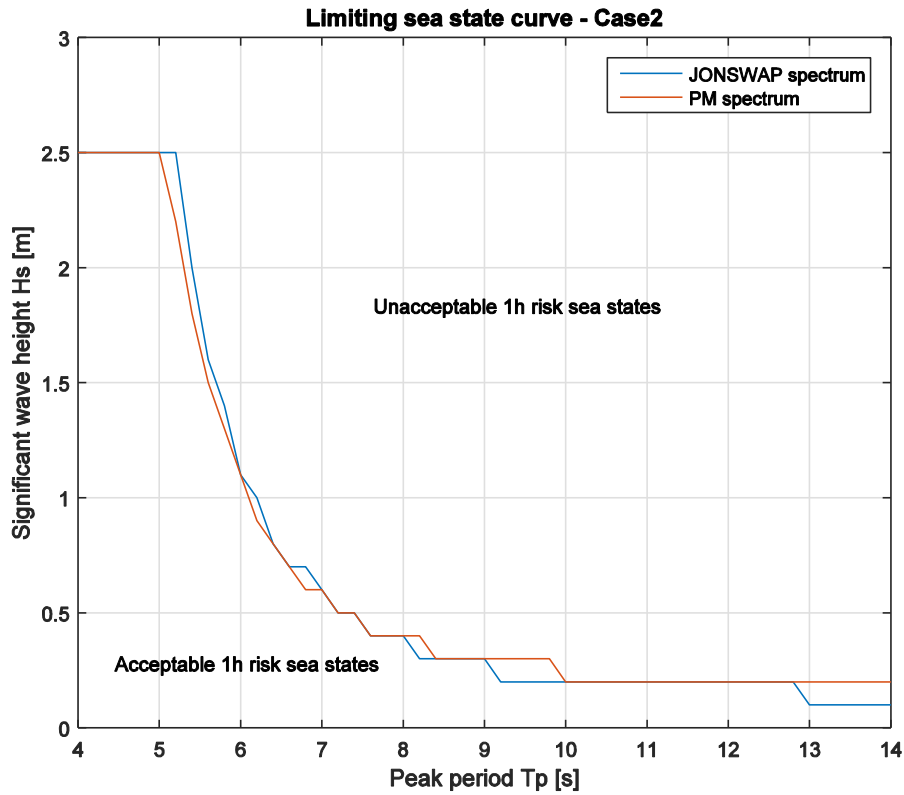
Figure 4.16 Limiting sea states in different wave spectra – Case2
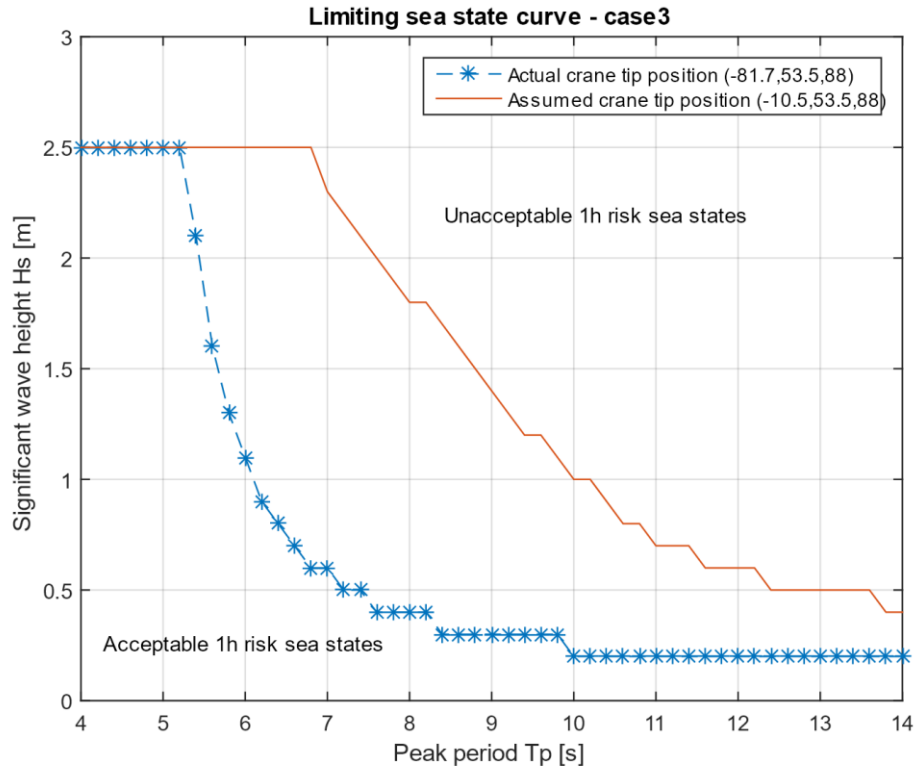
Figure 4.17 Limiting sea states in different crane tip positions – Case3

For the Case 3, it is strikingly clear from the Figure 4.17 that much more severe sea states can be tolerated with the assumed crane tip position during installation. It echoes the previous analysis and conclusion that it helps a lot to mitigate the motion response by orientating the crane tip toward mid ship as far as reasonable. In this study, the assumed position is impossible to reach due to limited working radius of the heave lifting crane. Considering the bulk size of the tripod foundation, it is not feasible to rotate and locate the crane tip closer to mid-ship, but the comparison-analysis verifies empirical assumption and performs as a good guideline for future similar marine operation.

5 Numerical modelling of the lifting system

Numerical modelling and simulation are to be carried out using the software SIMA SIMO from the company MARINTEC (MARINTEK, 2016a) (MARINTEK, 2016b). Lifting operation can be divided into several phases, lift-off, hanging in the air, lowering through splash zone and consequently deeply submerged until landing on seabed. This thesis study would cover all the phases except the landing, among which more attention is paid to the lowering process including the splash zone crossing. Moreover, numerical modelling and simulation for the lift-off operation would also conducted, taking into consideration the potential snap load or re-hit during the operation. To thoroughly investigate this critical lifting phase, two cases would be studied, lift-off from its own deck and lift-off from a barge.

5.1 General set up of the lifting system

The basic system comprises of two rigid bodies, a floating vessel and a tripod foundation. On the deck of the vessel, a rigidly connected crane has been modelled. Then, the two rigid bodies can be linked by lift wire which extends from a winch on the crane column to the top of the tripod via the crane tip. The lift wire is also considered to be rigidly connected to the lift point on the tripod.

Besides the wire coupling, a fender coupling will also be involved between the tripod and the HLV for onboard lift-off, or coupled with the transport barge for the case lift-off from barge.
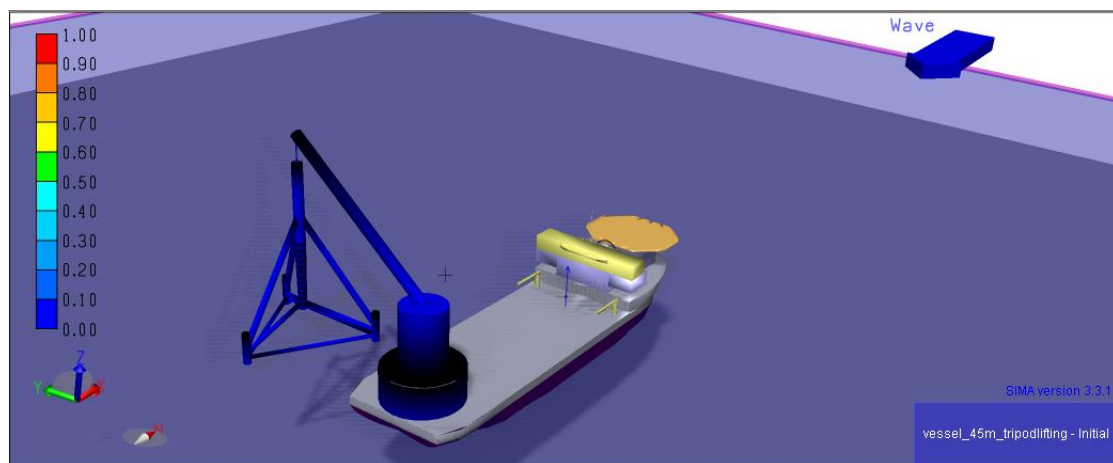
Figure 5.1 Numerical model for the simulation of the lowering process
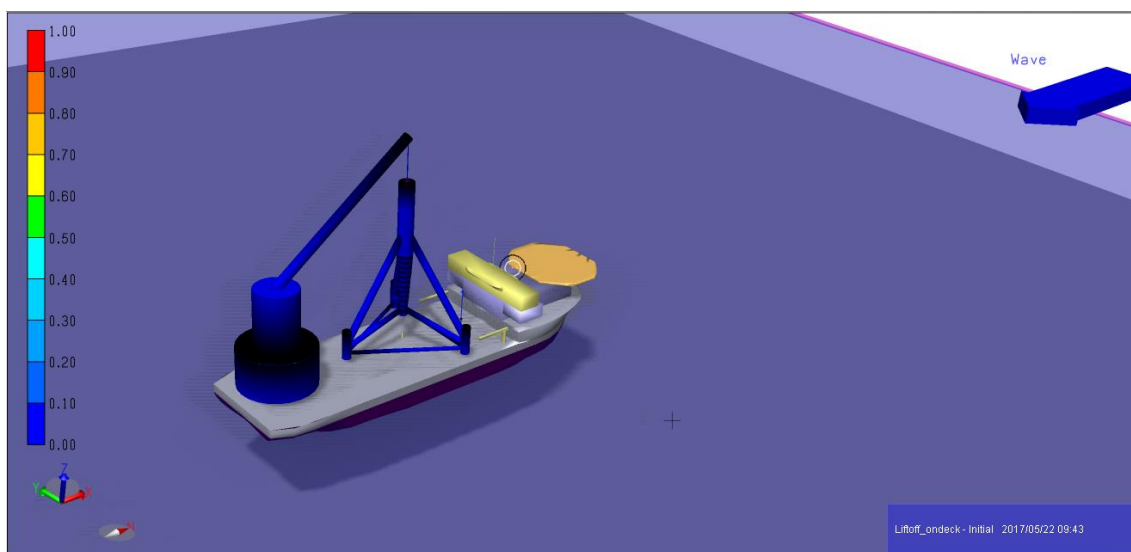
Figure 5.2 Numerical model for the simulation of onboard lift-off

31
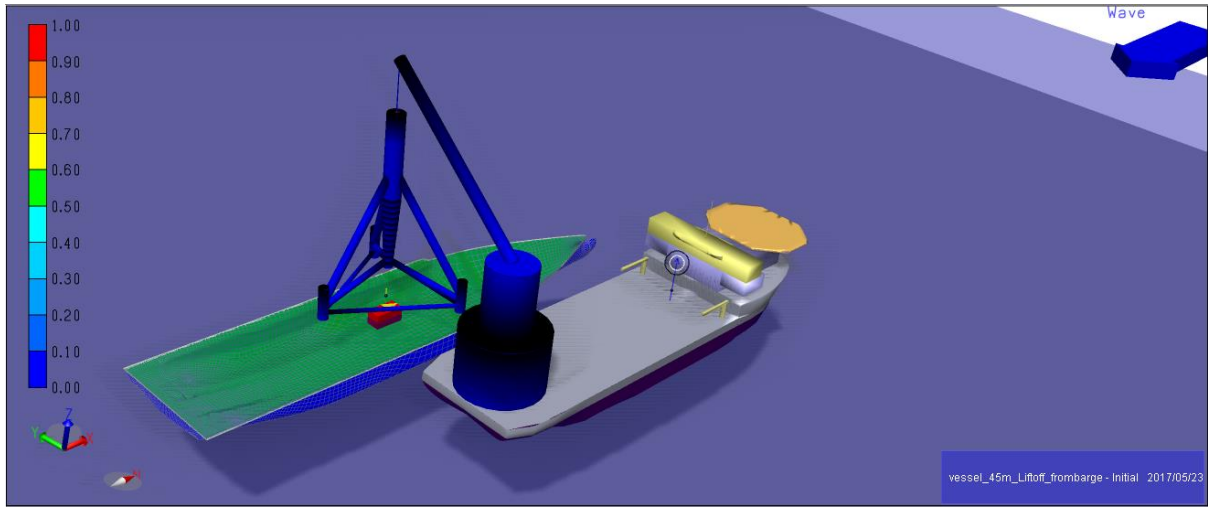
Figure 5.3 Numerical model for the simulation of lift-off from transport barge

The global coordinate system is a right-handed coordinate system with the X-axis pointing towards the bow, the Y-axis towards the port side and the Z-axis pointing upwards. The origin is located on the ship's centreline at the cross of the midship section and the sea water level (draft line) during the lifting operation.

5.2   Modelling and input

5.2.1   Numerical model of the heavy lift vessel (HLV)

Corresponding to the motion transfer functions used in frequency domain analysis, numerical model of the heavy lift vessel was received from Dr. Li. In the numerical model, information including but not limiting to, stress and damping coefficients, the first order motion and wave force transfer functions, is included.
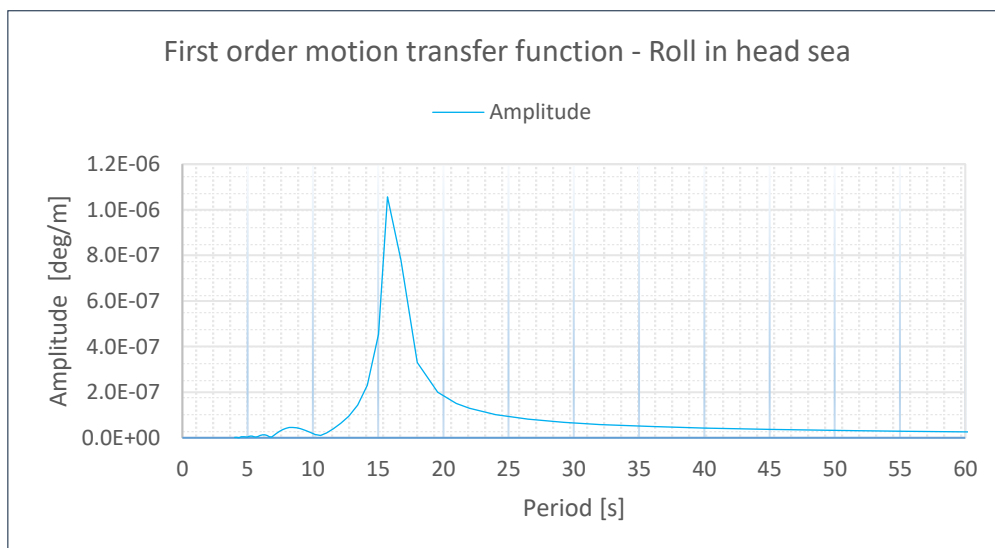
Figure 5.4 First order motion transfer function of roll in head sea (from SIMA)

32
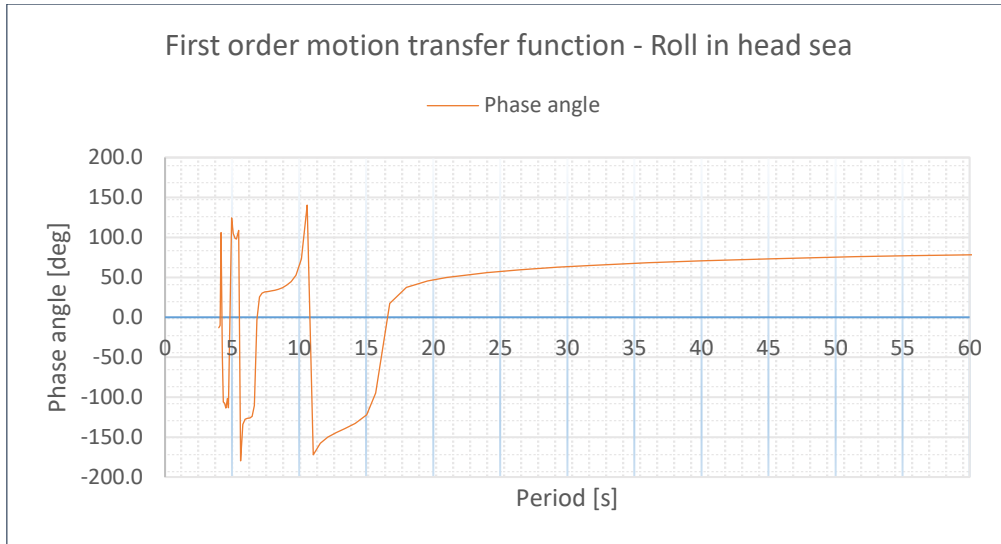
Figure 5.5 First order motion transfer function of roll in head sea (from SIMA)

Following simplifications are applied for the current vessel force model:

1) Waves are considered as main factor excluding any influence from wind or current

2) Mooring line systems of the HLV are simplified by using linear stiffness terms in surge, sway and yaw.

In practice, water ballasting is supposed to be carried out to counter the overturning moment from the lifted tripod. For simplicity, specified moment is introduced in the numerical model of lowering process to alleviate the huge roll motion. For the case lift-off from barge, time dependent ballasting is applied, corresponding to the time duration of the specific lift-off.

5.2.2   Modelling of the tripod foundation

Prior to the application of the Morison's formula, it shall be verified whether the member structures of the tripod foundation can be treated as slender element or not. For slender bodies with a ratio between diameter and wave length less than 0.2, the empirical Morison's equation is often used to calculate hydrodynamic forces (Morison, et al., 1950).

For the site No. 15 with 45m water depth, wave length can be calculated in terms of wave spectral peak periods T_p, following the equation (5-11). According to the 10-year scatter diagram at the installation site, wave conditions with T_p in the range of $3s - 15s$ are relatively common.

$$\lambda = \frac{g}{2\pi} T^2 \tanh \frac{2\pi}{\lambda} h \qquad (5\text{-}1)$$

Table 5-1 Calculated wave length

Wave period	T (s)	3	4	5	6	7	8	9	10	11	12	13	14	15
Wave length	λ (m)	14.1	25.0	39.0	56.2	76.4	99.3	123.9	149.2	174.6	199.8	224.5	248.8	272.8

Based on the largest diameter of the member structure – the upper part of the central column (5.7m), the limiting wave length can be calculated.

$$\lambda_{\text{limiting}} = 5D_{largest} = 5 \times 5.7 = 28.5 \, m \qquad (5\text{-}2)$$

33
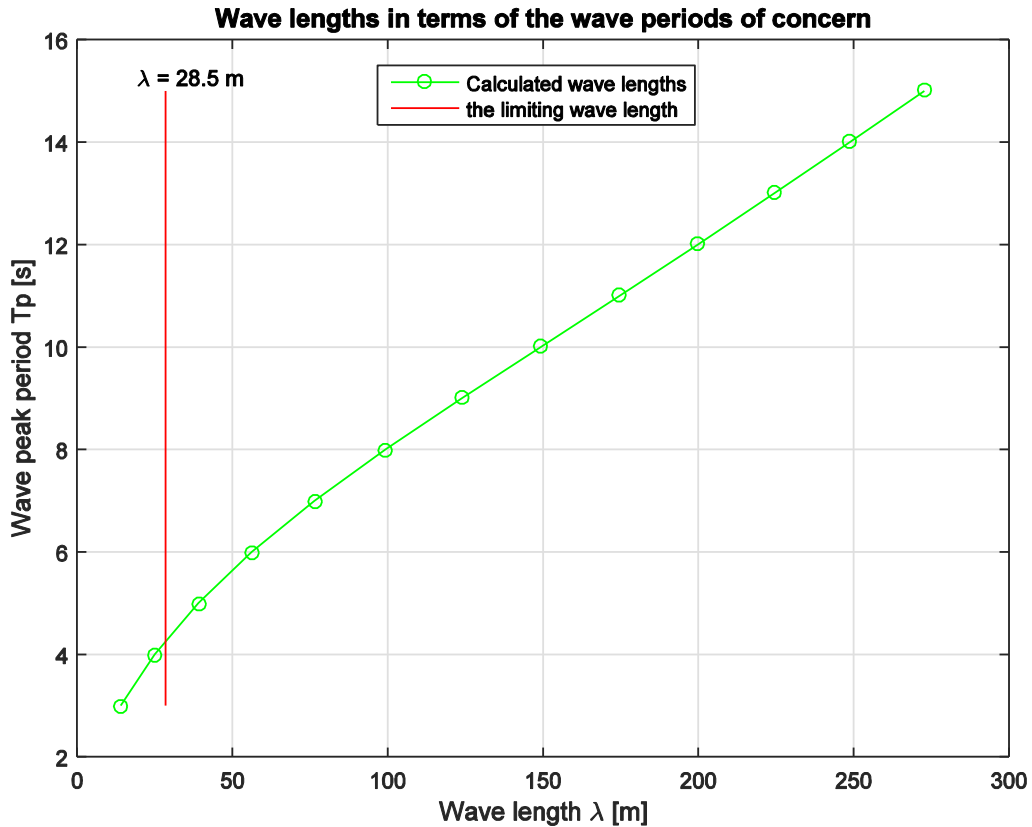
Figure 5.6 Calculated wave length in terms of spectral wave periods

As can be seen from the figure, the foundation structure can be treated as slender elements for roughly all the T_p concerned, even based on the most critical structure-dimensioning. Specifically, the wave peak periods between 5s and 12s can be perfectly covered by the slender body approximation based on the Morison formula.

5.2.3 Mechanical couplings

In the numerical model, the lift wire which links the crane and the tripod is modelled as a simple wire coupling. The simple wire coupling is modelled as a linear spring according to (MARINTEK, 2016a):

$$T = k \cdot \Delta l \tag{5-3}$$

Where T is the wire tension, K is effective axial stiffness and the Δl is the wire elongation. The effective axial stiffness, K, is given by:

$$\frac{1}{k} = \frac{l}{EA} \times \frac{1}{k_0} \tag{5-4}$$

Where E is the modulus of elasticity, A is the cross-section area, l is the unstretched wire length and the k_0 is crane flexibility. Material damping is set to be 2% of the EA value (MARINTEK, 2016a).

Table 5-2 Properties of the lift wire

Lift wire properties		
Flexibility [m/N]	Damping [Ns]	EA [N]
2.00E-09	1.58E+08	7.91E+09

34

Fender is a contact element between the tripod and the vessel on which the tripod is seated. It can give a compressive force normal to the defined sliding plane (freeboard deck of the vessel). In the model, the fender force acts upwards to counter the weight of the tripod. The friction coefficients are chosen based on the empirical data between steel and steel. The shear stiffness is decided on the assumption that the deformation due to the shear is within reasonable range.

Table 5-3 Characteristics of the fender coupling

Characteristics of the fender plate			
Dynamic friction coefficient	Static friction coefficient	Shear stiffness [N/m]	Damping exponent
0.42	0.78	4.68E+07	1.00

The compressive normal force is found by interpolation, from a specified relation between distance and force and from the specified internal damping (MARINTEK, 2016a). Linear interpolation is applied for the relationship between the distance and the normal force. It is assumed as reasonable to set the internal damping as 2% of the equivalent stiffness in normal direction.

Table 5-4 Cross section characteristics of the fendering coupling

Cross section characteristics			
Cross sections	Vertical distance [m]	Force [N]	Damping [Ns/m]
1	0.00	0	0
2	-0.03	1.00E+06	2.00E+04
3	-0.05	3.00E+06	6.00E+04

5.2.4   Hydrodynamic coefficients

For slender bodies with the ratio between diameter and wave length less than 0.2, Morison's load formula can be used to calculate the hydrodynamic forces. In the slender body approximation, effects of diffraction and radiation are considered insignificant. The main contribution of the wave force is normal to the axis of the slender members since tangential drag force is small compared to the normal drag force for bare cylinders (DNV, 2011a).

Morrison's load formula of the normal force, for moving structure in waves, can be applied,

$$f_N(t) = -\rho C_A A \ddot{r} + \rho C_M A \dot{v} + \frac{1}{2}\rho C_D D (v - \dot{r})|v - \dot{r}| \tag{5-5}$$

Where,

v and $\dot{v}$ are fluid particle velocity and acceleration respectively

$\dot{r}$ and $\ddot{r}$ are the sectional velocity and acceleration of the moving structure

D and A are the diameter and cross-section area of structure section

C_M, C_A and C_D are the mass, added mass and drag force coefficients respectively

The first term on the right of the equation is the inertial term resulting from radiation force of the moving body. The second term is the wave excitation force consisting of diffraction and Froude-Krylov

35

force. The last term is the quadratic drag term due to viscous damping (Li, et al., 2014). C_A and C_D are dependent on many parameters such as the Reynolds number (Re), the Keulegan- Carpenter number (K_C) and the surface roughness ratio (Δ).

$$C_D = C_D(R_e, K_C, \Delta) \qquad (5\text{-}6)$$

$$C_A = C_A(R_e, K_C, \Delta) \qquad (5\text{-}7)$$

Outer surface of the newly fabricated foundation can be assumed to be smooth. With Re in the magnitude of 10^6, combined with a small Kc number, the quadratic drag coefficient can be chosen as $C_D = 0.7$ (Li, et al., 2014). For cylinders in unbounded fluid with a small K_C, C_A can be assumed to be independent of K_C number and equal to the theoretical value $C_A = 1.0$ for both smooth and rough cylinders (DNV, 2011a).

While, the tripod is made of bottomless tube structures with diameters in the order of meters. Following the lowering process, the bottomless hollow structure members will be, in practice, flushed with sea water after the wave crossing. The water inside the hollow structure affects the hydrodynamic coefficients and excitation force on the structure members, meanwhile the influence depends on the wall thickness and submergence of the cylinders (Mavrakos, 1988). $C_M = C_A = 1.8$ is applied for all the bottomless tube structures of the tripod, referring to the further research (Li, et al., 2014).

Table 5-5 The drag and added mass coefficients

Hydrodynamic coefficients	
C_D	C_A
0.7	1.8

Based on the decided coefficients, the hydrodynamic coefficients C_q (quadratic drag in $N \cdot s^2/m^3$) and C_a (added mass in kg/m) as required in SIMA, can consequently be calculated following the equations.

$$C_q = \frac{1}{2}\rho C_D D \qquad (5\text{-}8)$$

$$C_a = \rho C_A A \qquad (5\text{-}9)$$

However, it is impossible to model hollow structure in SIMA by use of slender element. As clarified, hydrodynamic influence from the trapped water inside the bottomless-hollow structure has been incorporated in the selected added mass coefficient. Hence, reasonable hydrodynamic force can be guaranteed in the actual model with solid slender element, by use of the correct input from the above equations.

While, in terms of buoyancy force, now that it is impossible to build hollow structure modelling, all the tube structure members shall be modelled as solid slender element by adjusting (shrinking) its diameter based on the same distributed mass (cross-section area). For the modelling in SIMA, conversion in the dimensioning should be carried out following the equation.

$$\pi(D - t) \cdot t = \frac{\pi D_s^2}{4} \qquad (5\text{-}10)$$

Here, D and t are the original diameter and thickness of the tripod foundation while the D_s is the diameter of the slender element in SIMA.

5.3   Environmental conditions

Taking into consideration the location of the installation site, JONSWAP wave spectrum, characterised by significant wave height H_s and peak period T_p, is applied to represent the irregular wave condition of the real sea state. Following the analysis in the frequency domain, the HLV is to be orientated heading against the wave during the lifting operation - head sea with 180-degree wave propagation. Other than the wave, influence from swell, current or wind are not considered.

Referring to the calculated limiting sea states in the frequency domain as plotted in the Figure 4.17, some typical sea states with spectral peak period (T_p) in integer value, are collected. To cross check the validity of the calculation results, stationary simulations in SIMA under the calculated limiting sea states, are to be run. Case study based on the position of the tripod is to be carried out, hanging in air (13m above the sea level) and partly submerged (at the draft of 40m).

Table 5-6 Predicted limiting sea states using frequency domain method

	Calculated limiting sea state					
T_p [s]	5	6	7	8	9	10
H_s [m]	2.5	1.1	0.6	0.4	0.3	0.2

For the time variant (nonstationary) simulations, the lowering process and the lift-off, the following environmental condition is set to be default input. Aside from the fact that the significant wave height shall be no more than 2.5m following the operational requirement of the HLV, the waves with $T_p = 7$s is of the highest probability to be encountered referring to the scatter diagram Table 2-5.

Table 5-7 Main environmental condition used in the simulations

		Critical environmental condition			
Wave only	Direction	Spectrum	Spreading code	H_s [m]	T_p [s]
EC1	180	JONSWAP	Unidirectional	2.5	7

5.4   Eigenvalue analysis

The two rigid bodies with 6 degree of freedom (DOF) each, the tripod and the vessel, experience rigid body motions. It is vital to assess the eigen periods of the rigid body motions to understand what motion modes are dominating in the coupled or decoupled conditions.

Eigenvalue analysis is conducted in frequency domain, excluding any external force or effect of damping. The natural periods can be obtained by solving the equation,

$$[-\omega^2(M + A) + K] \cdot x = 0 \qquad (5\text{-}11)$$

Where, M is the mass matrix of the two-body system (the vessel and the tripod) and A is the added mass matrix. K is the restoring stiffness matrix, including hydrostatic restoring and the wire coupling between the two bodies. x is a vector which contains 6 DOF (uncoupled) or 12 DOF (coupled) for different rigid body motions.

For the coupled lifting system with 12 DOF, certain modes may be dominated by coupled motions or motions from different bodies. It is more challenging to interpret why motions are coupled or excited in the coupled 12 DOF lifting system. By investigating only one body alone, it can help understand the motion mode of each body and consequently facilitate analysing of the coupled system.

5.4.1 Eigenvalue of the heavy lift vessel (HLV)

After running static simulation, eigenvalue of the heavy lift vessel can be obtained. Eigen periods of the motions in each degree of freedom (DOF) are shown in the table. The roll period of the HLV is around 15.88s (Mode 3), larger than the value of the other two DOFs which are also of our interest, the heave around 9.5s (Mode 2) and the pitch 8.42s (Mode 1).

Table 5-8 Eigen values of the HLV

Body	Mode		1	2	3	4	5	6
HLV	SURGE	[m]	-0.23	0.05	0.00	-0.01	**1.00**	-0.01
HLV	SWAY	[m]	0.00	0.00	0.13	0.75	0.01	0.80
HLV	HEAVE	[m]	-0.12	**-1.00**	0.00	0.00	0.00	0.00
HLV	ROLL	[deg]	0.00	0.00	**1.00**	-0.08	0.00	-0.05
HLV	PITCH	[deg]	**1.00**	-0.10	0.00	0.00	0.00	0.00
HLV	YAW	[deg]	0.00	0.00	-0.02	**-1.00**	0.00	**1.00**
Natural period		[s]	8.42	9.50	15.88	68.57	70.07	72.12

5.4.2 Eigenvalue of the tripod hanging from a fixed crane

By setting the body HLV as prescribed (supposed to be fixed), eigen periods of the hanging tripod (in air, 13m above sea level) can be calculated in static simulation. While, the eigen period of the tripod yaw motion is too large to be calculated in SIMO. It is fortunately not of our concern since the yaw motion can be handled by tug wire through extra winch as necessary.

Table 5-9 Eigen values of the tripod

Body	Mode		1	2	3	4	5	6
Tripod	SURGE	[m]	-0.02	-0.51	0.52	0.48	-0.47	0.00
Tripod	SWAY	[m]	0.02	-0.51	-0.51	0.48	0.47	0.00
Tripod	HEAVE	[m]	**1.00**	0.00	0.01	0.00	0.01	0.00
Tripod	*ROLL*	[deg]	*-0.05*	***1.00***	***1.00***	**1.00**	***1.00***	*0.00*
Tripod	PITCH	[deg]	-0.05	**-1.00**	**1.00**	**-1.00**	**1.00**	0.00
Tripod	YAW	[deg]	0.00	0.00	0.00	0.00	0.00	**1.00**
Natural period		[s]	0.92	2.79	2.80	15.40	15.54	***

For the hanging tripod, Mode 1 is dominated by heave motion with natural period 0.92s. Stiffness in heave is mainly from the axial stiffness of the coupling lifting wire. Combination of both rotational and translational motions can be found in other modes. At the period 2.79s and 2.80s – with exactly same roll and sway motions, the pitch and surge are almost of the same amplitude but in opposite direction. So is between the period 15.40s and 15.54s, same in roll and sway but opposite in pitch and surge. For the two pairs, the modes around 2.8s (2.79s and 2.80s) and 15.5s (15.40s and 15.54s) seem rather similar, while the difference lies in the sign (direction) between roll and sway. The combination of positive roll and negative sway leads to faster motion cycle with the periods around 2.8s while the other combination with both positive motions result in pendulum motion with longer periods at around 15.5s.

5.4.3 Eigenvalue of the coupled system

For the coupled system with 12 degrees of freedom, eigenvalue can also be obtained after the static analysis. For the case with tripod located 13m above the sea level, the calculated values are listed in the below table, with critical excursions highlighted in colours.

Table 5-10 Eigen values of the coupled system

	Mode		1	2	3	4	5	6	7	8	9	10	11	12
HLV	SURGE	[m]	0.01	0.00	0.00	0.00	0.00	0.00	0.00	-0.02	0.40	-1.00	0.84	0.00
HLV	SWAY	[m]	-0.03	-0.01	0.00	-0.03	0.01	0.00	-0.01	0.00	0.26	0.75	1.00	0.00
HLV	HEAVE	[m]	0.00	0.00	0.00	0.00	-1.00	0.00	0.00	-0.01	0.01	0.01	0.00	0.00
HLV	ROLL	[deg]	-0.23	-0.09	0.00	-0.24	0.00	0.03	0.02	-0.04	0.23	0.05	-0.11	0.00
HLV	PITCH	[deg]	-0.02	0.00	-0.02	0.00	0.04	-0.04	0.01	0.14	-0.20	0.04	0.03	0.00
HLV	YAW	[deg]	0.00	0.00	0.00	0.00	0.00	0.02	0.00	-0.04	-1.00	-0.23	0.72	0.00
Tripod	SURGE	[m]	-0.01	-0.03	0.52	-0.02	0.11	0.13	-0.20	1.00	0.08	-0.41	0.20	0.00
Tripod	SWAY	[m]	-0.05	-0.53	-0.04	0.63	-0.02	0.11	0.32	0.27	0.71	0.90	0.32	0.00
Tripod	HEAVE	[m]	1.00	-0.12	-0.03	-0.30	-0.92	-0.03	0.06	0.22	-0.16	0.11	0.00	0.00
Tripod	ROLL	[deg]	0.08	1.00	0.07	-1.00	0.00	0.68	1.00	-0.04	-0.11	0.11	0.13	0.00
Tripod	PITCH	[deg]	-0.03	-0.05	1.00	-0.05	0.63	-1.00	0.66	0.52	-0.28	0.07	0.09	0.00
Tripod	YAW	[deg]	0.00	0.00	0.00	0.00	0.00	0.00	0.00	0.03	0.06	0.01	-0.06	1.00
Natural period		[s]	0.80	2.21	2.62	4.51	9.52	12.61	14.45	19.54	44.86	67.53	75.55	5358.30

For the lower eigenvalue, 0.80s, 2.21s, 2.62s and 4.51s (Modes 1 ~ 4), tripod motions dominate while the vessel motions are minor or small. The mode 5, with eigen period 9.52s, is dominated by heave motion of the HLV since the eigen period approaches the natural period of the HLV-heave. Meanwhile, drastic heave motion on the tripod which is excited by the resonant heave motion of the HLV, together with obvious pitch motion on the tripod, can be observed in the Mode 5. In the eigen-periods 67.53s and 75.55s, the system performance is still dominated by the motions of the HLV while some translational motions on the tripod can also be found. While, for the Mode 6 and 7 with the eigen value 12.61s and 14.45s respectively, the system is again dominated by tripod motions, exactly by the motion combination between pitch and roll.

5.4.4 Eigenvalue of the coupled system at various tripod positions

The properties of the coupled system vary during the lowering process including the eigenvalue. As the simulation goes with running winch, the length of the coupling lift wire increases which changes the restoring stiffness of the coupled system. Moreover, following the lowering operation of the tripod, hydrodynamic added mass arises from wave as soon as the tripod dips into the wave splash zone and keeps changing following the continual submergence of the tripod. At every 5m interval, eigenvalue of the coupled system is calculated and collected.

Table 5-11 Eigen period of the coupled system following the position of the tripod

Z_Tripod	Wire length	Eigen period in different modes											
[m]	[m]	1	2	3	4	5	6	7	8	9	10	11	12
13.00	102.50	0.8	2.21	2.62	4.51	9.52	12.61	14.45	44.86	67.53	75.55	19.54	5358.3
8.00	107.5	0.82	2.62	3.05	5.36	9.52	11.73	14.43	31.82	65.19	73.49	67.55	2236.5
3.00	112.5	0.83	2.96	3.39	6.12	9.52	10.95	14.5	23.7	62.91	72.69	102.36	2109.3
-2.00	117.5	0.85	3.39	3.84	6.79	9.52	11.18	18.13	24.89	61.54	72.45	84.26	2228.7
-7.00	122.5	0.86	3.72	4.2	7.44	9.51	11	24.14	30.29	61.68	72.33	81.42	10482
-12.00	127.5	0.88	4.02	4.49	8.05	9.51	10.64	28.52	34.84	61.83	72.4	81	5812.8
-17.00	132.5	0.89	4.28	4.73	8.63	9.5	10.32	29.33	35.8	61.41	72.37	79.71	5746.3
-22.00	137.5	0.91	4.55	4.99	9.24	9.49	10.09	30.34	37.06	61.1	72.39	79.07	6701.2
-27.00	142.5	0.92	5.08	5.53	10.04	9.48	9.97	32.39	39.6	61.2	72.44	79.93	6448.1
-32.00	147.5	0.93	5.41	5.86	10.67	9.47	9.86	33.37	40.79	60.9	72.49	79.82	4700.7
-37.00	152.5	0.95	5.84	6.28	11.36	9.46	9.82	34.37	42.02	60.65	72.56	79.88	5128
-42.00	157.5	0.96	7.26	7.78	12.64	9.51	10.33	36.23	44.23	60.94	72.61	82.12	2571.3

Same logic as the analysis in the Sec. 5.4.3, one critical excursion or coupled excursions can be identified corresponding to each eigenmode, at certain draft. Following the lowering down of the tripod, certain trend can be figured out concerning the mode dependent critical excursions.
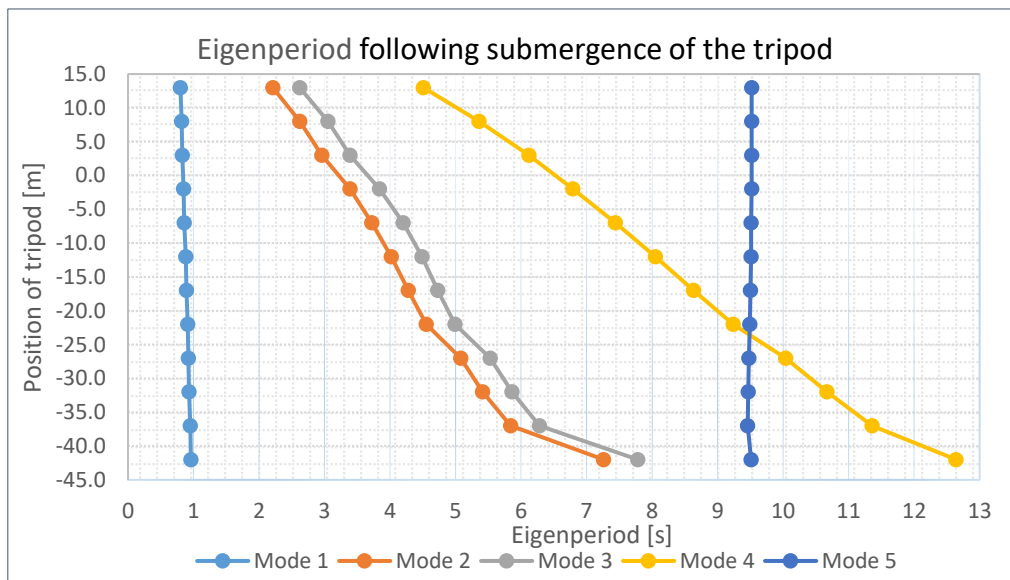
Figure 5.7 Eigenperiod with varying position of the tripod

The Modes 1 ~ 4 are dominated by tripod motions while the Mode 5 is mainly dominated by the HLV although its influence fades gradually with increasing submergence. The Mode 1 and 5 which are dominated by heave motion of the tripod and the HLV respectively, are barely affected during the lowering. The Mode 2 and 4 are both dominated by coupled motions between tripod sway and tripod roll, while relatively more roll motion from HLV will arise for Mode 4 since it approaches the HLV's natural period of roll. Similar as the Mode 2 and 4, the Mode 3 which is dominated by the coupled motions between tripod pitch and tripod surge, also depends on the submergence a lot as can be read in the figure. Furthermore, for the three Modes 2 ~ 4 which are all dominated by coupled motions of the tripod between certain translation and rotation, while the latter (rotational) motion plays more critical role.

Figure 5.8 Eigenperiod with increasing submergence of the tripod

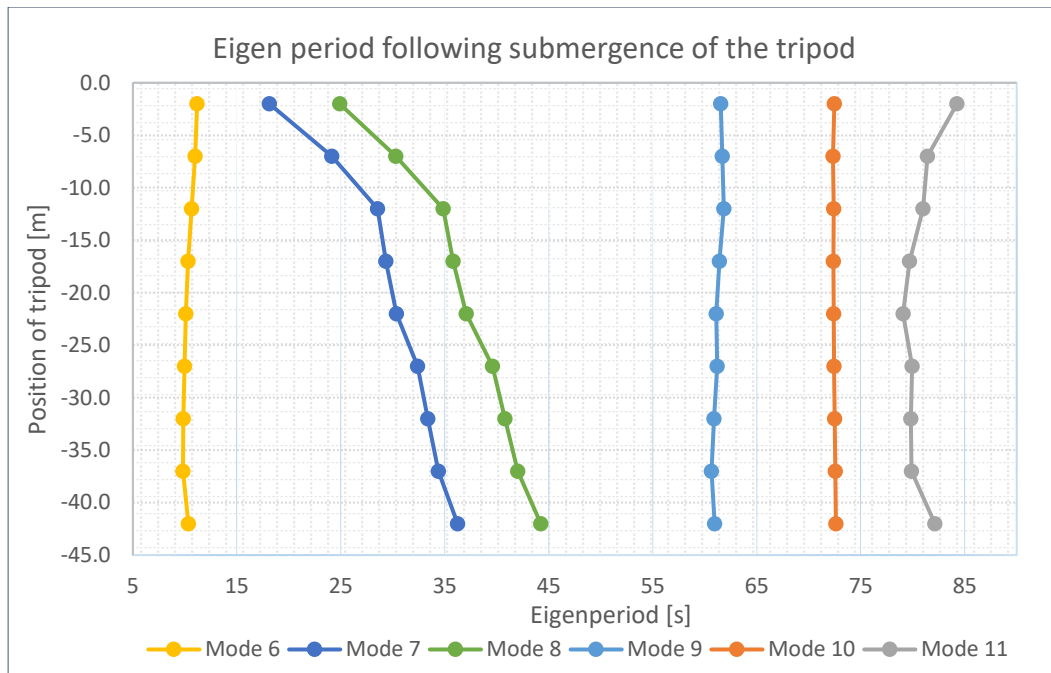For the Modes 6 ~ 8, they are still dominated by the tripod while obvious variation in eigen values can be found before and after its entry into sea, owing to the extra damping from sea water. For the remaining Modes excluding the 12th one, there are significant motion contributions from HLV involved, especially the Mode 10 since the eigen values are approaching the natural periods of certain HLV motions like sway. The Mode 12 is dominated by the yaw motion of tripod which can be easily controlled by extra pulling wire through winch as necessary. To pursue vivid trend of the eigen periods for the Modes 6 ~ 11, the data are tracked and plotted after the tripod is lowered into sea.

Referring to the 10-year scatter diagram at the installation site Table 2-5, the spectral peak period T_p is in the range from 5s to 15s, corresponding to the concerned limiting $H_s = 2.5\ m$. Hence, for the coupled system, the modes whose natural period is out of the range [5s,15s] would not be of our interest.

Now that only the modes with the eigenvalue ranged from 5s to 15s are of our concern, attention shall be paid to the Modes 2 ~ 6. Both the Mode 5 and 6 stabilize around 10s while the other 3 modes depend clearly on the changing position of the tripod. In addition, all the three mode-trajectory cover the period-range from 5s to 7s which are of high probability to be encountered according to the previously discussed scatter diagram.

5.4.4.1   Time domain simulation and analysis

The wave elevation can be in short term modelled as a stationary, zero mean Gaussian process. Then, the sea state can be represented by means of a wave spectrum, as clarified in the theory related chapter. For analysis of marine operations, the wave spectrum is normally assumed to be invariant for a period of 3 hours.

The predicted limiting sea states using frequency domain method are cross checked in time domain by running stationary simulations. Consequently, the attention is shifted to the time-varying non-stationary processes, the lowering and the lift-off. Potential critical events may occur during the processes, such as slack wire, collision with the lifting vessel due to excessive tip motion of the tripod or even re-hit between the tripod and transport barge during the lift-off.

5.5   Simulation of stationary process

Stationary simulations under the calculated limiting sea states are run at two positions, one hanging in air with 13m clearance from the sea level and the other with extended lift-wire located at 5m above the sea bed.

5.5.1   Environmental conditions and model setup

The calculated limiting sea states in frequency domain can only be treated as preliminary assessments since it is carried out based on the decoupled rigid body motion (HLV only). Besides, the wave induced motions are supposed to follow the linear response process. The calculated limiting sea states in frequency domain are to be verified in time domain through running stationary simulations under the predicted sea states.

Table 5-12 Predicted limiting sea states using frequency domain method

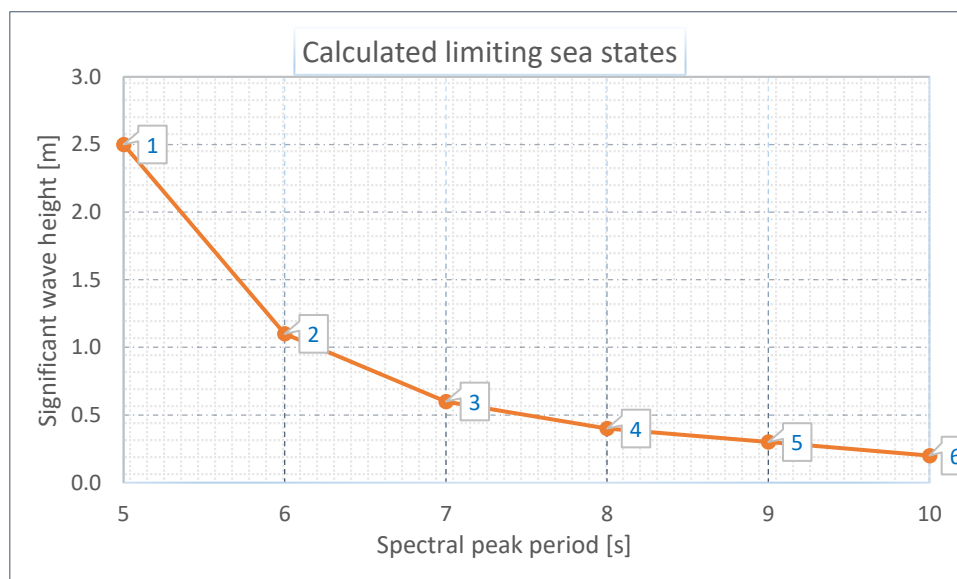|	**Calculated limiting sea states**					
	1	2	3	4	5	6
Hs [m]	2.5	1.1	0.6	0.4	0.3	0.2
T_p [s]	5	6	7	8	9	10

Figure 5.9 Predicted limiting sea states with serial number

To efficiently cover the variability of the stochastic irregular sea, 3-hour stationary simulation under the calculated limiting sea states are expected to be carried out. While, rather than continuous 3-hour simulation, 1-hour stationary running with 3 seeds, will be proceeded now that the calculation in frequency domain is based on 1-hour global response maxima.

Following the concept of rigid body motion calculation in the frequency domain, vertical motion of the crane tip can be deduced and plotted in time domain also, through combining the relevant motions of the HLV referring to the equation (3-16).
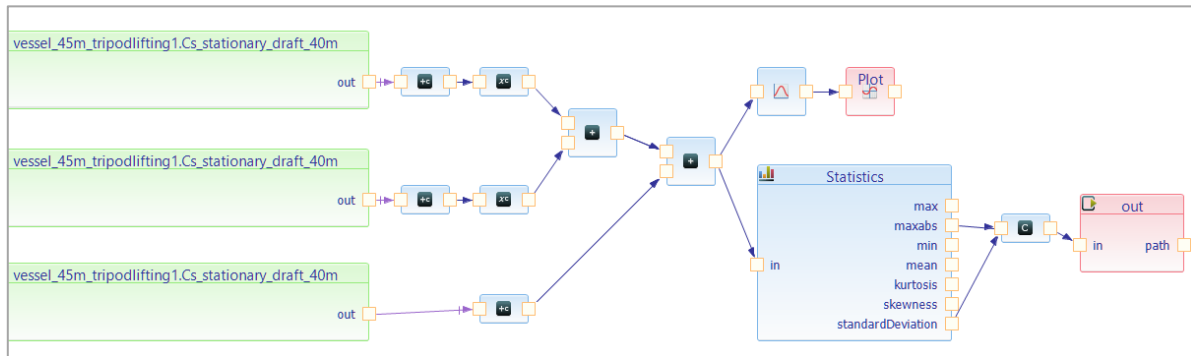
Figure 5.10 Setup for postprocessing

All relevant motions of the HLV, heave, roll and pitch, shall be output respectively. To sum up the effects from all three motions, Scale-function under the arithmetic-tools shall be applied first to transform the rotations (pitch and roll) to equivalent translational distance. Prior to the summation, the static motions resulting from the tripod shall be deducted since it is neither considered in the frequency domain calculation. Consequently, the integrated vertical motion of the crane tip can be plotted or further handled through functions like Statistics, Condition Result Merger and File Output.

5.5.2   Results and discussion

By use of the postprocessing as clarified, statistical extreme values can be collected corresponding to the concerned limiting sea states.

Figure 5.11 Statistical extreme vertical motions at crane tip

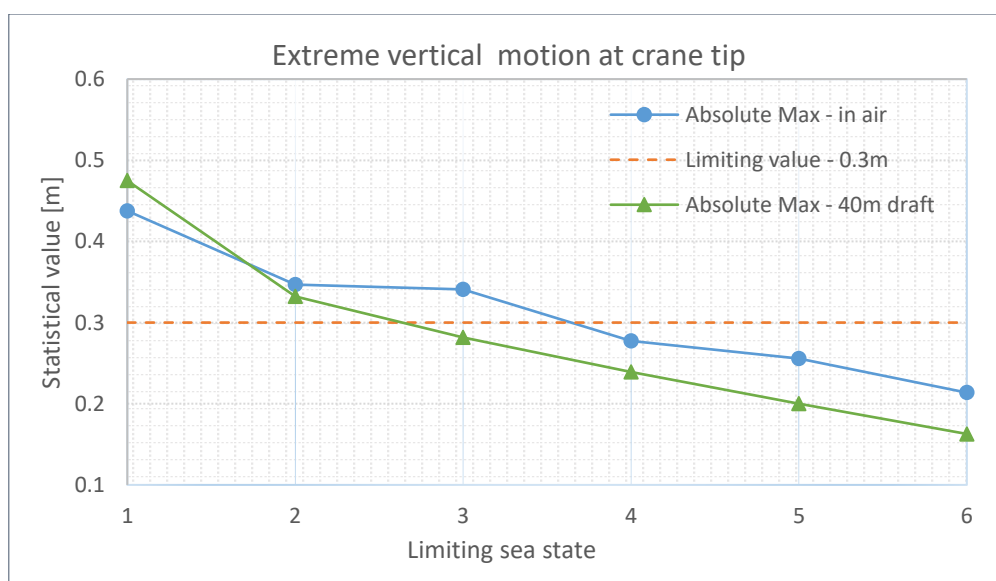Reading from the Figure 5.11, the extreme vertical motion of the crane tip becomes smaller following the limiting sea states with rising T_p, which is valid for both the positions. For the sea states number 4, 5 and 6 with the spectral peak period T_p equal to 8s, 9s and 10s respectively, the extreme vertical motions are even lower than the limiting criteria (0.3m).

In retrospect, the utilized limiting sea states were calculated in frequency domain on the basis that vertical motion at crane tip could be higher than the limiting value 0.3m while the probability of exceedance should be within certain limit (0.05). Judging from the above figure, it is hard to tell whether the first 2 sea sates were overestimated in frequency-domain calculation. Although higher than 0.3m extreme motion occurs, the probability of exceedance is unclear. While, it is certain that the calculated limiting H_s are underestimated for the last three sea states (with T_p equal to 8s, 9s and 10s respectively) since their most critical vertical motion is still lower than the limiting criteria. The discrepancy results from the coupling effects in the time domain simulation. The calculation in frequency domain is based purely on motions (pitch, heave and roll) of the vessel whose natural periods (Table 5-8) are closer to the T_p of the last three cases. Around the natural periods of the HLV, more critical crane tip motions are anticipated due to the resonance response of the vessel. While, due to the coupling, as clarified in the Sec. 5.4.3, there are not that much response from the HLV around the concerned T_p (8s, 9s and 10s). It is the reason why the calculation in frequency domain is imperfect and it underestimates the allowable sea state or weather window at certain spectral peak periods.

Regarding the difference of the crane tip motion between the two positions, it can be observed that extreme motions of crane tip in the submerged case are generally lower than the values in the case hanging in air. The extra hydrodynamic force (on the tripod) due to submergence contributes a lot to the deviation. The motions of the tripod would be more critical due to the extra hydrodynamic force. Furthermore, rather than the motions of the HLV, the rotational motions of the tripod are supposed to dominate the coupled system after the submergence, referring to the eigenvalue analysis. Pitch motion of the two rigid bodies are collected, as shown in the Figure 5.12.To further clarify on the difference of combined crane tip motion between the two positions, especially in the first 3 sea states with T_p equal to 5s, 6s and 7s respectively, the Sec. 5.4.4 is the basis for detailed explanation. In the figure on draft dependent eigen period, it can be found that response of the coupled system may be dominated by the Mode 2, 3 and 4 in the T_p range [5s, 7s] which covers the sea states 1, 2 and 3. Resonance response could be induced by proper combination of the draft and T_p. Through the combination 13m above sea level and 5s, the system responses would be dominated by the Mode 4 in which the motion of HLV plays more role as clarified. While, at the draft -40m combined with T_p approaching 7s, the system responses would be controlled by the Mode 2 or 3 in which the motion of tripod plays the key role. Now that the crane tip motion is the combination of vessel heave, pitch and roll, the combined extreme motion would be higher when the motions of HLV play more role in the system response.

Although the pitch motion of the HLV plays important role in the vertical motion of crane tip, it is insufficient to represent the motion or trend of the concerned crane-tip vertical motion. One-hour time history in the sea states 3 are represented in the Figure 5.13. It can be observed that the combined vertical motion for the submerged case is located perfectly within the limited range while there are few moments with excessive extreme motion for the case with the tripod hanging in air. It is in concert with the statistical comparison in the first figure of this section.
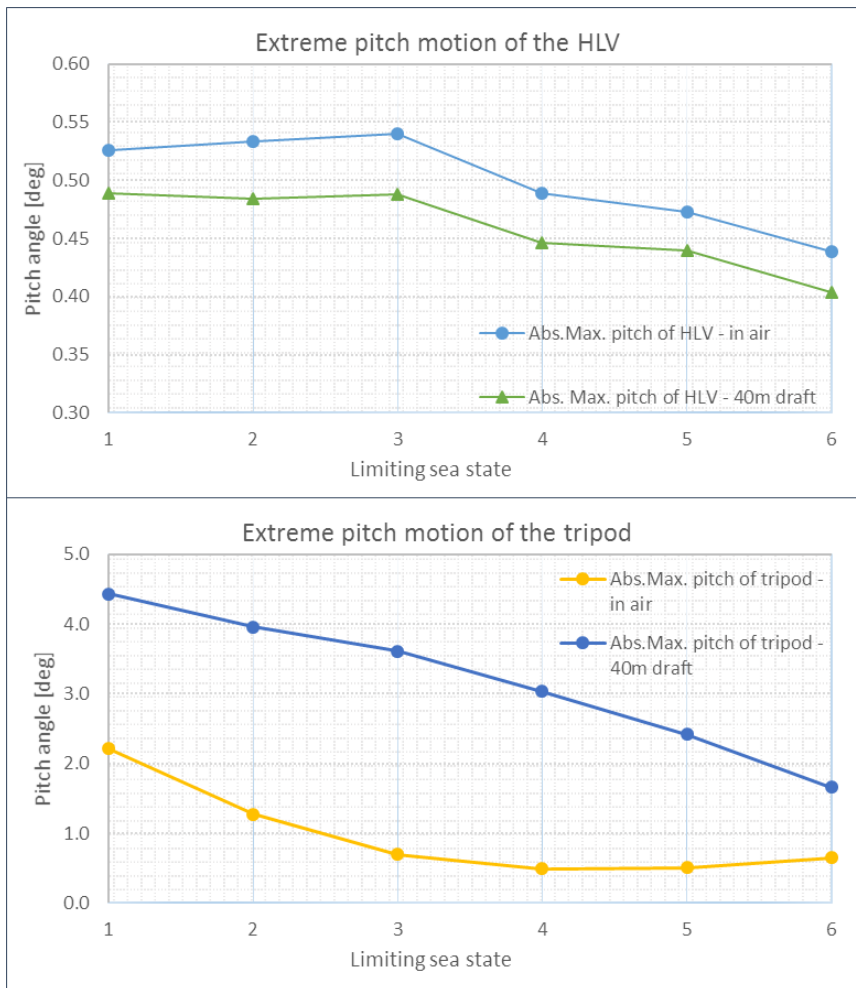
Figure 5.12 Statistical extreme pitch motions of the two rigid bodies
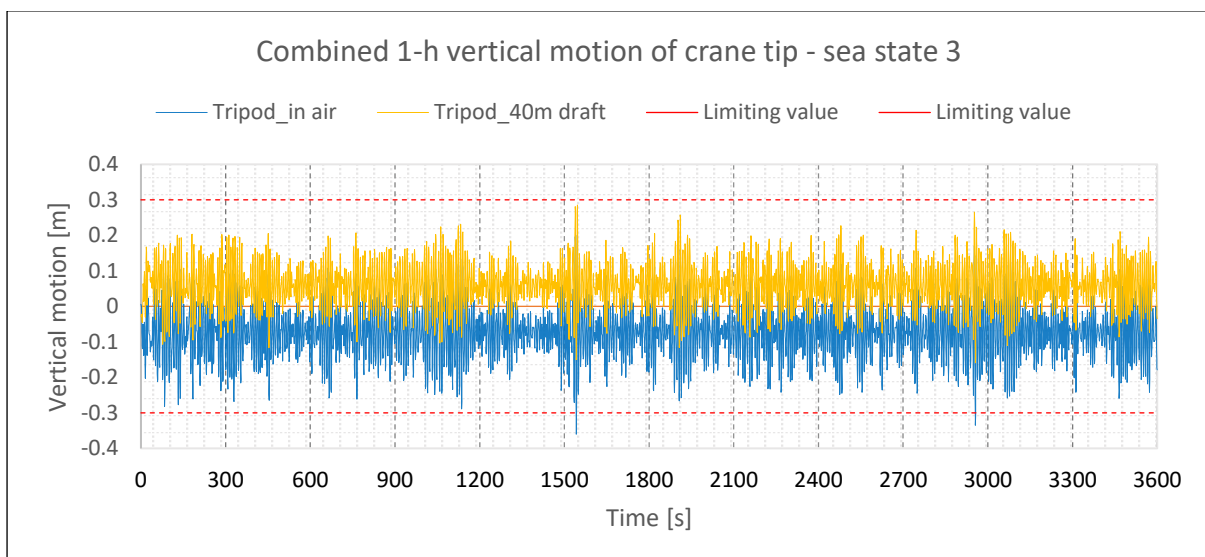

Figure 5.13 Time series of the vertical motion of crane tip

5.6   Simulation of lowering process

Due to the characteristic of time varying and non-stationary of the process, more critical responses may occur taking into the nonlinear transient loads. Attention shall be paid to extreme tension in the lift wire and extreme motions of the bodies during this process. Performance of the coupled system is investigated, under the primary limiting sea state with a significant wave height $H_s = 2.5$ m and a spectral peak period $T_p = 7$ s.

Winch speed, 0.05 m/s, is selected as the basic input. The winch is set to run from 300s until 1400s, equivalent to 55m wire releasing, which will lower the tripod from 13m above still water level until 3m above sea bed. Together with the 300s time allowance before and after the winch-engagement respectively, the length of each simulation is set to be 1700s.

5.6.1   Convergence study

Compared to the stationary simulation, the lowering process is subject to transient effects by nonlinear loads due to waves (Li, et al., 2013). To guarantee the reliability of simulation results, it is important to ensure a good convergence of the numerical simulation. To verify the convergence, 30 different realizations (random seed number) are supposed to be run. Consequently, extreme motion and response can be compared with their mean value of all the 30 samples. Moreover, cumulative averaged value in terms of seed number are also calculated.
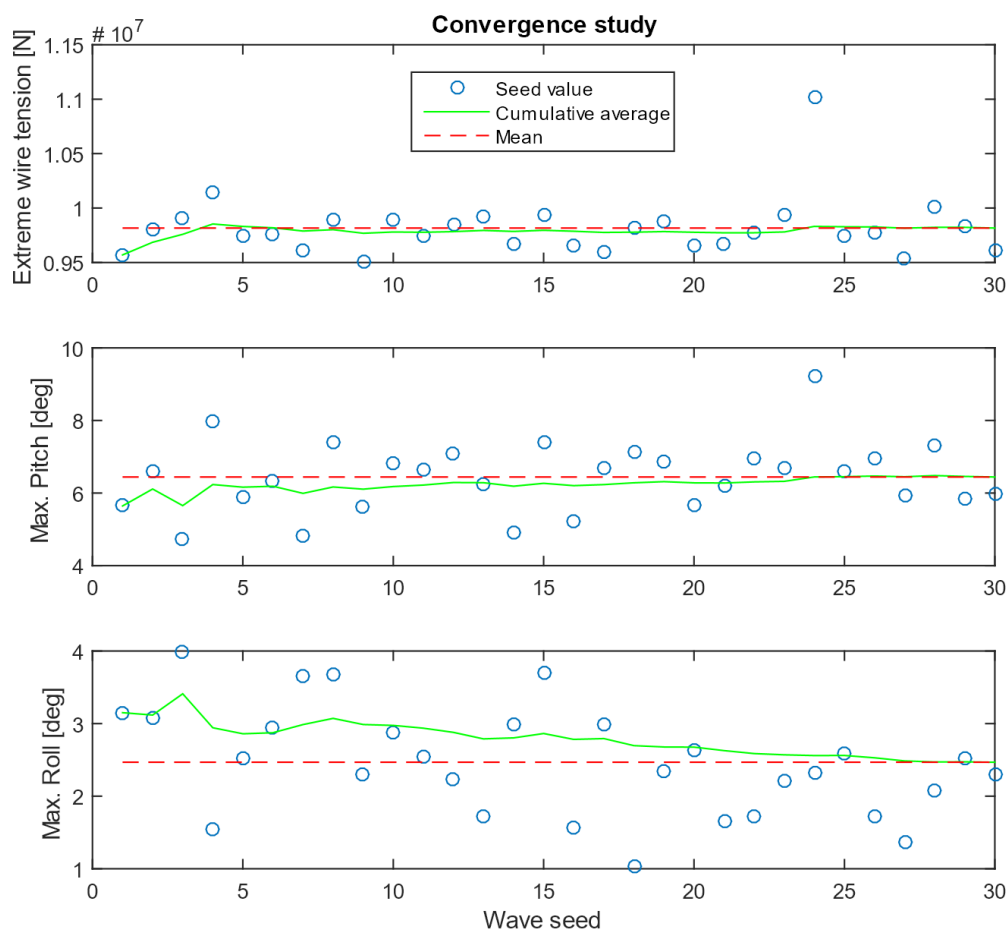

Figure 5.14 Convergence study in terms of critical responses

Reading from the Figure 5.14, 30 seeds are sufficient to obtain convergent results for the extreme responses concerned. Furthermore, good convergence can be reached after 25 seeds judging from the first two graphs which are generally in accord with each other. It suggests that the extreme tension force in the lift wire is more consistent with the extreme pitch motion of the tripod during the lowering process. To precisely represent the system performance during the lowering process, at least 25 seeds shall be applied.

Following the eigen period analysis in the Sec. 5.4.4, under the sea sate with the spectral peak period 7s, resonance response may occur at certain draft corresponding to the eigen Mode 2 to 4. As clarified, all the three modes are dominated by coupled motions by the tripod and especially the rotational motions (roll or pitch). Hence, the extreme responses on the lift wire tension, pitch and roll of the tripod will be of high concern.

5.6.2   Time series of the extreme responses

Concerning the extreme lift wire tension, it can be observed that the value obtained from seed 2 is highly close to the mean value of all the samples. Now that the mean extreme value of all the seeds is reasonable to represent the process, simulation results in wave seed 2 are supposed to be good references on the time series study.
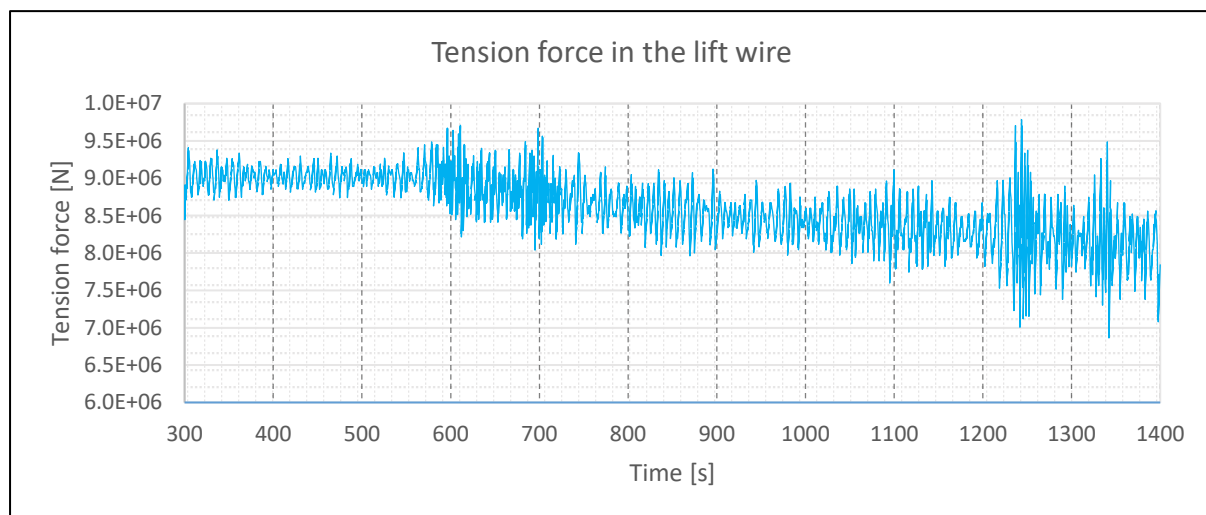

Figure 5.15 Time series of the pitch motion of the tripod

During the running of the winch from 300s to 1400s, the tripod is lowered from 13m above sea level down to the position 3m above sea bed. During the process, the tripod experiences splash zone crossing which is the reason behind the obvious tension fluctuation around 600s. Following the increasing submergence, the buoyance force will keep rising which can explain the slope-down trend of the lift wire tension. Furthermore, some surges on the tension force can be seen around 1250s and 1330s which probably result from resonance response of the coupled system. Hence, it is necessary to take a look at the pitch and roll motion of the tripod which are supposed to be the dominant motions on the wire tension.

As shown in the Figure 5.16, drastic pitch motions can be found in line with the timeline when the lift wire tension surges. In general, same trend can be observed from the time history of the roll motion (Figure 5.16) while the amplitudes of the roll motion are much less. It verifies the inference made in last section that the tension force is closely related to the pitch motion of the tripod during the

47

lowering process. Moreover, the position where the most drastic pitch occurs, -38.5m in draft (around 1330s), is consistent with the eigen analysis in Sec. 5.4.4 and corresponding to the Mode 3.
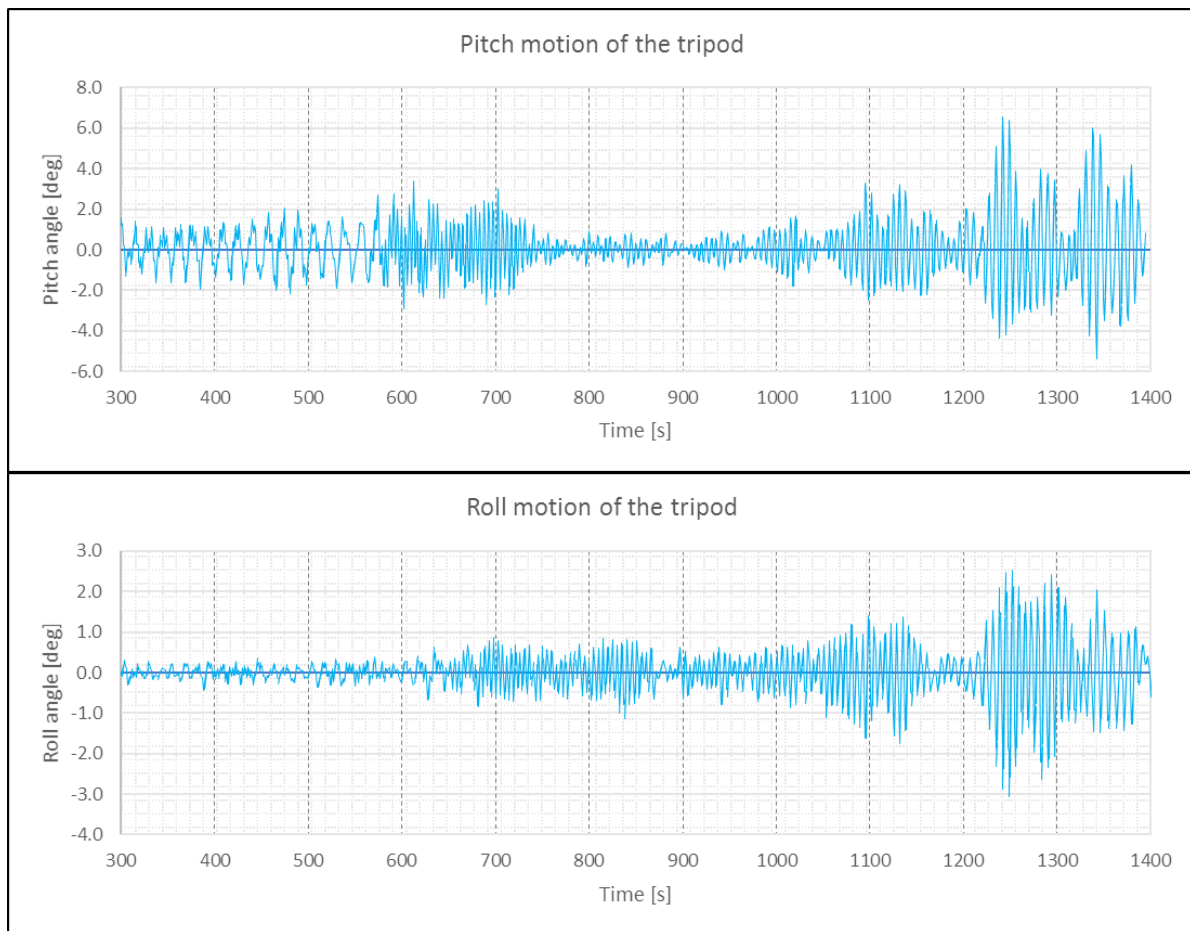
Figure 5.16 Time series of the pitch and roll motion of the tripod

5.6.3   Tip motion of tripod at its lower end

Special attention shall be drawn to the lower tip motion of the tripod at its pile-sleeves especially the one adjacent to the HLV. Figure 5.17 shows the initial layout of the lifting system. During the lowering down of the tripod, slight rotation around its local centre may lead to quite a bit horizontal displacements at its footprint owing to the outstanding height beneath the local centre (45m). To guarantee safe clearance from the vessel and ensure precise landing for smooth installation, lower tip motion of the tripod shall never be neglected.

Figure 5.17 Initial layout of the lifting system for the lowering operation

The horizontal displacement, in each direction longitudinal and transversal, can be attributed to the translational and rotational motion in th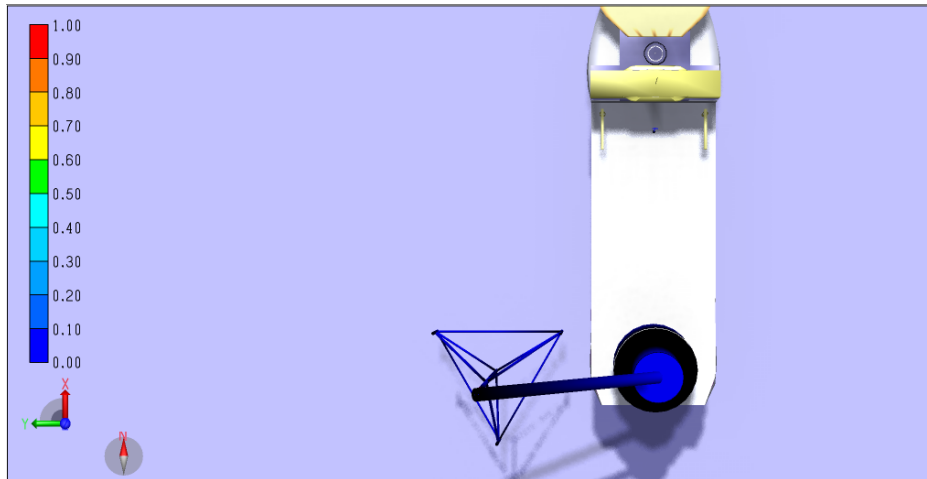at direction respectively. Surge and pitch motion of the tripod will contribute to scaled-up lower-tip displacement in the X direction (longitudinal). So do the sway and roll to the transverse displacement. To superimpose the translation and rotation, the rotations (pitch and roll) shall be transformed to equivalent translational distance through Scale-function. Prior to summation of the signal through Add-function, the translational signal is 'relocated' to the zero-axis through Add-constant function. Then it is possible to plot the integrated signal – the horizontal displacement.
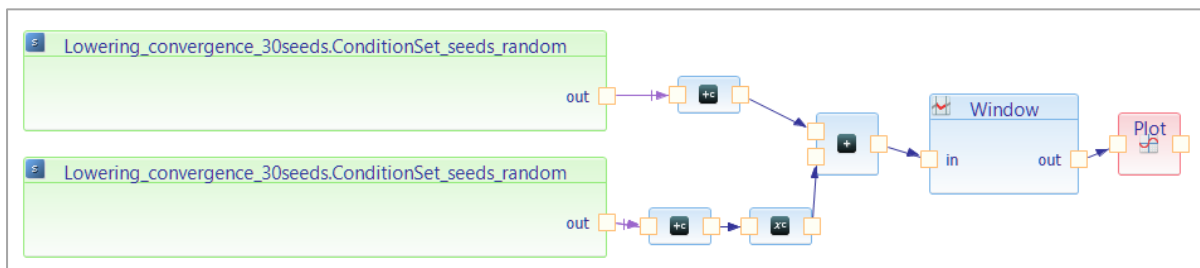
Figure 5.18 Setup of postprocessing

5.6.3.1 Results and discussion

Regarding the longitudinal displacement at lower tips as shown in the below figure, extreme offset can be observed in the time interval between 1200s and 1400s, which correlates with the enlarged pitch motion of the tripod. Moreover, large offset can be observed prior to submergence of the tripod which arises from the large pendulum motion in air, while it is damped out following the entry into sea waves. After diving into water, the amplitude of the tip motion becomes comparatively smaller until reaching the critical-draft region where the tripod motions are excited.

Figure 5.19 Time history of the horizontal displacement (X-offset) at the lower tip of the tripod

Besides the request for precision during landing, the transversal offset is the critical parameter to verify any potential collision with the vessel during the lowering, especially in air owing to the large pendulum motion. While, the collected results shown in the below figure are far away from th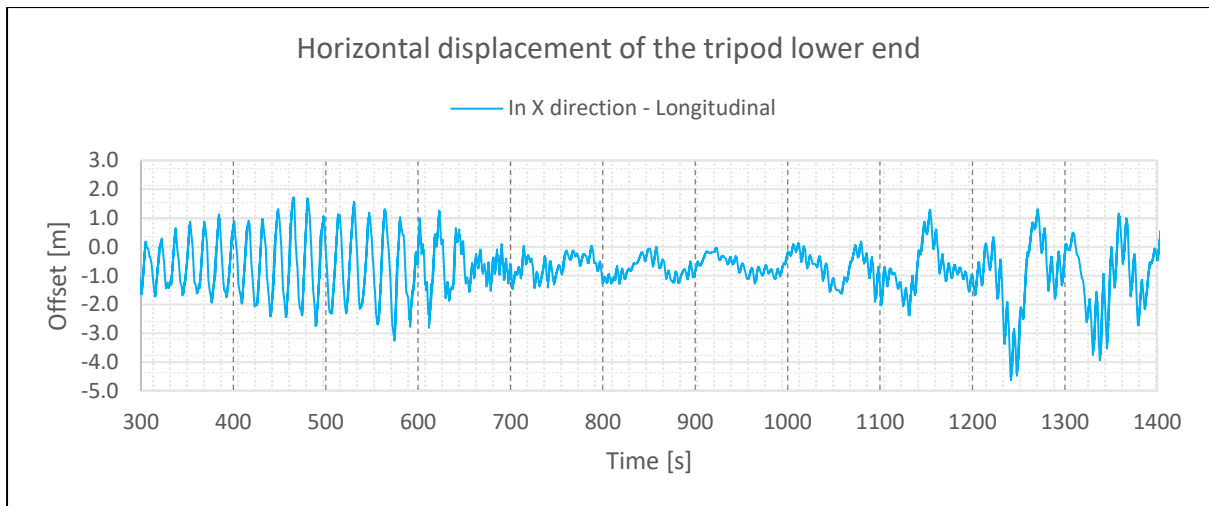e anticipated. It is expected to oscillate around certain axis, roughly similar as the motion in X direction. The abnormal tip motion can be traced back to the abnormal sway-motion as shown in the following figure. The reason behind the weird figures lies in the roll motion of the HLV. Specified moment has been applied on the HLV to counter the turning moment from the hanging tripod. Although equilibrium of moment is guaranteed in air based on the dry weight of the tripod, the balance is broken once the tripod dips into the waves. Following the submergence of the tripod, the decreasing wet weight of the tripod leads to the overbalance of the specified moment, which causes the continuous positive rolling of the HLV (Figure 5.21). In this study, the tripod is originally positioned 8m away from the portside of the vessel, which can accommodate the present extreme offset (more than 4m toward the HLV) excluding the influence from the vessel roll.

Taking its importance of the parameter (Y-offset) into account, countermeasures such as time dependent roll-counteracting ballasting on the HLV or tugger line through the tripod are recommended for future work to have a better control on it, in the case of tight original clearance.
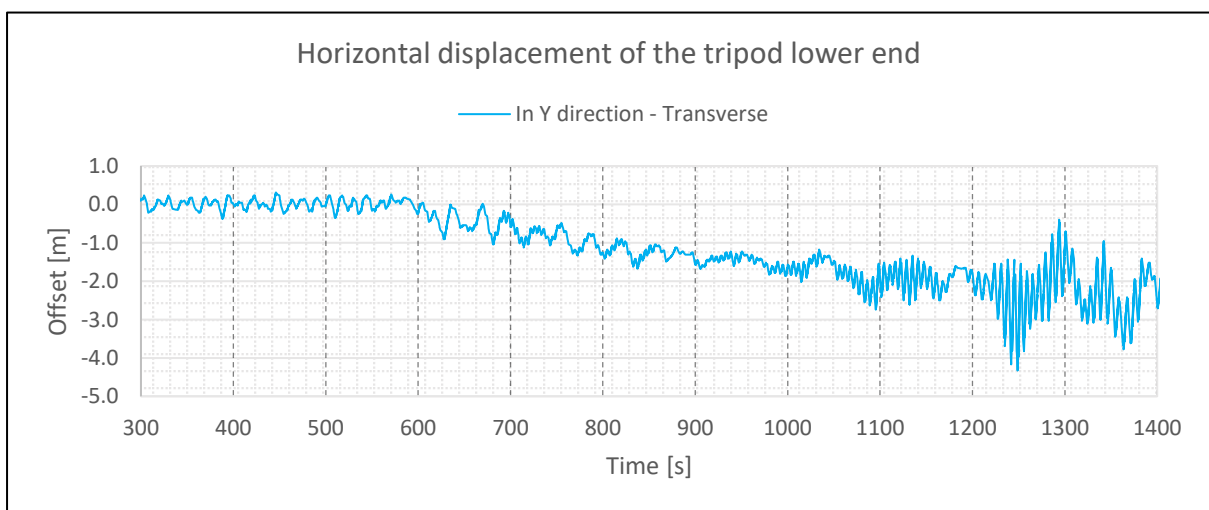

Figure 5.20 Time history of the horizontal displacement (Y-offset) at the lower tip of the tripod
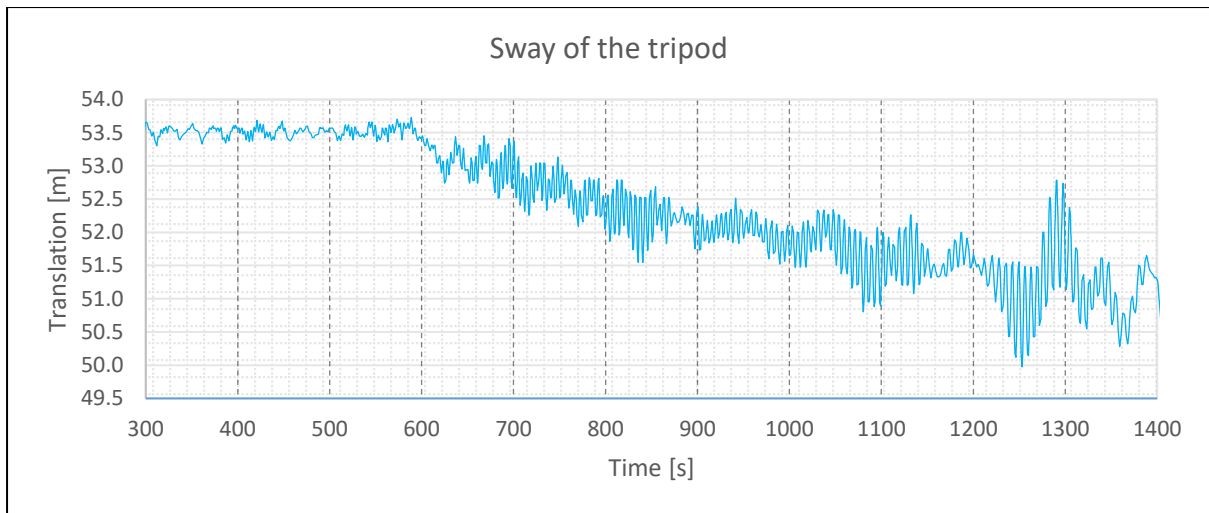
50

Figure 5.21 Time history of the sway motion of the tripod

5.6.4   Comparison between a floating vessel and a jack-up vessel

Compared to the floating lift vessel, a jack-up acts as a bottom-fixed structure and provides a stable working platform for the lifting operation. It is supposed to help relieve the motions of lifted object although its installation and retrieval are time consuming and weather sensitive.

As can be seen from the figure, the difference mainly lies in the process during its lowering in air. Compared to the evident pitch motion in air for the HLV, nil can be found on the tripod in the case of jack-up since there is no motion transferred through lift wire from the fixed vessel (jack-up). With the onset of the wave-crossing, obvious difference in pitch motion, arising from the varied vessel types, can still be observed. While, the motions by and large agree with each other as the lowering continues. Since the motion of the tripod are more affected by the wave forces instead of the influence from the floating HLV.

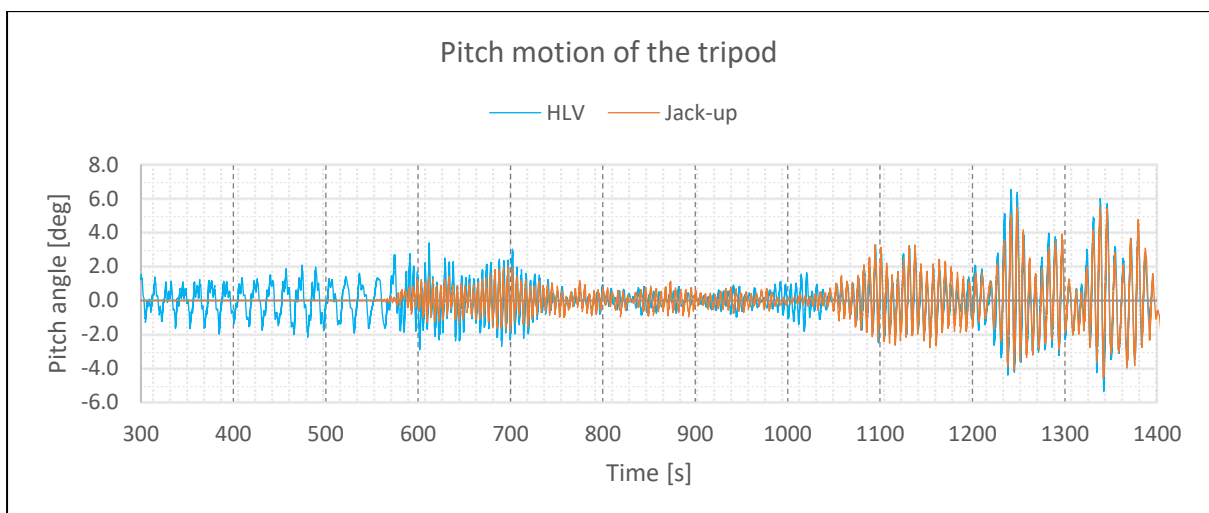*Figure 5.22 Time history of the pitch motions of the tripod, coupled with different vessels*

Compared to the roll motion of the tripod coupled with the HLV – Figure 5.22, there is barely any roll for the jack-up, since there is no motion transfer from the fixed vessel, combined the fact that it is simulated in the ideal head sea. This extra roll motion will lead to larger wire tension for HLV, as can

51

be seen in the below figure, since the tension force is mainly subject to the rotational motion of the tripod as studied and concluded in previous sections. In addition, in the case of the floating HLV, the relative motion between crane tip and the lift point on the tripod may contribute to easing of the wire tension (Li, et al., 2013).
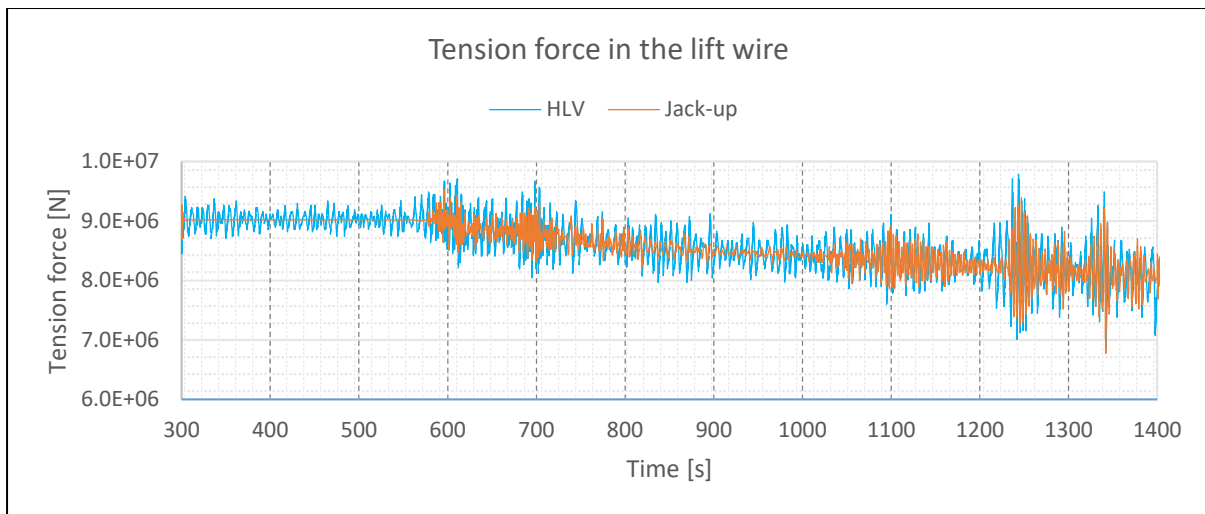
Figure 5.23 Time history of the tension force in the lift wire in terms of different vessels

Taking into consideration the minor roll motion of tripod (sway also) in the case jack-up, there is no doubt that the transversal offset in HLV will be much more severe. The results are not plotted because it is kind of impractical for the HLV in this study as explained in the above section. Regarding the tip motion in the X direction (Figure 5.24), similar trend as shown and analysed in the pitch motions can be found.
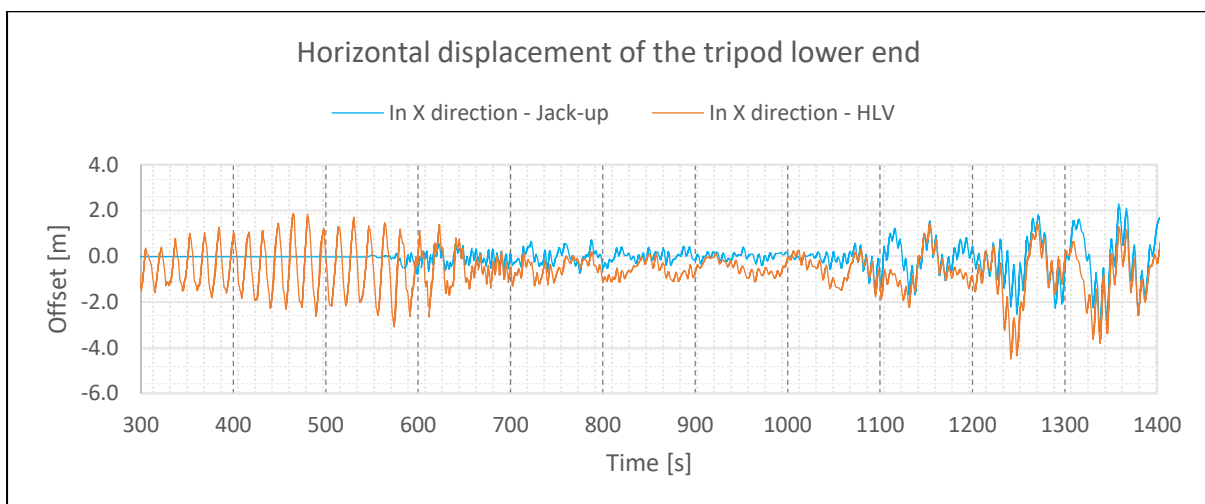
Figure 5.24 Time history of tip motion (X-offset) of the tripod in terms of different vessels

5.7   Simulation of lift-off operation

Lift-off operation could be severely critical since some hazards may be encountered, such as intolerable tension in lift wire, unacceptable horizontal motion of object during the lift off or even re-hit after lift-off from barge. To thoroughly investigate this critical lifting phase, modelling and simulations would be carried out for two cases, lift-off onboard from its own deck and lift-off from a barge.

In case the transport has taken place on the crane vessel, the lift off operation itself is a simple operation since the relative motion between the crane-top and the vessel is marginal (DNV, 2011b). When lifting an object from the barge by means of a crane onboard a crane vessel positioned side by side with the barge as in this study, the relative motion between crane hook and the barge at the position of the lifted object, will play a key role to determine the probability of re-hit after the lift off.

Moreover, following parameters could also determine whether the lift-off operation is feasible (DNV, 2011b).

- The hoisting speed of the crane (depends on the weight of the object to be lifted, a lower limit is usually taken to be in the order of 0.1 m/s).

- The combined motion characteristics of the barge and the crane vessel.

- The weather condition, combined with the orientation of the two vessels.

In this study, barge is modelled with the same hydrodynamic characteristics as the crane vessel (HLV). They are positioned side by side, both heading against the wave propagation (in head sea). Concerning the hoisting speed, the lower limit 0.1m/s is set as the default input for winch and influence from different speeds will be investigated.

The winch is set to run from 200s and it would firstly pay-in the pre-set loose wire which is 1.5m in length. It would be kept engaged until the tripod is lifted 5m upward from its original sitting position which takes 65s at the hoisting speed 0.1m/s. Total length of dynamic simulation is set to be 450s so that the system will stay in steady state for certain period after the winch disengages.

5.7.1 Lift off from self-deck

Following the same logic as in the Sec. 5.6, it is found from the Figure 5.25 that 30 random seeds are sufficient to achieve convergence on extreme wire tension. To guarantee reasonable representation of the operation concerning extreme tension force in the lift wire, statistical peak values of all the necessary sample seeds shall be collected and averaged. Consequently, sample seed will be taken, seed 18 (close to the mean) in this case, and its time series responses are to be investigated in the following subchapter to have a full understanding of the process.
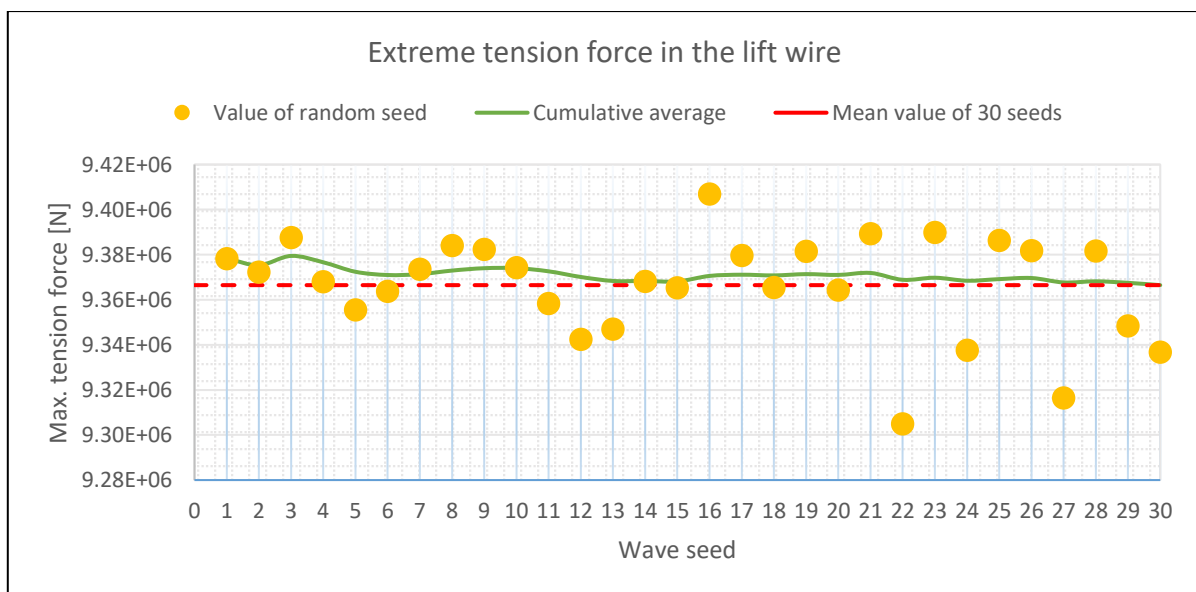

Figure 5.25 Convergence study in terms of extreme tension force

5.7.1.1 Results and analysis at the hoisting speed 0.1 m/s

Firstly, investigation is carried out with the basic hoisting speed 0.1m/s. As clarified, attention should be drawn to the wire tension and horizontal motion of the tripod after lift-off.

Concerning the wire tension, it turns out that there is barely any variation in the beginning or the end, compared to the fluctuation due to involvement of the winch. Hence, only the time window covering the duration of running-winch is shortlisted. Reading from the Figure 5.26, fluctuation in wire tension can be found following the completion of the lift-off around 215s and the deactivating of the winch at 265s. It can be further noticed that the tension-variation after the lift-off is relatively minor and even slighter than the counterpart resulting from the winch-off.
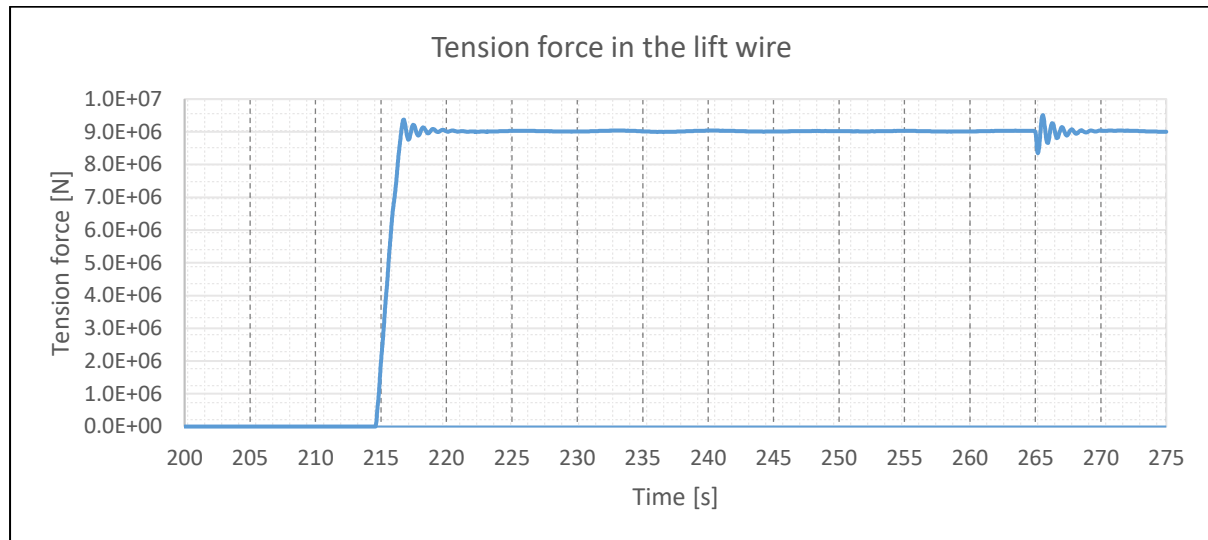
Figure 5.26 Time history of tension force in the lift wire during the lift-off

Regarding motions of the tripod following completion of the lift-off, the simulation results show that there is barely any sway or roll compared to the motions in surge and pitch. It is not beyond our expectation as the simulation was run in the condition of head sea. In addition, no critical or severe surge translation is identified during and followed immediately after the lift-off around 217s, as shown in the Figure 5.27.
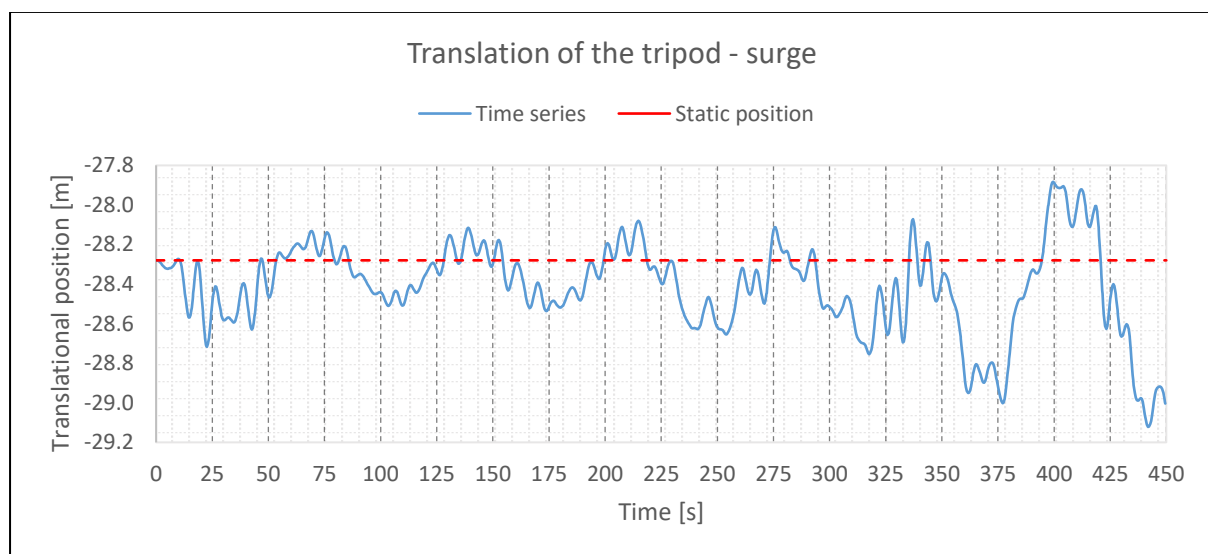
Figure 5.27 Time history of surge motion of the tripod

For pitch motion, it can be observed in the Figure 5.28 Figure 5.28that the motions of the two bodies are not in the same pace any more after the lift off completed. The amplitude of the tripod pitch is scaled up but still allowable (within 1 degree). After smooth lift-off, the motion of the tripod is subject to motion of the crane top through the wire coupling, as clarified in previous sections.
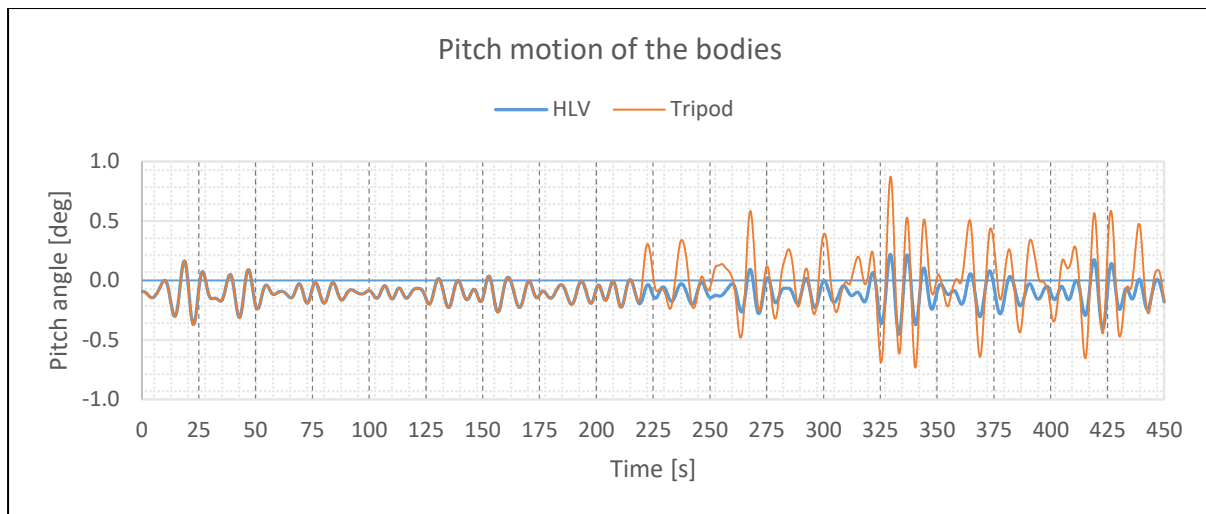
Figure 5.28 Time history of pitch motions of the two bodies

5.7.1.2 Influence from hoisting speed

Winch speed is marked as negative since default positive direction is downward-pointing in the modelling. Winch is set to run from 200s until the tripod is lifted by 5m. The process will experience twice tension-fluctuation following the completion of the lift off and the deactivating of the winch, as clarified in above section. Instead of the second fluctuation, attention is paid to the wire-tension variation immediately after the lift off with the time interval between 200s to 220s.

Table 5-13 Predefined winch speeds

	Winch speed [m/s]			
1	2	3	4	5
-0.1	-0.2	-0.3	-0.4	-0.5

Table 5-14 Setup for the winch

Winch speed [m/s]	Running duration [s]	Stop-time [s]
-0.1	65.00	265.00
-0.2	32.50	232.50
-0.3	21.67	221.67
-0.4	16.25	216.25
-0.5	13.00	213.00

It can be expected that the lifting would commence at varying time points as the time duration spent on the slack wire retrieving is different due to the varied winch speed. As can be observed from the

time series – the Figure 5.29, lift-off starts earlier and completes sooner with higher hoisting speed, together with larger extreme wire tension.
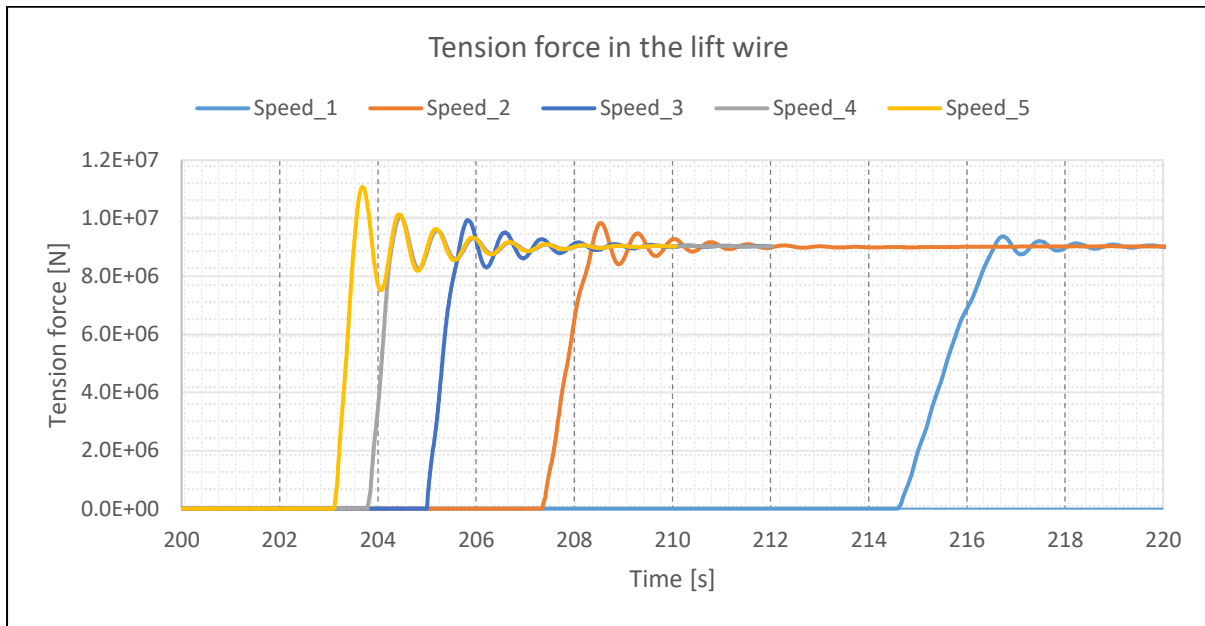
Figure 5.29 Time history of the tension force during onboard lift-off

It is necessary to turn to the statistical values through postprocessing to precisely identify and compare the extreme tension force resulting from various hoisting speeds. It can be observed from the statistical values that the extreme wire tension keeps rising with increasing hoisting speed from 0.1 m/s. Furthermore, significant hike up can be seen with the hoisting speed at 0.5m/s, compared to the slight ascent in extreme tension with the speed between 0.2m/s and 0.4m/s. Hence, it is critical to control the hoisting speed during the lift-off, slight exceedance of the allowable hoisting speed corresponding to the safety criterion of the lift wire, may lead to catastrophe due to the surge in extreme wire tension.
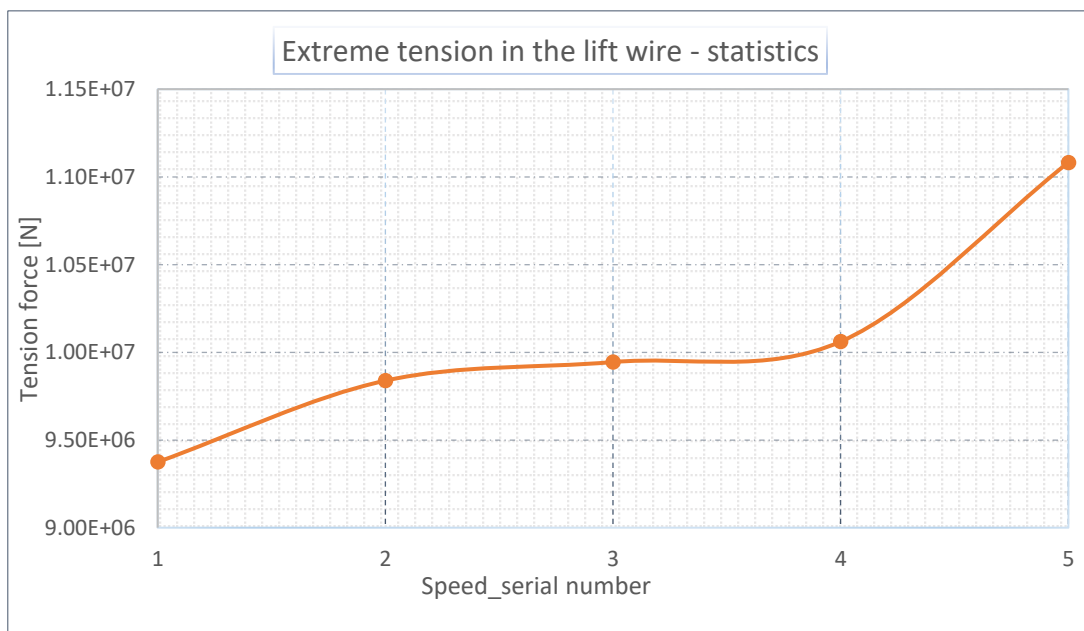
Figure 5.30 Statistical extreme tensions during the onboard lift-off

5.7.2 Lift off from barge

It is common practice to transport structures with feed barge so that the HLV can focusing on the installation work. For offshore wind farm installation, usually quite a lot turbines are involved. It does not make sense to do the transportation work back and forth by use of the expensive HLV, which places it as a necessity to study the lift-off from the barge.

Considering the extra coupling with the barge, more wave seeds may be needed to reach reasonable convergence (Acero, et al., 2015). Same setting as the previous section is applied (with the hoisting speed 0.1m/s), e.g. wire and fendering coupling, environmental condition, the winch start-off and duration. Concerning statistics of the extreme wire tension during lift-off, it turns out that 45 seeds are sufficient to achieve good convergence, as shown in the Figure 5.31.
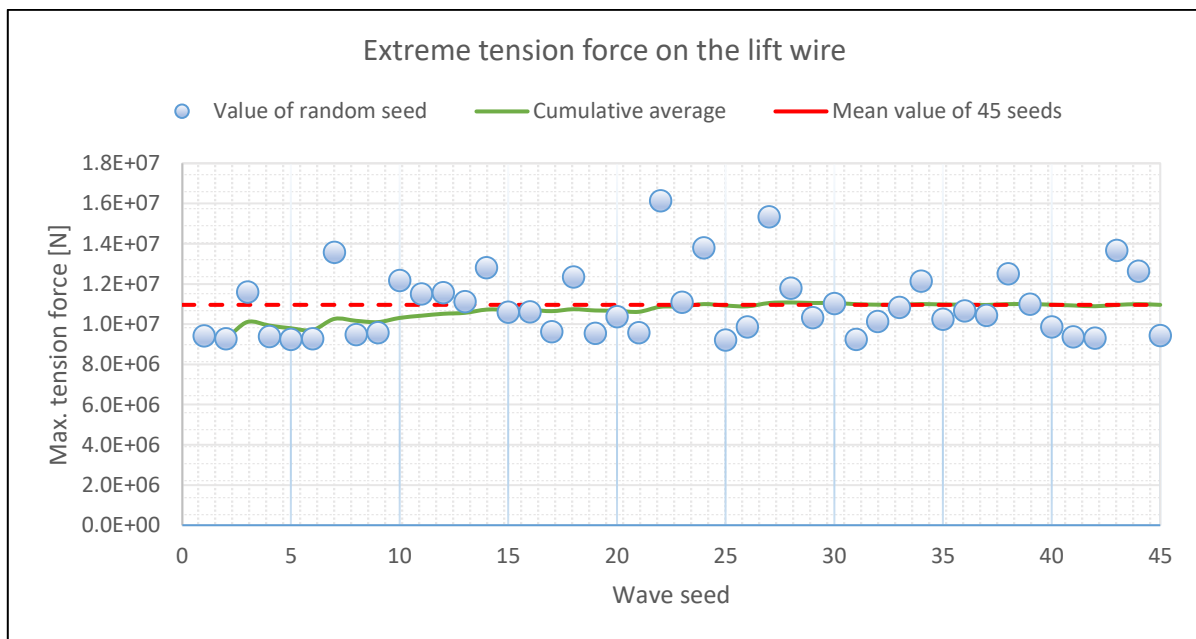
Figure 5.31 Convergence study in terms of extreme wire tension

5.7.2.1 Extreme coupling forces

Based on the convergence study, seed 22 (the most extreme) and 39 (close to the mean) are selected for time-history investigation.

Compared to the smooth lift-off operation carried out on the deck of the HLV, the process in this case is far more volatile and stark peak force can be observed as shown in the figure. The peaks in the wire tension result from snap load following the slack in lift wire, entitled snap force. The extreme snap force is evidently larger than the expected normal force and almost twice the normal value in the extreme wave seed. It is the reason why slack sling or wire is recommended to be avoided (DNV, 2011b) (Sarkar & Gudmestad, 2010).

Although same settings are applied in the simulation, such as the loose wire length and winch speed, the lift wire gets stretched as early as 210s instead of around 214s in the case of lift-off onboard, as can be observed in both the coupling related figures, the Figure 5.32 and the Figure 5.33. It is the result of the relative motions between the HLV and the barge. At the beginning of the load transfer,

amplitude of the snap force can almost reach the level of the normal mean tension and it scales upper with the following slack-wire cases until it is successfully lifted off.
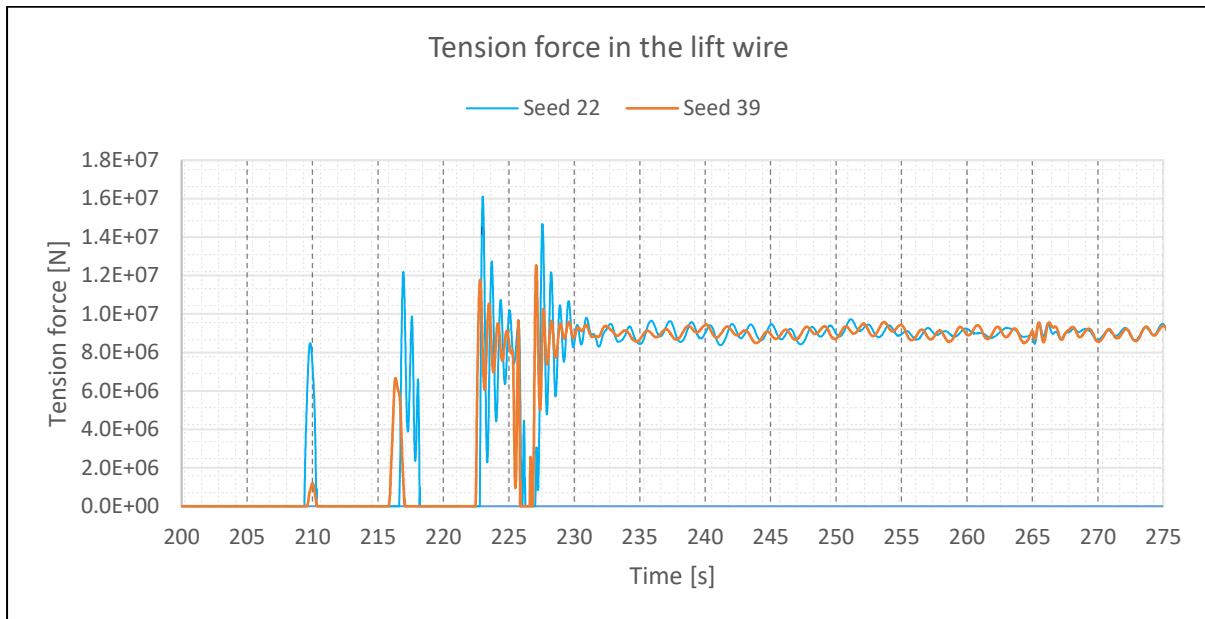
Figure 5.32 Time history of wire tension in the case lift-off from barge
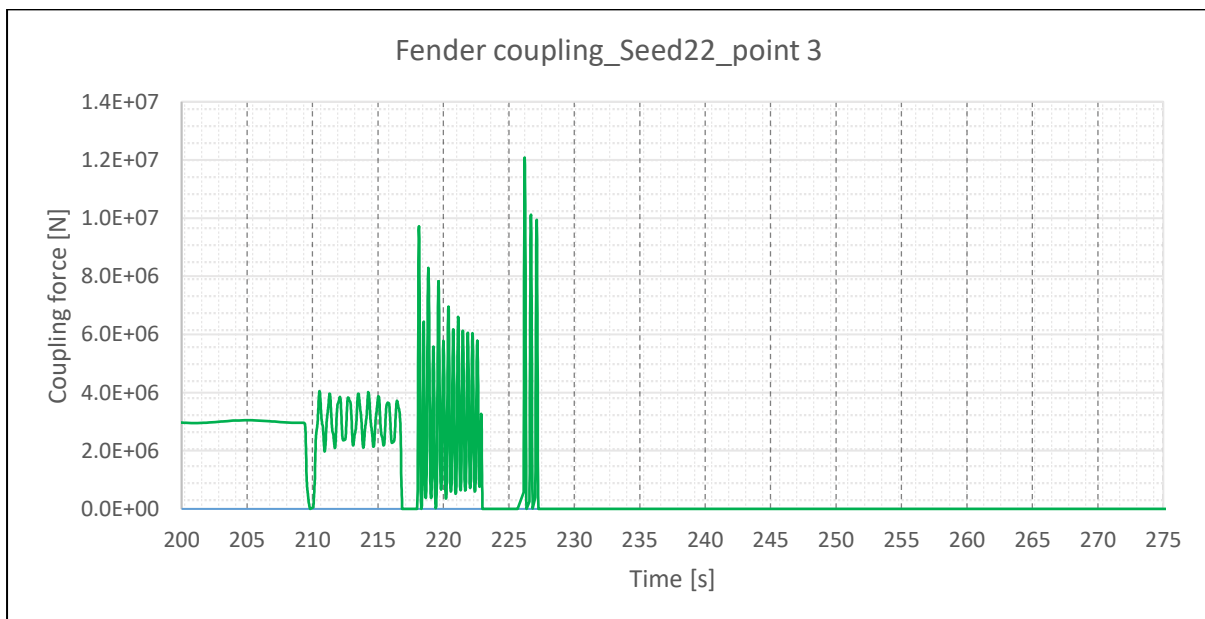
Figure 5.33 Time history of fender compression in the case lift-off from barge

Concerning the snap force due to slack wire or re-hit between the lifted object and the barge, it may be affected by many factors, such as stiffness of the wire coupling (Sarkar & Gudmestad, 2010) (Acero, 2016), wave heading direction and hoisting speed during lift-off (Jeong, et al., 2015), which can be further investigated in future work.

5.7.2.2 Critical motions of the system

Regarding motions of the system, the whole process can be divided into three phases. Phase one lasts until the lift wire gets taut (around 209s). It can be treated as two separate systems, the barge with tripod seated on and the free floating HLV, excluding shielding effects or any hydrodynamic interaction between the two floating vessels. The hydrodynamic interaction between the two floaters which share same hydrodynamic characteristics in this study, can be ignored based on the research (Baar, et al., 1992). While, the shielding effects will influence the lifting operation and shall be taken into consideration (Li, et al., 2014), which it is not in the reach of this study. The continuous lifting after successful lift-off (around 227s) and the consequent steady state hanging in air is the last phase which also comprises of two separate systems, the free barge and the HLV with the lifted tripod. Slack and re-hit occurs in between, which is the second phase.

In the first phase, the motions of the tripod are similar as the case onboard lift-off in the corresponding time interval now that the HLV and the barge share the same hydrodynamic characteristics. For the tripod, same motions as the barge can be observed and barely any roll due to the ideal wave condition of head sea, which contributes to the near-nil tip motion in Y direction and mild offset in the X direction, as can be seen in the Figure 5.34. During the phase two, tripod motions (bumping) are involved but of less concern in this study. More attention is drawn to the motions immediately after the successful lift-off. Significant motions arise following the completion of the lift-off, which consequently induces noticeable tip motions both longitudinally and transversally.
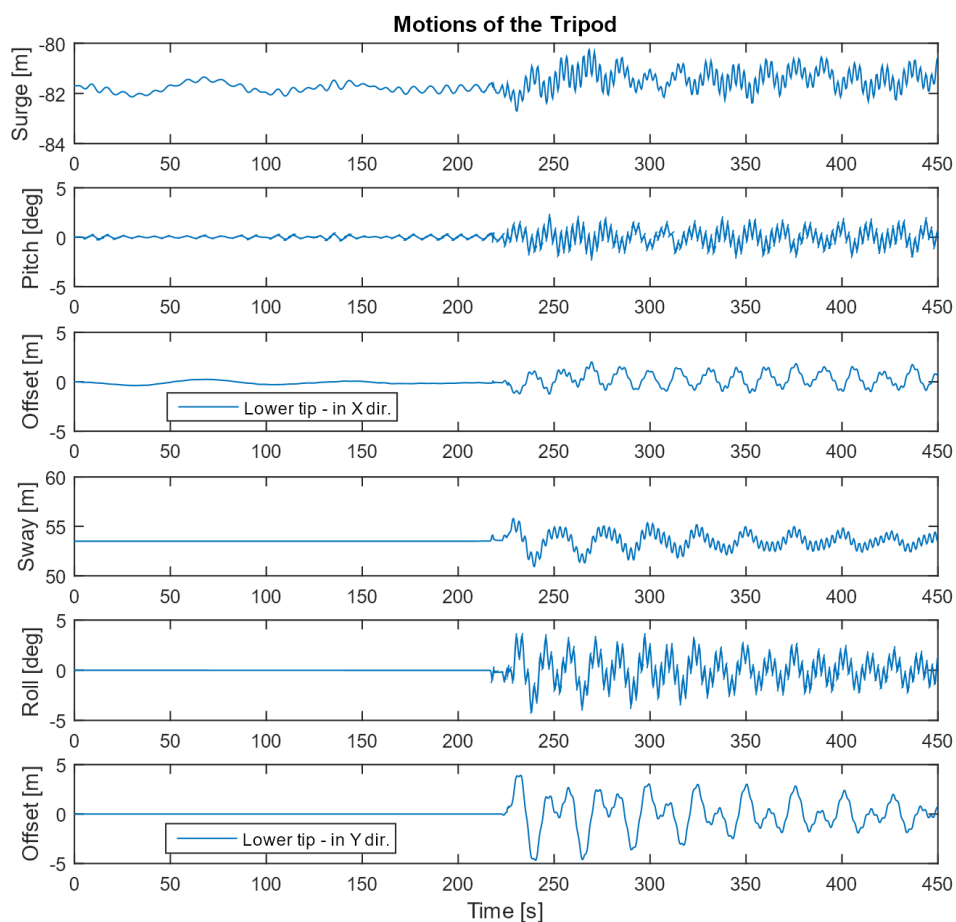
Figure 5.34 Time history of motions of the tripod

Concerning some critical motions of the HLV and the barge, the Figure 5.35 can be interpreted in detail as following. Regarding the two floaters, there are barely any sway or roll can be observed in the first phase thanks to the ideal condition of head sea. As soon as the lift wire gets stretched, coupled motions are involved for both the floaters due to the couplings, the lift wire and the fender. The HLV is subject to passive roll and sway due to the coupling force transferred from the lift wire, since the tripod is so heavy as to force the HLV into moving. Time dependent de-ballasting on the portside of HLV (same side as the barge) has been set to run from 220s to counter the turning moment from the wire tension. The de-ballasting serves two purposes, acting as righting moment and reducing the draft of the HLV to help avoid or ease re-hit between the tripod and the barge. With completion of the lift-off, the roll motion of the barge damps out gradually, while the motions of the HLV follow the pattern of the coupled system between the HLV and tripod as analysed in previous sections.

Figure 5.35 Time history of motions of the HLV and the barge

6 Conclusions and future work

The installation of tripod foundations by a heavy lifting vessel (HLV), in the site 15 North Sea Centre, was studied in this thesis. Much time was devoted to the calculation of limiting sea state in frequency domain and its verification in time domain. In the frequency domain analysis, case studies involving different variables, such as direction of coming wave, wave spectrum and crane tip location, are carried out to have a better understanding of their influence on the r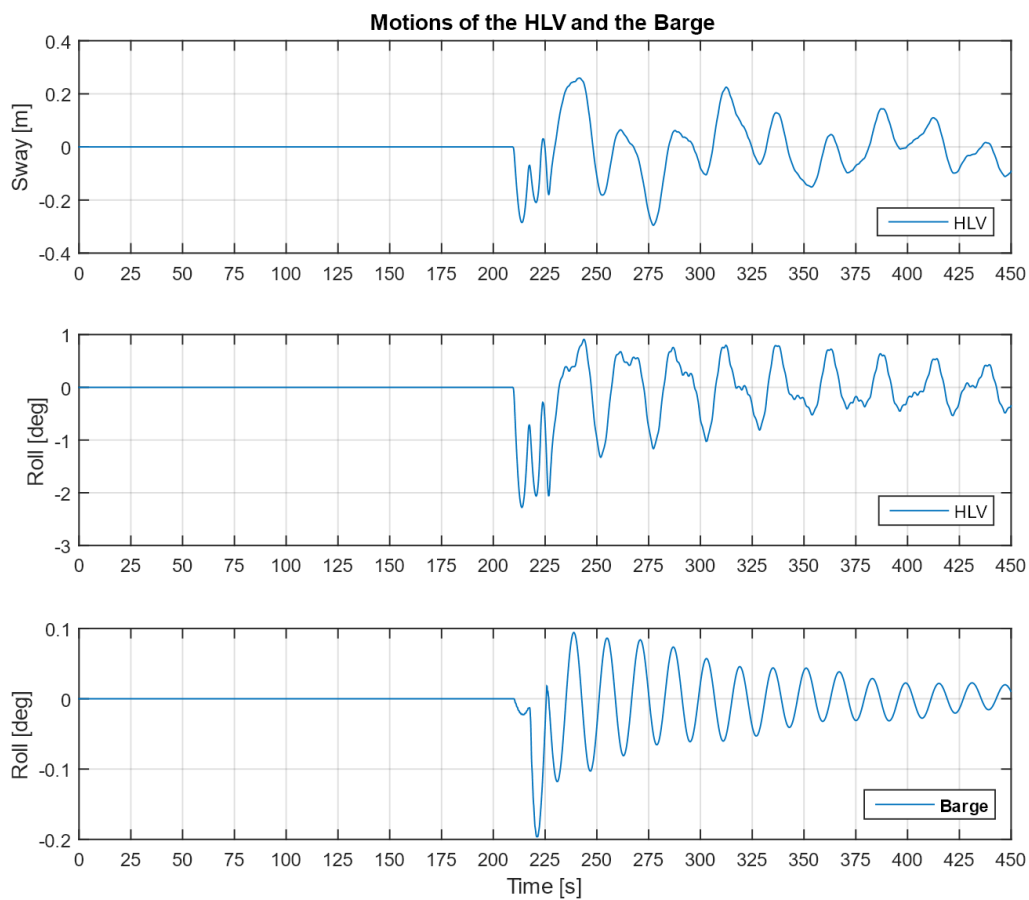esponse and consequently on the predicted limiting weather. Eigenvalue analysis were conducted to assess the eigen periods of the rigid body motions and understand what motion modes are dominating in the coupled or decoupled conditions.

Besides, more attention was paid to numerical modelling and simulation of the coupled nonlinear processes during the installation. The two lifting phases, the lowering and the lift-off, were thoroughly investigated concerning the potential risk like slack wire, collision with the lifting vessel due to excessive tip motion of the tripod or re-hit between the tripod and transport barge during the lift-off. Comparative studies in response during the lowering using two types of installation vessel, the HLV and the Jack-up, were investigated. Case study on various hoisting speeds during the onboard lift-off was also presented.

6.1 Conclusion

Based on the investigations in this thesis work, some essential findings can be summarised as follows:

1) For different crane-tip locations during installation, response spectrum for that point can vary a lot. The responses are more critical, correspondingly more gentle sea states required, should the crane tip be located further away from COG or roll centre of the HLV.

2) Direction of wave propagation to the vessel heading has a significant impact on the vessel response. By aligning the HLV against the primary wave direction (incoming wave in 180-degree), rougher sea states can be tolerated due to much milder response compared to beam sea condition.

3) For the coupled system, the Modes 2 ~ 4 which are dominated by the rotational motions of the tripod are of our concern since their natural periods may coincide with the spectral peak periods of the waves according to the hindcast data. Furthermore, their eigenfrequencies are strongly dependent on the level of submergence of the tripod.

4) The predicted limiting weather using frequency domain method is found inaccurate. The calculated limiting H_s seems underestimated with T_p approaching the natural periods of the installation vessel. The shortcoming of the prediction in frequency domain arise from the simplification of linear response and decoupled system.

5) Besides the critical response during the splash zone crossing, attention shall also be brought to the resonance rotational response of the tripod which can occur after submerged. Critical wire tension and volatile tripod motions can be induced due to the resonance response as presented in the lowering process analysis.

6) Compared to the floating installation vessel, the wire tension and response of the tripod using the jack-up are comparatively smaller under the predefined conditions in this study. Especially during the lowering in air, huge difference exists between the two types of installation vessels and barely any tripod motion is induced for the jack-up case thanks to the great bottom-fixed stability.

7) Compared to the onboard lift-off, there would be much more challenges for the lift-off from barge. Under the considered wave condition, the onboard lift-off operation can be smoothly implemented while the operation from the barge experiences snap load and re-hit. In addition, hoisting speed during the lift-off shall be decided with care for safety reason since it has big influence on the extreme tension of the lift wire.

6.2 Recommendation for future work

Numerical simulations are particularly helpful for analysis of the coupled dynamic system while the accuracy of the numerical model plays key role in the simulation results. Taking into consideration the simplifications in the present numerical model, many improvements can be applied in future. The following list presents recommendations for future work.

1) The numerical modelling could be further refined. Instead of direct connection to the tripod top through lift wire, hook with sling wires should better be integrated into the modelling. Furthermore, the characteristics of the couplings, like stiffness and damping of the lift wire and fender, should be double checked with maker or ship owner.

2) The effects from wave spreading could be considered. This study was conducted in long crested, head sea wave conditions. In reality, the offshore installation might be carried out in the sea conditions resembling the short-crested waves. The directional waves would certainly have influence on the system responses.

3) The potential damping could be take into consideration. For slender structures, Morison's formula was based on to calculate the excitation force. While, this method neglected the potential damping of the structures. According to the research (Li, et al., 2015a), correct damping is particularly important for the resonant motions of the lifting system.

4) Shielding effects could be taken into account. The simulations in this study were carried out in undisturbed waves. Referring to the investigation (Li, et al., 2014), If the lowering operation is performed in the vicinity of a properly positioned HLV, shielding effects are significant especially in short waves.

References

4Coffshore, 2013. *Tripod support structures.* [Online]
Available at: http://www.4coffshore.com/windfarms/tripod-support-structures-aid7.html
[Accessed 05 02 2017].

Acero, W. G., Gao, Z. & Moan, T., 2015. Assessment of the dynamic responses and allowable sea states for a novel offshore wind turbine installation concept based on the inverted pendulum principle. *Energy Procedia,* Volume 94, pp. 61-71.

Acero, W. I. G., 2016. *Assessment of Marine Operations for Offshore Wind Turbine Installation with Emphasis on Response-Based Operational Limits. Doctoral thesis.* Trondheim: Norwegian University of Science and Technology.

Andersen, C. E., 2012. *Numerical simulation for installation of offshore monopile wind turbines. Master thesis.* Trondheim: Norwegian University of Science and Technology.

Baar, J. J. M., Pijfers, J. G. L. & van Santen, J. A., 1992. *Hydromechanically coupled motions of a crane vessel and a transport barge..* Houston, Texas, Offshore Technology Conference.

Birkeland, F. M., 2016. *Numerical Simulation for Installation of XL Monopile for Offshore Wind Turbine.* Trondheim: Norwegian University of Science and Technology.

Chakrabarti, S., 1987. *Hydro Dynamics of offshore structures.* Southampton: Computational Mechanics Publications.

Clauss, G., Riekert, T. & al., e., 1990. *Operational limitations of offshore crane vessels.* s.l., Offshore Technology Conference.

DNV, 2011a. *Recommended Practice DNV-RP-C205, Environmental conditions and environmental loads.* s.l.:Det Norske Veritas.

DNV, 2011b. *Recommended Practice DNV-RP-H103, Modelling and analysis of marine operations.* s.l.:Det Norske Veritas.

Faltinsen, O. M., 1990. *Sea loads on ships and offshore structures.* Cambridge: Cambridge University Press.

Gudmestad, O., 2015. *Marine technology and operations, theory & practice.* Southampton: WIT Press.

GWEC, 2016. *Market forecast for 2017- 2021. Global wind energy council. Website:.* [Online]
Available at: http://www.gwec.net/global-figures/market-forecast-2012-2016
[Accessed 05 02 2017].

Haver, S., 2007. *Prediction of characteristic response for design purposes. Draft version..* s.l.:s.n.

Haver, S., 2016. *Lecture notes in Marine Operations.* Stavanger: University of Stavanger.

HeavyLiftSpecialist, 2013. *There are a large number and different types of floating cranes around the world.* [Online]
Available at: http://www.heavyliftspecialist.com/cranes/floating-cranes-world/
[Accessed 10 02 2017].

IEA, 2013. *Technology roadmap: Wind energy.* [Online]
Available at:
http://www.iea.org/publications/freepublications/publication/Wind_2013_Roadmap.pdf
[Accessed 02 02 2017].

Jeong, D. H., Roh, M. I. & Ham, S. H., 2015. Lifting off simulation of an offshore supply vessel considering ocean environmental loads and lifting off velocity. *Ocean Systems Engineering,* 5(3), pp. 181-198.

Journée, J. & Massie, W., 2001. *Offshore hydromechanics.* 1st ed. s.l.:Delft University of Technology.

Li, L., Acero, W. G., Gao, Z. & Moan, T., 2016a. Assessment of allowable sea states during installation of offshore wind turbine monopiles with shallow penetration in the seabed. *Journal of Offshore Mechanics and Arctic Engineering,* 138(041902), p. 4.

Li, L., Gao, Z. & Moan, T., 2013. *Numerical simulations for installation of offshore wind turbine monopiles using floating vessels.* Nantes, American Society of Mechanical Engineers.

Li, L., Gao, Z. & Moan, T., 2015a. Response analysis of a nonstationary lowering operation for an offshore wind turbine monopile substructure. *Journal of Offshore Mechanics and Arctic Engineering,* 137(051902), p. 9.

Li, L., Gao, Z. & Moan, T., 2015b. Joint distribution of environmental condition at five European offshore sites for design of combined wind and wave energy devices. *Journal of Offshore Mechanics and Arctic Engineering,* 137(3).

Li, L., Gao, Z. & Moan, T., 2016b. Operability analysis of monopole lowering operation using different numerical approaches (ISSN 1053-5381). *International Journal of Offshore and Polar Engineering,* 26(2), pp. 88-99.

Li, L., Gao, Z. & Moan, T., 2016c. Operability analysis of monopole lowering operation using different numerical approaches. *International Journal of Offshore and Polar Engineering (ISSN 1053-5381),* 26(2), pp. 88-89.

Li, L., Gao, Z., Moan, T. & Ormbrg, H., 2014. Analysis of lifting operation of a monopile considering vessel shielding effect. *Marine Structures,* Volume 39, pp. 287-314.

MARINTEK, 2016a. *SIMO Theory Manual, Version 4.8.2,.* s.l.:MARINTEK.

MARINTEK, 2016b. *SIMO User Guide, Version 4.8.2.* s.l.:MARINTEK.

Mavrakos, S., 1988. Hydrodynamic coefficients for a thick-walled bottomless cylindrical body floating in water of finite depth.. *Ocean Engineering,* 15(3), pp. 213-229..

Morison, J., Johnson, J. & Schaaf, S., 1950. The Force Exerted by Surface Waves on Piles. *Journal of Petroleum Technology,* 2(05).

Overdick GmbH & Co KG, 2012. *Seafastening for Tripod Foundations.* [Online]
Available at: https://overdick-offshore.com/projects/service_division/seafastening_for_tripod_foundations
[Accessed 10 02 2017].

Sarkar, A. & Gudmestad, O. T., 2010. Splash zone lifting analysis of subsea structures. *In ASME 2010 29th International Conference on Ocean, Offshore and Arctic Engineering*, pp. 303-312.

WindEurope, 2017. *The European offshore wind industry – key trends and statistics 2016,* s.l.: windeurope.org.

Xu, D., 2016. *Master thesis on Numerical modelling and simulations for lowering of an offshore wind turbine tripod.* Trondheim: Norwegian University of Science and Technology.
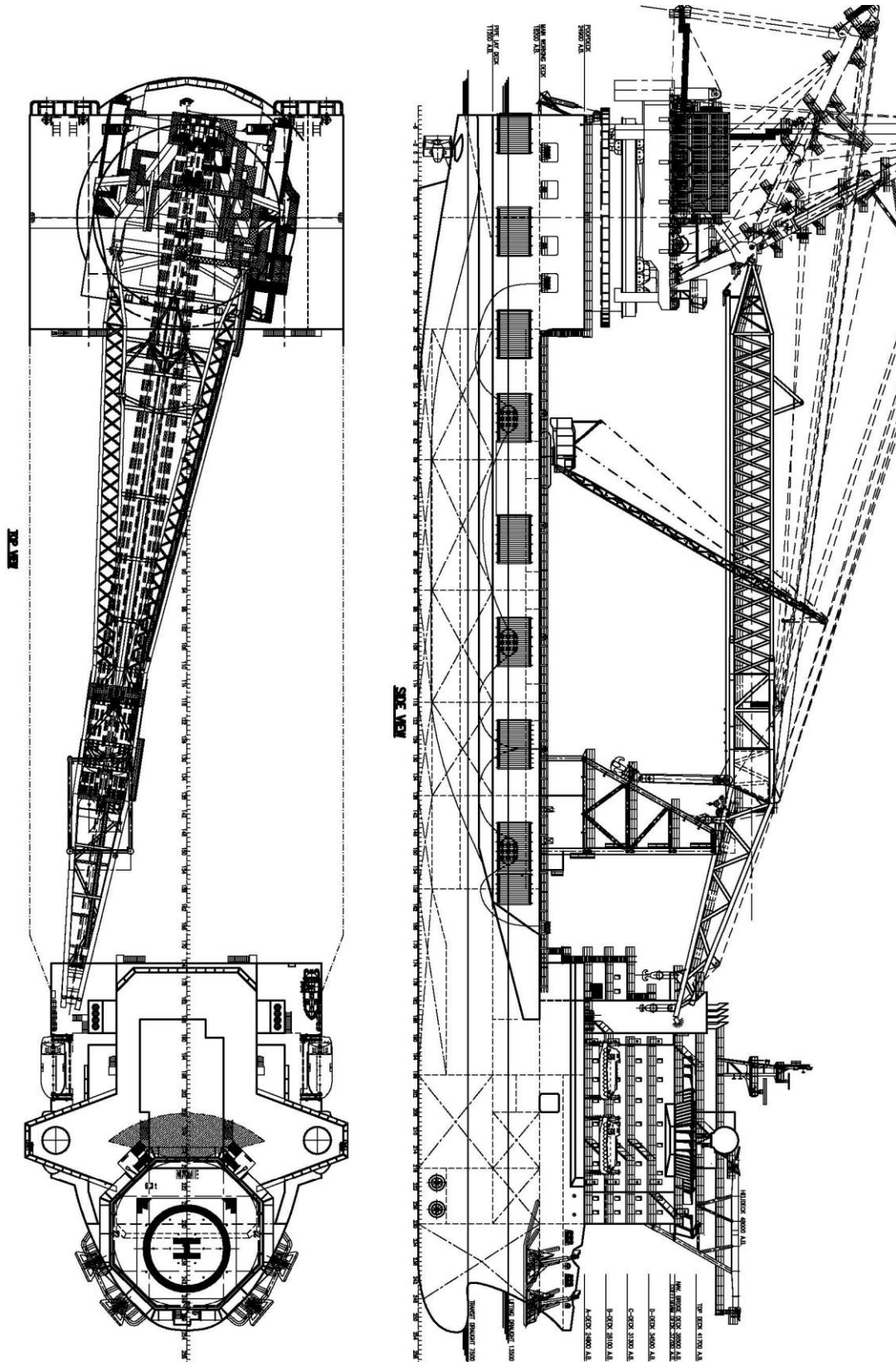
Appendix A
Layout of Heavy Lift Vessel

Figure A.1 - Layout of HLV

Appendix B

MATLAB scripts

JONSWAP (S) versus PM spectrum

```matlab
function [S,PM]=JONSWAPDNVbackup(Hs,Tp)
    wp=2*pi/Tp;
    gamma=3.3;
%   k=2*pi/(wp*sqrt(Hs));
%     if k <= 3.6
%        gamma = 5;
%     elseif k <= 5
%        gamma = exp(5.75-1.15*k);
%     else % k > 5
%        gamma = 1;
%        disp('PM spectrum')
%     end
    W=linspace(0.0959,1.568,59); %wave frequency following RAO data
    S=zeros(1,length(W));
    PM=zeros(1,length(W));
    for k=1:1:length(W),
        if  W(k) < wp,
            sigma=0.07;
        else
            sigma=0.09;
        end
        PM(k)=(5/16)*Hs^2*wp^4*(W(k)^(-5))*exp(-(5/4)*(W(k)/wp)^(-4));
        S2=gamma^(exp(-(W(k)-wp)^2/(2*(sigma*wp)^2)));
        Agamma=1-0.287*log(gamma);
        S(k)=Agamma*PM(k)*S2;
    end
end
```

Plotting of the JONSWAP versus PM spectrum (Hs=5m, Tp=6/8/10s) - Figure 3.4

```matlab
%Spectrum curves between JONSWAP and PM in various Tp, based on Hs=5m

W=linspace(0.0959,1.568,59); %wave frequency following RAO data

[SJ6,PM6]=JONSWAPDNVbackup(5,6); %Hs=5m and Tp=6s
[SJ8,PM8]=JONSWAPDNVbackup(5,8); %Hs=5m and Tp=8s
[SJ10,PM10]=JONSWAPDNVbackup(5,10); %Hs=5m and Tp=10s

plot(W,SJ6,W,PM6,'--',W,SJ8,W,PM8,'--',W,SJ10,W,PM10,'--');
title('Comparison between JONSWAP and PM spectrum');
axis([0,1.6,0,9]);
legend('JONSWAP spectrum','PM spectrum');
xlabel('Wave Frequency \omega [rad/s]');
ylabel('Spectral density [m^2 s]');
gtext('Tp=10s')
gtext('Tp=8s')
gtext('Tp=6s')
gtext('Hs=5m')
```

RAO plotting - Figure 4.2 ~ 4.6

```matlab
%First, extract data from "System Description SIMO" (from Lin) to get the
%transfer functions of the Heave motion, Roll motion and Pitch motion
%respectively which are saved as independent files in dxt format.

%Then, import data of the independent .txt to Matlab and entitled as
%amplitudeHeave / phaseHeave etc. as shown in the following coding

%coordinates of crane tip (x,y) of interest regarding vertical motion RAO
%for crane tip, (-81.7, 53.5, 80) is decided as the installation position
%take (-10.5,53.5, 80) for comparison - influence from pitch

%%
%import data from seperate motion transfer function files
Heave=importdata('Heave motion TF.txt');
HMTF=Heave.data;
Roll=importdata('Roll motion TF.txt');
RMTF=Roll.data;
Pitch=importdata('Pitch motion TF.txt');
PMTF=Pitch.data;

aH=HMTF(:,3);
pH=pi*HMTF(:,4)/180; %convert phase angle from degree to radians
aR=RMTF(:,3);
pR=pi*RMTF(:,4)/180;  %convert phase angle from degree to radians
aP=PMTF(:,3);
pP=pi*RMTF(:,4)/180; %convert phase angle from degree to radians

W=linspace(0.0959,1.568,59); %wave frequency following RAO data

%%
%RAO for vessel heave
plot(W,aH(355:413),'--',W,aH(414:472),W,aH(473:531),':k',W,aH(532:590),'--
',W,aH(591:649),W,aH(650:708),':b',W,aH(709:767))
grid on
legend('idir7','idir8','idir9','idir10','idir11','idir12','idir13');
title('RAO - vessel heave');
xlabel('Frequency \omega [rad/s]');
ylabel('RAO [m/m]')

%%
%RAO for vessel roll
plot(W,aR(355:413),'--',W,aR(414:472),W,aR(473:531),':k',W,aR(532:590),'--
',W,aR(591:649),W,aR(650:708),':b',W,aR(709:767))
legend('idir7','idir8','idir9','idir10','idir11','idir12','idir13');
title('RAO - vessel roll');
xlabel('Frequency \omega [rad/s]');
ylabel('RAO [rad/m]')

%%
%RAO for vessel pitch
plot(W,aP(355:413),'--',W,aP(414:472),W,aP(473:531),':k',W,aP(532:590),'--
',W,aP(591:649),W,aP(650:708),':b',W,aP(709:767))
legend('idir7','idir8','idir9','idir10','idir11','idir12','idir13');
title('RAO - vessel pitch');
xlabel('Frequency \omega [rad/s]');
```

```matlab
ylabel('RAO [rad/m]')

%%
%RAO of vertical motion for crane tip
DW=repmat(W,1,13); %replicate the frequency data for various directions as the RAO file

Hv=zeros(1,length(DW));
RAOV=zeros(1,length(DW));
for k=1:1:length(DW)
    %Hv(k)=aH(k)*exp(1i*pH(k))+53.5*aR(k)*exp(1i*pR(k))+10.5*aP(k)*exp(1i*pP(k));
    Hv(k)=aH(k)*exp(1i*pH(k))+53.5*aR(k)*exp(1i*pR(k))+81.7*aP(k)*exp(1i*pP(k));
    RAOV=abs(Hv);
end

plot(W,RAOV(355:413),'--r',W,RAOV(414:472),'g',W,RAOV(473:531),':b',...
    W,RAOV(532:590),'--',W,RAOV(591:649),W,RAOV(650:708),':k',...
    W,RAOV(709:767));
 grid on
legend('idir7','idir8','idir9','idir10','idir11','idir12','idir13');
title('RAO - vertical motion of crane tip');
xlabel('Frequency \omega [rad/s]');
ylabel('RAO [m/m]')
```

Response spectra of the crane tip at two positions - Figure 4.8 (similar to Figure 4.9 and 4.10)

```matlab
%First, extract data from "System Description SIMO" (from Lin) to get the
%transfer functions of the Heave motion, Roll motion and Pitch motion
%respectively which are saved as independent files in dxt format.

%Then, import data of the independent .txt to Matlab and entitled as
%amplitudeHeave / phaseHeave etc. as shown in the following coding

%coordinates of crane tip (x,y) of interest regarding vertical motion RAO
%for crane tip, (-81.7, 53.5, 80) is decided as the installation position
%take (-10.5,53.5, 80) for comparison - influence from pitch

%%import data from seperate motion transfer function files
Heave=importdata('Heave motion TF.txt');
HMTF=Heave.data;
Roll=importdata('Roll motion TF.txt');
RMTF=Roll.data;
Pitch=importdata('Pitch motion TF.txt');
PMTF=Pitch.data;

aH=HMTF(:,3);
pH=pi*HMTF(:,4)/180; %convert phase angle from degree to radians
aR=RMTF(:,3);
pR=pi*RMTF(:,4)/180;  %convert phase angle from degree to radians
aP=PMTF(:,3);
pP=pi*RMTF(:,4)/180; %convert phase angle from degree to radians

%%wave spectrum
S=JONSWAPDNV(1.25,6); %take for example,Hs=1.25m and Tp=6s
W=linspace(0.0959,1.568,59); %wave frequency following RAO data
```

```matlab
DW=repmat(W,1,13); %replicate the frequency data for various directions as the RAO file
DS=repmat(S,1,13); %replicate the Wave Spectrum data to the same dimension as the Transfer function data
(various directions)


%Response - vertical motion of crane tip (-81.7, 53.5, 80)
Hv1=zeros(1,length(DW));
Srv1=zeros(1,length(DW));
for k=1:1:length(DW)
    Hv1(k)=aH(k)*exp(1i*pH(k))+53.5*aR(k)*exp(1i*pR(k))+81.7*aP(k)*exp(1i*pP(k));
%   Hv2(k)=aH(k)*exp(1i*pH(k))+53.5*aR(k)*exp(1i*pR(k))+10.5*aP(k)*exp(1i*pP(k));
    Srv1(k)=(abs(Hv1(k)))^2*DS(k);
end


%Response - vertical motion of crane tip (-10.5, 53.5, 80)
Hv2=zeros(1,length(DW));
Srv2=zeros(1,length(DW));
for k=1:1:length(DW)
    Hv2(k)=aH(k)*exp(1i*pH(k))+53.5*aR(k)*exp(1i*pR(k))+10.5*aP(k)*exp(1i*pP(k));
    Srv2(k)=(abs(Hv2(k)))^2*DS(k);
end


figure
subplot(1,2,1)
plot(W,Srv1(355:413),'--r',W,Srv1(414:472),'g',W,Srv1(473:531),':b',W,Srv1(532:590),'--
',W,Srv1(591:649),W,Srv1(650:708),':',W,Srv1(709:767));
grid on
legend('idir7','idir8','idir9','idir10','idir11','idir12','idir13');
title('Response spectrum - crane tip (determined position)');
xlabel('Frequency \omega [rad/s]');
ylabel('Response(\omega) [m^2 s/rad]')
axis([0.4,1.6,0,0.35])

subplot(1,2,2)
plot(W,Srv2(355:413),'--r',W,Srv2(414:472),'g',W,Srv2(473:531),':b',W,Srv2(532:590),'--
',W,Srv2(591:649),W,Srv2(650:708),':',W,Srv2(709:767));
grid on
legend('idir7','idir8','idir9','idir10','idir11','idir12','idir13');
title('Response spectrum - crane tip (assumed position)');
xlabel('Frequency \omega [rad/s]');
ylabel('Response(\omega) [m^2 s/rad]')
axis([0.4,1.6,0,0.35])
```

Limiting sea state – Figure 4.13

```matlab
%%import data from seperate motion transfer function files
Heave=importdata('Heave motion TF.txt');
HMTF=Heave.data;
Roll=importdata('Roll motion TF.txt');
RMTF=Roll.data;
Pitch=importdata('Pitch motion TF.txt');
PMTF=Pitch.data;

aH=HMTF(:,3);
pH=pi*HMTF(:,4)/180; %convert phase angle from degree to radians
```

```matlab
aR=RMTF(:,3);
pR=pi*RMTF(:,4)/180;  %convert phase angle from degree to radians
aP=PMTF(:,3);
pP=pi*RMTF(:,4)/180; %convert phase angle from degree to radians

%% idir 13 with 180 degree wave direction
W=linspace(0.0959,1.568,59); %wave frequency following RAO data
Hv13=zeros(1,length(W)); % idir 13 with 180 degree wave direction
for k=1:1:length(W)
%
Hv13(k)=aH(k+708)*exp(1i*pH(k+708))+53.5*aR(k+708)*exp(1i*pR(k+708))+10.5*aP(k+708)*exp(1i*pP(k+708));

Hv13(k)=aH(k+708)*exp(1i*pH(k+708))+53.5*aR(k+708)*exp(1i*pR(k+708))+81.7*aP(k+708)*exp(1i*pP(k+708));
end

%% idir 9 with 120 degree wave direction
W=linspace(0.0959,1.568,59); %wave frequency following RAO data

Hv9=zeros(1,length(W)); % idir 9 with 120 degree wave direction
for k=1:1:length(W)
%
Hv9(k)=aH(k+472)*exp(1i*pH(k+472))+53.5*aR(k+472)*exp(1i*pR(k+472))+10.5*aP(k+472)*exp(1i*pP(k+472));

Hv9(k)=aH(k+472)*exp(1i*pH(k+472))+53.5*aR(k+472)*exp(1i*pR(k+472))+81.7*aP(k+472)*exp(1i*pP(k+472));
end

%% critical parameters
Zlim=0.3; %limiting value of vertical motion of crane tip
q=0.05; % assumed allowable probability of exceeding the above limit value

%%
%wave and response spectrum in various [Hs,Tp]
Tp=4:0.2:14;
Srv=zeros(1,length(W)); %assign response spectrum
Hsl=zeros(1,length(Tp)); %assign limiting Hs
for k=1:1:length(Tp)
   Hs=0;
   Sigma=0;
   Sigma0=0;
   while Sigma<=Sigma0
      Hs=Hs+0.1;
      S=JONSWAPDNV(Hs,Tp(k));
      Srv=(abs(Hv9)).^2.*S; %response spectrum
      m0=trapz(W,Srv);
      Sigma=sqrt(m0); % response variance
      Sm02=Srv.*W.^2; %for calculation of 2nd order spectral moment
      m2=trapz(W,Sm02);
      tm02=2*pi*sqrt(m0/m2); %expected zero-up crossing wave period
      N=3600/tm02; % expected No. of waves in 1 hour
      Sigma0=Zlim/(sqrt(-2*log(1-(1-q)^(1/N))));
      Hsl(k)=Hs-0.1;
   end
   if Hsl(k)>2.5
      Hsl(k)=2.5; %limiting wave condition due to vessel operating specification
   end
end
```

```matlab
%%
plot(Tp,Hsl);
grid on
title('Limiting sea state curve');
xlabel('Peak period Tp [s]');
ylabel('Significant wave height Hs [m]');
axis([4,14,0,3])
% gtext('Acceptable 1 hour risk sea states')
% gtext('Unacceptable 1 hour risk sea states')
```